Simulations of 2017 Hydrodynamics and Water Quality in the Massachusetts Bay System using the Bays Eutrophication Model

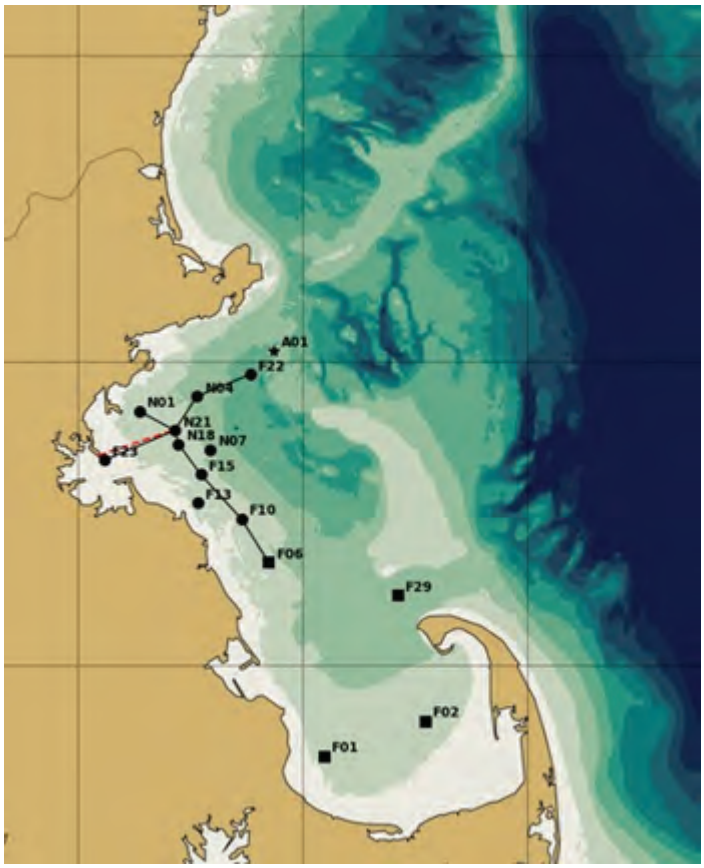

Massachusetts Water Resources Authority
Environmental Quality Department
Report 2021-12

Citation:

Deltares, 2022**. Simulations of 2017 Hydrodynamics and Water Quality in the Massachusetts Bay System using the Bays Eutrophication Model.** Boston: Massachusetts Water Resources Authority. Report 2021-12. 107 p.

MWRA Environmental Quality Department reports can be downloaded from http://www.mwra.com/harbor/enquad/trlist.html.

Summary

This report presents hydrodynamic and water quality model results for the Massachusetts Bays system (Massachusetts Bay, Cape Cod Bay, and Boston Harbor) during 2017. Treated effluent containing nutrients is released from the Massachusetts Water Resources Authority (MWRA) treatment plant at an outfall 15 km (9.5 mi) offshore in Massachusetts Bay. Nutrients are necessary and important to support healthy and diverse marine ecosystems. However, excess nutrients can cause eutrophication, the overgrowth of phytoplankton (microscopic marine algae) which degrades water quality and can harm marine life by depleting oxygen when it decays. To address potential eutrophication and other concerns, MWRA maintains an extensive bay and harbor field monitoring program, which this modelling complements.

The modelling methods are described in Deltares (2021). The hydrodynamic model simulates temperature, salinity, and currents, and is the foundation for the water quality model, which simulates key eutrophication parameters including nutrients, chlorophyll (a measure of phytoplankton), and oxygen. Hydrodynamic results agree well with available observations and capture the geographic and vertical structure, and temporal variability, of temperature and salinity distributions and density stratification, as well as tidal and non-tidal currents.

The 2017 water quality simulation captured general patterns in observed seasonal variations, geographic distributions, and vertical structure for many variables. This included the late spring reduction in near-surface dissolved inorganic nitrogen (DIN) due to phytoplankton uptake, and its replenishment after mixing in fall due to cooling and storms. It also included seasonal dissolved oxygen variations, with peak values in spring at shallow depths due to colder water and phytoplankton growth, and late summer minima at depth where stratification inhibits reaeration by air-sea exchange. In addition to those more bay-wide patterns, in the model as in observations, DIN was elevated persistently within about 10 km (6 mi) of the outfall and intermittently as far as about 20 km (12 mi) away, mainly due to nitrogen from ammonium in the treated effluent. The model captured the observed vertical structure of this effluent influence, which reached the surface through the winter months and remained at depth from about May through October when the bay was stratified. Consistent with field observations, the model did not show effects of effluent on chlorophyll or oxygen, nor indications that eutrophication was occurring.

In 2017 the river flow, surface heat flux, and winds driving the model were mostly in ranges typical of past years and consequently results generally did not deviate strongly from past simulations. Model chlorophyll was less variable than in past years. Metrics for agreement with observations were lower than for past years, which is believed to result from mismatch of temporal variability at timescales shorter than are the focus of the model. Phytoplankton biomass was composed of a succession of diatoms and flagellate species typical of past years, and *Phaeocystis* biomass was essentially absent, consistent with available 2017 observations.

Overall, the 2017 simulation supports the conclusions from field monitoring, that eutrophication was not a concern and bay-wide ecological function was not appreciably influenced by the outfall.

Contents

List of Figures

List of Tables

1 Introduction

The Massachusetts Water Resources Authority (MWRA) has established a long-term monitoring program to evaluate the impact of its sewage treatment plant effluent, which is discharged 15 km (9.5 mi) offshore, on the water quality and ecosystem function of Massachusetts Bay, Cape Cod Bay, and Boston Harbor. The monitoring program primarily consists of a series of ongoing field observation surveys and includes complementary water quality modeling as required by the discharge permit. The water quality simulations are carried out using the Bays Eutrophication Model (BEM), as recently updated (Deltares, 2021). This report presents simulation results for the 2017 calendar year. The content of this report is from Deltares internal document 11203379-005-ZKS-0001, dated 2 February, 2022.

1.1 Background on oceanographic processes influencing water quality

Massachusetts Bay and Cape Cod Bay (Figure 1-1) comprise a temperate coastal embayment system. Readers unfamiliar with the geography and/or the current understanding of the physical and biological oceanographic processes characterizing the system are referred to the introductory summaries found in sections 1.2 and 1.3 of MWRA Technical Report 2011-13 (Zhao et al., 2012), in the annual MWRA water column monitoring reports (e.g., for calendar year 2020, Libby et al., 2021), and in references cited by them. (All MWRA Technical Reports, including those just cited, are available online at http://www.mwra.state.ma.us/harbor/enquad/trlist.html.) A brief summary follows here. In this subsection the focus is on processes and influences other than effluent from the MWRA outfall, which has been shown in past studies to have a minor system-wide effect.

System hydrodynamics are characterized by a persistent general circulation pattern driving the flow of offshore Gulf of Maine waters into Massachusetts Bay via the Western Maine Coastal Current off Cape Ann, then southward before returning offshore just to the north of Cape Cod, with a portion of the flow first passing through Cape Cod Bay to the south (Figure 1-1). Rough estimates of the water residence time are about a month based on the surface currents, somewhat longer at mid-depth or deeper, where currents are weaker, and also longer in Cape Cod Bay than in Massachusetts Bay. While this slow general circulation is important in determining long-term average transport pathways, superposed on it are stronger and more variable wind-driven currents, and oscillatory tidal motions. Temperatures follow the characteristic temperate seasonal pattern of minima in late winter and peaks in late summer. Salinities are freshest inshore and in the upper several meters; in addition to the influence of offshore oceanographic conditions, they vary mainly in response to riverine inputs including primarily those brought by the Western Maine Coastal Current and the Merrimack River outflow to the north, and to a lesser extent the smaller amounts delivered via Boston Harbor. There is a seasonal cycle in vertical structure that includes transitions between well-mixed conditions, present from fall through early spring due to higher winds and atmospheric cooling, and strong density stratification during the late spring and summer due mainly to increased surface temperatures resulting from atmospheric heating.

The biology of the system is plankton-based and exhibits clear seasonal cycles that are tied closely to those hydrodynamic features, but with more pronounced spatial and interannual variability. Phytoplankton abundance typically peaks most strongly during bloom-favorable

conditions in the late winter and early spring, as temperatures rise, light increases, and nutrients remain plentiful near the surface due to the active vertical mixing. Following the transition from spring to summer, near-surface nutrient concentrations become depleted as density stratification impedes the vertical mixing that replenishes them. Zooplankton abundance and biomass generally peak in late summer, following the spring increase in phytoplankton prey levels. Primary productivity is commonly sustained at modest levels through summer and typically there is a second increase in phytoplankton during fall, when vertical mixing increases again and delivers nutrients to the surface while temperature and light conditions are still favorable before winter. Dissolved oxygen concentrations are influenced by a combination of biological and physical processes; the net result is a seasonal peak in late spring, due to phytoplankton production increasing winter levels already high due to strong reaeration, then steady decreases to a late summer minimum due to respiration and reduced reaeration. The summer oxygen minimum is lower at depth, where stratification limits reaeration.

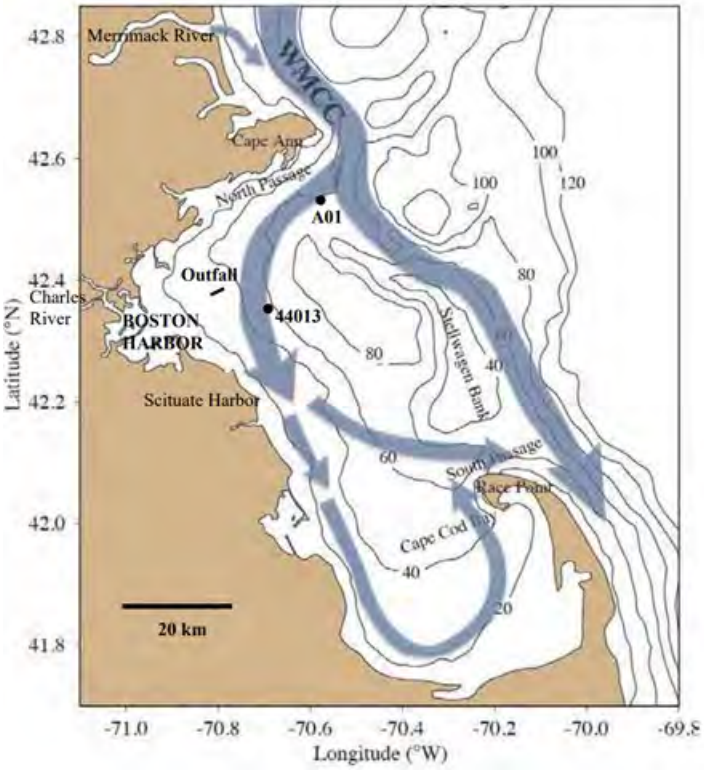

Figure 1-1 Geography, bathymetry, schematic long-term mean circulation. WMCC = Western Maine Coastal Current. A01 = Oceanographic mooring (Northeastern Regional Association of Coastal and Ocean Observing Systems). 44013 = Weather buoy (National Data Buoy Center). Contours = water depth in meters. Figure from Zhao et al. (2017), adapted from Xue et al. (2014).

1.2 Summary of observed 2017 conditions

To provide context for descriptions of model simulations of 2017 throughout this report, a brief summary is given here of observed 2017 conditions based on monitoring results (Libby et al., 2018). Temperatures were sharply warmer than typical during the winter (January to March), and also warmer than typical during the fall (October to December), but in the range of a typical year during the spring and summer. Early spring river runoff was higher than average, leading to lower

springtime salinities than typical and development of stratification in April, somewhat earlier than in a typical year. There was no particularly large winter-spring diatom or *Phaeocystis* bloom. Nutrient concentrations were in the range of past years, including the seasonal cycle with drawdown in spring and replenishment in fall. There were nor'easter storms in May and early June, followed by extended period of upwelling-favorable winds through June and July. Chlorophyll was moderate and phytoplankton was slightly less abundant than in a typical year. Offshore in the Gulf of Maine to the north there was a sustained *Alexandrium* bloom and paralytic shellfish poison (PSP) impacts; the spring nor'easters advected *Alexandrium* into Massachusetts Bay, but the subsequent upwelling winds limited its highest concentrations to the outer portions of the bay and there were no PSP impacts on bay shellfishing. Fall destratification occurred later than usual, so bottom DO minima were lower than typical, and would have been lower but for a storm-driven increase that occurred in June.

2 Methods

Use has been made of the updated BEM, as delivered in 2021. A complete model description with more details is documented in MWRA's technical report 2021-02 and its appendices (Deltares, 2021). The model is set up in the Delft3D Flexible Mesh Suite, developed by Deltares. Technical details on the model set-up, its grid and forcing is presented in Appendix A of Deltares (2021). A description of the software package and underlying hydrodynamic and water quality equations are available in Section A1 of Deltares (2021), and in Deltares (2019a, b). The model has been calibrated for the years 2012-2016, as described in Appendix B of Deltares (2021). The results of the model validation are given in the main report body of Deltares (2021).

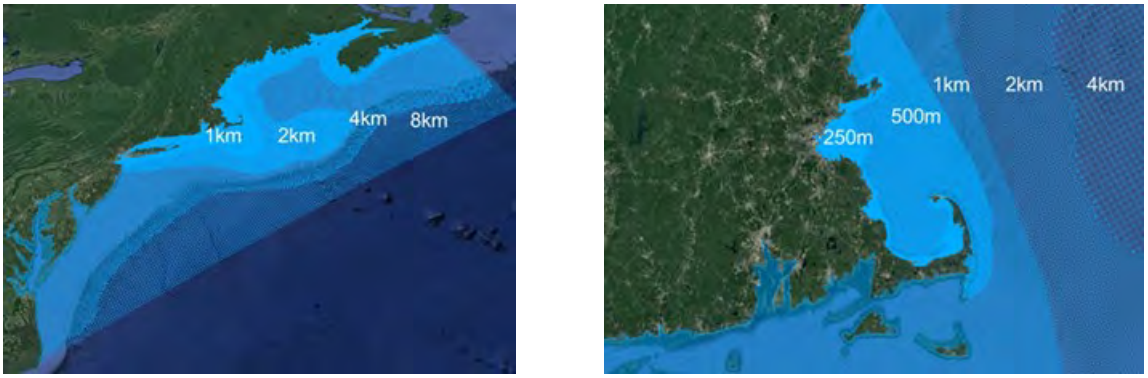

Figure 2-1 Model grid of the entire model domain (left) and zoomed-in for Massachusetts Bay (right)

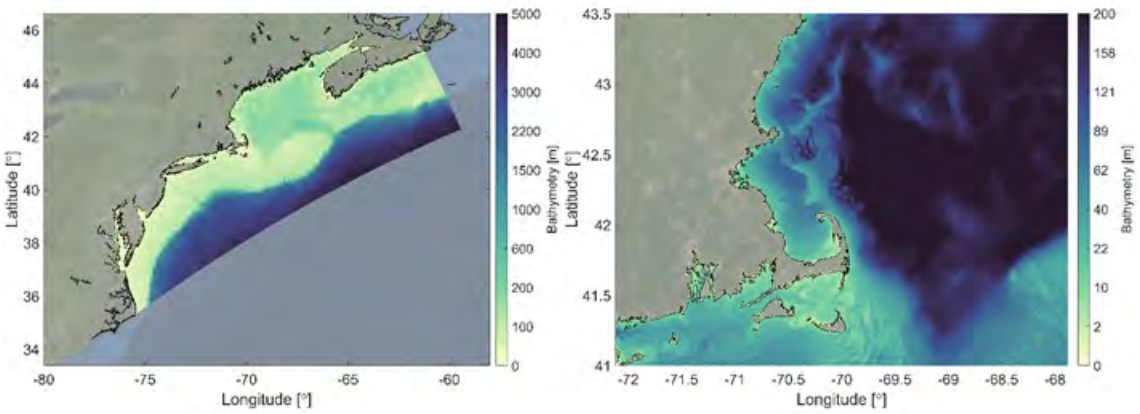

Figure 2-2 Model bathymetry of the entire model domain (left) and zoomed-in for Massachusetts Bay (right)

The model domain is large in order to best handle influences of offshore boundaries, as explained in Deltares (2021); it covers the entire Gulf of Maine region as well as the coastal region to the south, down to and including Chesapeake Bay (Figure 2-1 and Figure 2-2). Model performance in comparison to field measurements has been demonstrated most carefully in the area of Massachusetts Bay nearest the outfall, using MWRA observations (Deltares, 2021). The horizontal resolution is roughly 8km at the open ocean and is gradually refined toward the coast,

with a maximum resolution of 250m in Boston Harbor and along the surrounding coastline (including at the outfall location).

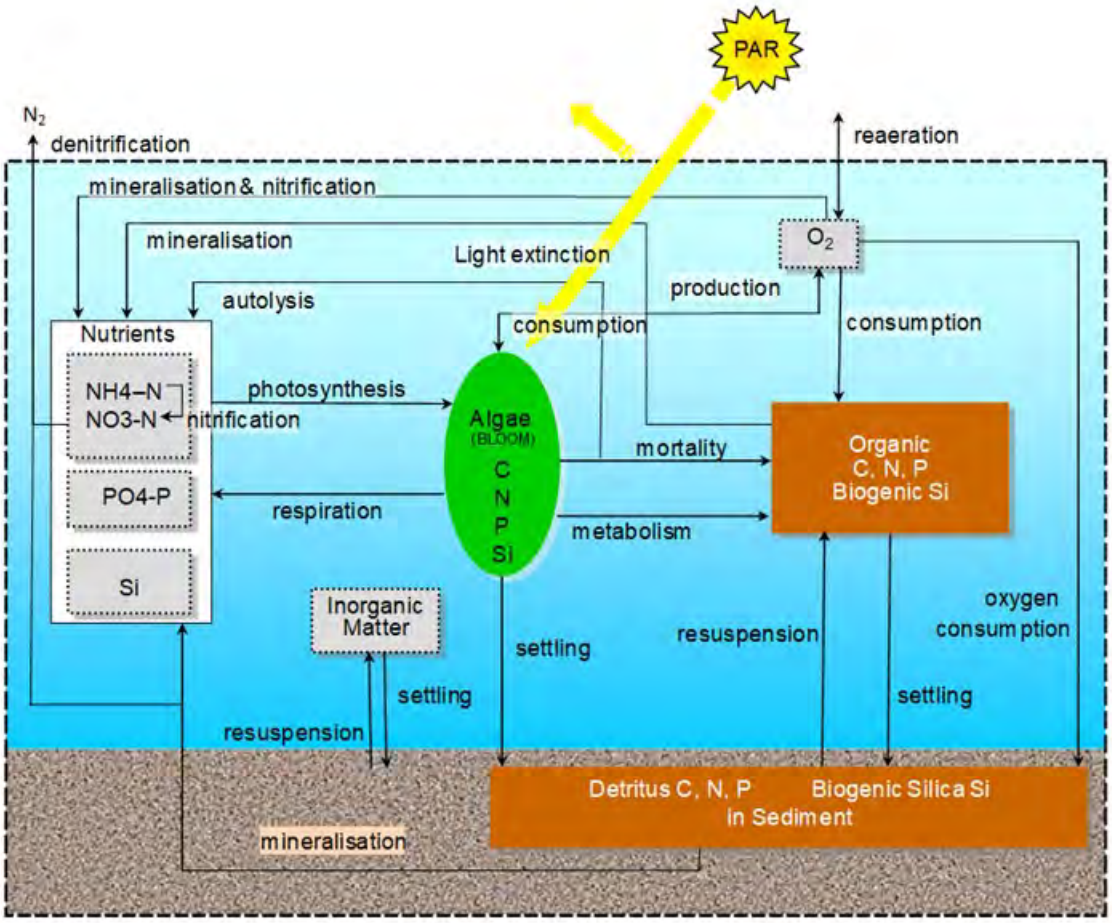

Figure 2-3 Schematic overview of all state variables and processes. Reproduced from Deltares (2021). Note that Inorganic Matter, Algae and Detritus affect light extinction in the water column.

Figure 2-3 provides an overview of the simulated state variables and processes for the water quality component. Four functional groups of pelagic phytoplankton are simulated ("Algae" in the figure): diatoms, dinoflagellates, other flagellates, and *Phaeocystis*.

The monitoring stations used to assess model performance and the transects along which water quality variables are examined are mapped in Figure 2-4. Model-observation comparison time-series are plotted for a representative selection of eight stations: N01 in the Northern Mass Bay, F22 with a greater oceanic influence, F23 near the outlet of Boston Harbor, N18 close to the MWRA outfall, N07 southeast of the outfall, F13 and F06 toward the south shore, and F02 in Cape Cod Bay.

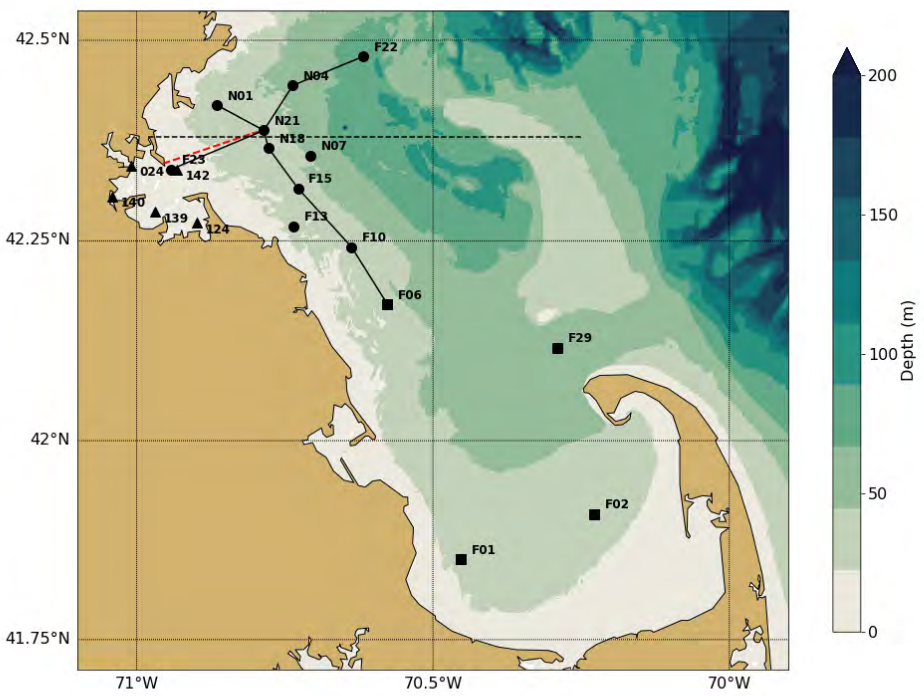

Figure 2-4 Location of MWRA monitoring locations (circles=Northern stations, squares=Southern stations, triangles=Harbor stations). The red dashed line indicates the tunnel between the DITP and the outfall diffusers. The black lines are the West-East and North-South transects used for model-observation comparisons of water quality constituents. The horizontal black dashed line represents the transect through the DITP outfall on which model results are presented in later figures.

2.1 Update to methods

In the 2017 BEM run, the representation of nutrient concentrations in the effluent has been corrected. In previous runs, MWRA monitoring data of total Kjeldahl nitrogen (TKN), NH_4, NO_2, NO_3, total phosphorus (TP) and PO_4 was misinterpreted as molecular weights per volume of water instead of atomic weights (expressed in gN/L and gP/L). This has led to a slight underestimation of TN, and an overestimation of the proportions of organic N in TN and of organic P in TP coming from the outfall. The 2017 results in this report are based on the correct loads.

The effect of this correction on the overall model performance has been assessed for the 2016 validation simulation of the BEM. The results of this assessment are given below and show that the effects of correcting the loads are minor and localized in the direct vicinity of the outfall. The outcome of this additional assessment is that the conclusions in MWRA's technical report 2021-

02 and its appendices (Deltares, 2021) regarding the setup, calibration and validation of the BEM do not need to be modified in any way.

To check the effects of the change in nutrient loads, skill metrics computed during the BEM validation phase (Deltares, 2021) were re-calculated for the updated representation of the DITP for DIN (Table 2-1), chlorophyll a (Table 2-2), and dissolved oxygen concentrations (Table 2-3). These metrics include bias, unbiased RMSE (uRMSE), total RMSE, normalized bias (bias* - normalized by the standard deviation of the observations) and normalized uRMSE (uRMSE*). It should be noted that skill metrics at station N21 were not reported in Deltares (2021).

Comparison plots between the former representation of the loads (Deltares, 2021) and the corrected representation are provided in Appendix B. These plots include:

- Model-observation time-series plots for DIN (Fig. B-1), chlorophyll a (Fig. B-2) and dissolved oxygen (DO) concentrations (Fig. B-3);
- Taylor diagrams for DIN (Fig. B-4), chlorophyll a (Fig. B-5) and dissolved oxygen (DO) concentrations (Fig. B-6);
- Cross-sections plots through the DITP outfall for DIN (Fig. B-7), chlorophyll a (Fig. B-8) and dissolved oxygen (DO) concentrations (Fig. B-9).

These results show that the correction of the representation of nutrients in the effluent has a negligible impact on DIN, chlorophyll a and DO concentrations in general. As expected, DIN concentrations are higher directly above the outfall, leading to an even higher overestimation of concentrations near the seabed at station N21 and a slight overestimation at near the surface (still in the range of model-observation discrepancies at other stations, see Table 2-1). The differences between the former and corrected representations are very limited at other monitoring stations and barely visible on the model-observation comparison plots. Furthermore, this has very little effect on chlorophyll a and DO concentrations, even at station N21.

Table 2-1 Comparison of skill metrics for computed DIN in 2016

Station	Depth	Former representation					Corrected representation				
		Bias	uRMSE	RMSE	bias*	uRMSE*	Bias	uRMSE	RMSE	bias*	uRMSE*
DIN											
N21	top	-0.12	7.96	7.96	-0.02	1.40	1.01	9.21	9.27	0.18	1.62
	bottom	25.34	7.25	26.36	6.97	1.99	31.39	8.79	32.60	8.64	2.42
F22	top	-1.24	2.99	3.24	-0.42	1.02	-1.20	3.00	3.23	-0.41	1.02
	bottom	0.34	1.16	1.20	0.17	0.60	0.34	1.16	1.21	0.18	0.60
N01	top	-1.11	2.72	2.94	-0.35	0.85	-0.93	2.88	3.02	-0.29	0.90
	bottom	2.77	3.41	4.39	1.42	1.74	2.98	3.55	4.63	1.52	1.81
N04	top	-1.06	3.09	3.27	-0.36	1.05	-1.01	3.16	3.32	-0.34	1.07
	bottom	1.41	0.80	1.62	0.73	0.41	1.42	0.81	1.63	0.73	0.42
N07	top	-1.89	3.70	4.15	-0.59	1.16	-1.85	3.75	4.18	-0.58	1.17
	bottom	1.56	2.16	2.66	0.94	1.31	1.61	2.23	2.75	0.98	1.35
F10	top	-0.75	3.49	3.57	-0.28	1.32	-0.72	3.57	3.64	-0.27	1.34
	bottom	0.20	2.59	2.60	0.06	0.83	0.33	2.61	2.63	0.10	0.84
N18	top	1.62	6.06	6.28	0.59	2.19	2.45	6.96	7.38	0.88	2.51
	bottom	1.43	5.33	5.52	0.33	1.23	1.81	5.63	5.92	0.42	1.30
F15	top	-1.96	3.39	3.92	-0.51	0.88	-1.97	3.54	4.05	-0.51	0.92
	bottom	1.55	1.26	2.00	0.69	0.56	1.62	1.27	2.05	0.72	0.56
F13	top	-0.87	3.01	3.14	-0.25	0.85	-0.73	3.21	3.29	-0.21	0.91
	bottom	0.75	2.88	2.98	0.38	1.47	0.95	3.04	3.18	0.48	1.55
F23	top	-2.12	2.47	3.25	-0.64	0.75	-1.99	2.55	3.24	-0.60	0.77
	bottom	-1.85	2.85	3.40	-0.65	1.00	-1.71	2.92	3.38	-0.60	1.02

Table 2-2 Comparison of skill metrics for computed chlorophyll a in 2016

Station	Depth	Former representation					Corrected representation				
		Bias	uRMSE	RMSE	bias*	uRMSE*	Bias	uRMSE	RMSE	bias*	uRMSE*
Chlorophyll a											
N21	top	-0.70	1.87	2.00	-0.86	2.32	-0.64	1.96	2.07	-0.80	2.43
	bottom	-0.82	0.97	1.27	-0.88	1.04	-0.81	0.97	1.27	-0.88	1.05
F22	top	-0.58	1.57	1.68	-0.76	2.05	-0.58	1.57	1.67	-0.76	2.05
	bottom	-0.75	1.05	1.29	-0.70	0.99	-0.75	1.05	1.29	-0.70	0.99
N01	top	-0.59	1.47	1.58	-0.98	2.45	-0.58	1.47	1.58	-0.97	2.46
	bottom	-0.88	0.88	1.25	-0.91	0.91	-0.88	0.88	1.25	-0.91	0.91
N04	top	-1.05	2.09	2.34	-1.00	1.98	-1.06	2.08	2.33	-1.00	1.97
	bottom	-0.68	0.93	1.15	-0.71	0.97	-0.68	0.93	1.15	-0.71	0.97
N07	top	-1.62	2.14	2.68	-1.00	1.32	-1.61	2.14	2.68	-1.00	1.32
	bottom	-0.95	1.29	1.61	-0.72	0.98	-0.95	1.29	1.61	-0.72	0.98
F10	top	-1.19	1.62	2.01	-1.11	1.51	-1.17	1.66	2.03	-1.09	1.55
	bottom	-0.98	1.46	1.75	-1.00	1.49	-0.97	1.47	1.76	-1.00	1.51
N18	top	-0.80	1.27	1.50	-0.97	1.54	-0.77	1.32	1.53	-0.94	1.60
	bottom	-1.11	1.07	1.54	-1.40	1.35	-1.11	1.09	1.55	-1.39	1.37
F15	top	-1.62	1.86	2.47	-0.95	1.09	-1.54	2.03	2.55	-0.91	1.19
	bottom	-1.03	0.95	1.40	-1.04	0.96	-1.03	0.95	1.40	-1.04	0.96
F13	top	-0.84	1.66	1.86	-0.49	0.96	-0.77	1.72	1.88	-0.44	1.00
	bottom	-0.63	1.19	1.35	-0.84	1.60	-0.63	1.21	1.36	-0.84	1.62
F23	top	-0.50	1.70	1.77	-0.35	1.18	-0.47	1.72	1.79	-0.33	1.20
	bottom	-1.21	2.15	2.47	-0.62	1.11	-1.19	2.16	2.47	-0.61	1.11

Table 2-3 Comparison of skill metrics for computed dissolved oxygen concentrations in 2016

Station	Depth	Former representation					Corrected representation				
		Bias	uRMSE	RMSE	bias*	uRMSE*	Bias	uRMSE	RMSE	bias*	uRMSE*
Dissolved oxygen											
N21	top	0.06	0.34	0.34	0.06	0.34	0.07	0.35	0.36	0.08	0.36
	bottom	0.31	0.26	0.41	0.37	0.30	0.31	0.27	0.41	0.36	0.31
F22	top	-0.12	0.39	0.41	-0.13	0.43	-0.12	0.39	0.41	-0.13	0.42
	bottom	0.57	0.43	0.71	0.50	0.38	0.57	0.43	0.71	0.50	0.38
N01	top	-0.11	0.48	0.49	-0.12	0.52	-0.11	0.48	0.49	-0.12	0.52
	bottom	0.15	0.32	0.35	0.16	0.34	0.14	0.32	0.35	0.15	0.35
N04	top	-0.24	0.45	0.51	-0.26	0.50	-0.24	0.45	0.51	-0.26	0.49
	bottom	0.44	0.25	0.50	0.37	0.21	0.43	0.25	0.50	0.37	0.21
N07	top	-0.15	0.37	0.40	-0.16	0.41	-0.15	0.37	0.40	-0.16	0.41
	bottom	0.42	0.37	0.57	0.34	0.30	0.42	0.37	0.56	0.34	0.30
F10	top	-0.04	0.32	0.32	-0.04	0.34	-0.03	0.32	0.32	-0.03	0.34
	bottom	0.38	0.18	0.42	0.38	0.18	0.38	0.18	0.42	0.37	0.18
N18	top	-0.11	0.39	0.40	-0.11	0.40	-0.10	0.40	0.41	-0.10	0.40
	bottom	0.20	0.30	0.36	0.22	0.33	0.20	0.31	0.37	0.21	0.34
F15	top	-0.19	0.34	0.39	-0.21	0.39	-0.17	0.37	0.41	-0.20	0.42
	bottom	0.28	0.24	0.37	0.29	0.25	0.28	0.24	0.37	0.28	0.25
F13	top	0.03	0.32	0.32	0.04	0.36	0.05	0.33	0.34	0.05	0.37
	bottom	0.31	0.32	0.44	0.31	0.33	0.30	0.32	0.44	0.31	0.33
F23	top	0.25	0.31	0.40	0.25	0.31	0.25	0.31	0.40	0.25	0.30
	bottom	0.46	0.21	0.50	0.46	0.21	0.46	0.21	0.50	0.46	0.21

3 Forcing

3.1 Wind, heat flux, solar radiation, and rivers

3.1.1 Wind

In Figure 3-1 the main characteristics of the monthly-mean wind forcing for the simulated year 2017 are compared to the means of the previous 20 years (1996-2016). The presented values are from mooring A01 (Figure 2-4). Additionally, ranges of the standard deviation and of the minimum and maximum values are given.

The seasonal pattern of the vector-averaged velocities (top frame) largely followed the means of previous years. Mean winds in February and March had a slightly stronger eastward component than usual. In April and October, the northward component was stronger than usual. Mean wind in September was rather strong to the south, where in previous years it was weaker and directed to the west-southwest.

Wind speeds (second frame) were largely within the ranges of the previous years. An exception occurred in March, when wind speeds were 2 m/s above average.

Monthly-mean wind stress magnitudes (third frame) were derived from the wind speeds and therefore show the same pattern.

North-south wind stresses (bottom frame) are an indicator for upwelling. These were largely within the ranges of the previous years. An exception was the monthly average of September, when a rather strong storm event occurred, resulting in stronger than usual downwelling (negative north-south wind stress).

3.1.2 Heat flux

A comparison between time series of the calculated net air-sea heat flux for 2017 and for the previous 5 years is given in Figure 3-2. A moving average with a window of 3 days is applied, consistent with how the water quality model output is handled below. The time series of the net flux includes the ranges of the standard deviation from the mean and of the minimum and maximum values. The cumulative flux is presented without any filtering.

The seasonal pattern in 2017 (top frame) showed an overall negative heat flux in winter (loss of heat from the surface, cooling of the ocean) and an overall positive heat flux in summer (heating of the ocean). This was in line with the average pattern in the previous years.

The cumulative heat flux (middle frame) was overall more positive than in the previous years. Mainly the winter cooling was weaker in January and February, while the onset of cooling at the end of the year was delayed. Nevertheless, the heat flux surplus at the end of the year was similar to previous years, mainly due to stronger cooling in March and the end of December.

The same pattern was visible in the anomaly of the cumulative heat flux (bottom frame, blue line) with strong cooling, compensating for the previous months, in March and December, the end of year anomaly was slightly negative with 0.1 GJ/m^2. The cumulative anomaly for the year (bottom

frame, green line) was positive at about 10 GJ/m2, so on an annual-mean basis, there was a greater cumulative surface heat flux surplus in 2017 compared to a typical year.

3.1.3 Solar radiation

The solar radiation from ERA5 is given in Figure 3-3. In general, the solar radiation in 2017 was very similar to the previous 20 years. There was however a slight negative anomaly (less solar radiation) from January to February, and from June to December (bottom frame, blue line). This led to a negative cumulative anomaly of solar radiation in 2017 of about 6 GJ/m2 (bottom frame, green line), so on an annual-mean basis, 2017 had less incident surface radiation than a typical year.

The higher surface heat flux in 2017 than a typical year occurred despite the lower than typical incident radiation in 2017. The surface heat flux in this case was more influenced by other factors like, for example, wind stress and wind-driven upwelling phenomena.

3.1.4 Rivers

In Figure 3-4 the volume transport for the Merrimack River, with results from the prior 20 years, is presented similarly to Figure 3.3.

The discharge (top frame) during the first two months of 2017 was slightly lower than the long-term mean, but still within or close to the plotted ranges. In the rest of the year the discharge was slightly higher during major discharge events in April-June and November. The last event exceeds the maximum of the previous years.

Overall, the discharges were similar to the long-term mean. This is clearly visible in the total discharged volume as well (middle frame). The anomaly of the discharged volume (bottom frame) was almost 0 km^3 at the end of the year.

The combined volume transport for the rivers discharging in Massachusetts Bay and Cape Cod Bay is presented in Figure 3-5. These rivers are Saugus, Mystic, Charles, Neponset, North and Jones. The combined discharges were slightly lower than average in the months March and October-December (top frame). This resulted in a negative anomaly of the discharged volume (bottom frame) of -10 km^3 at the end of the year

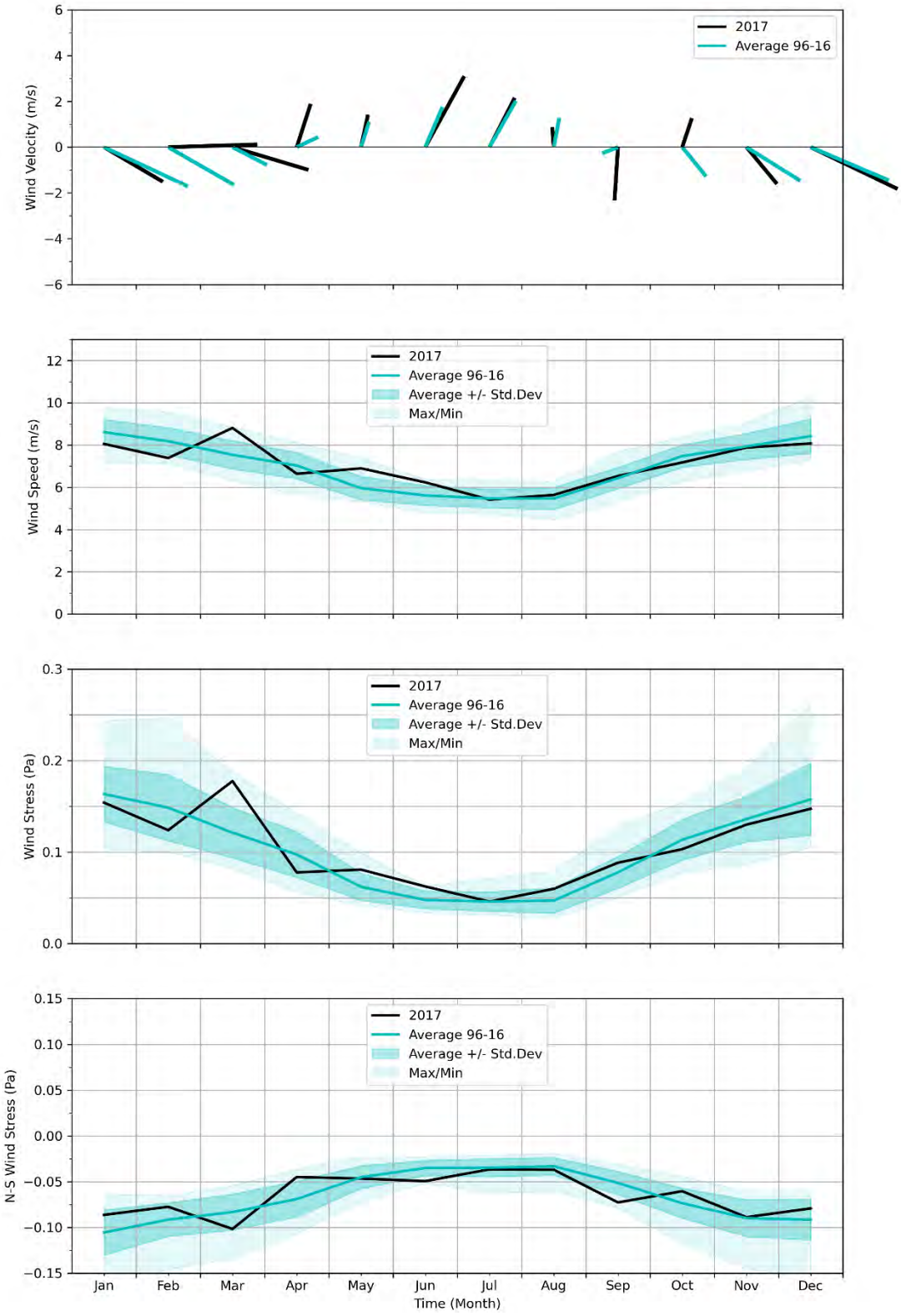

Figure 3-1 Surface wind forcing, monthly averages, compared to prior 20-year period.

Top frame: Vector-averaged wind velocities. Second frame: Wind speed. Third frame: Wind stress magnitude. Bottom frame: North-south component of wind stress, an indicator for wind-driven upwelling.

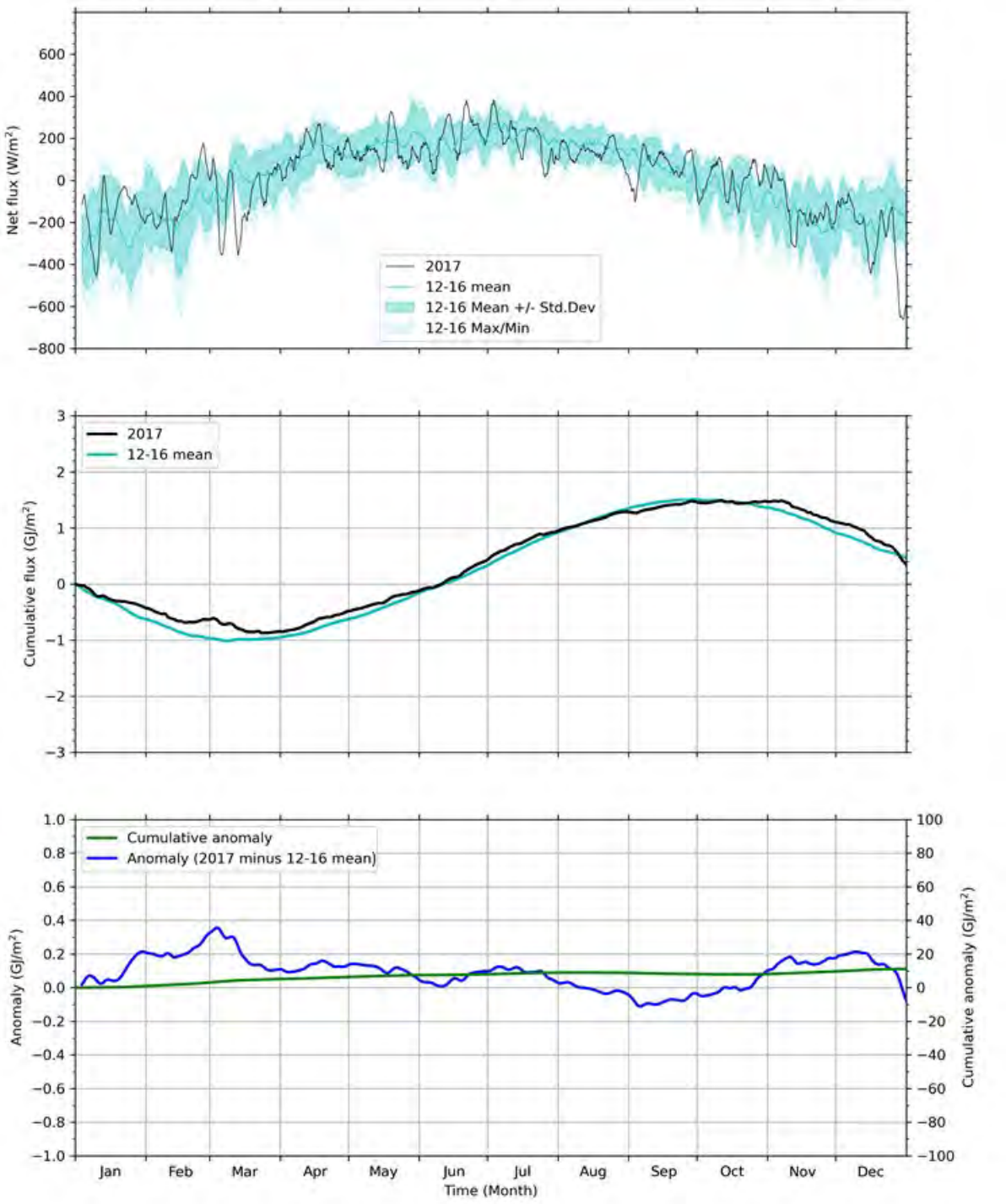

Figure 3-2 Surface heat flux, compared to prior 5-year period.

Top frame: Net heat flux into ocean. Middle frame: Cumulative net heat flux starting from January 1. Bottom frame: Anomaly (blue, left axis) and cumulative anomaly (=cumulative sum of daily mean anomaly; green, right axis) of 2017 net cumulative heat flux (relative to 2012-2016 average, NB. this is a shorter period than the 20 years used for the long-term mean, because direct simulation output from the 2012-2016 calibration period is used).

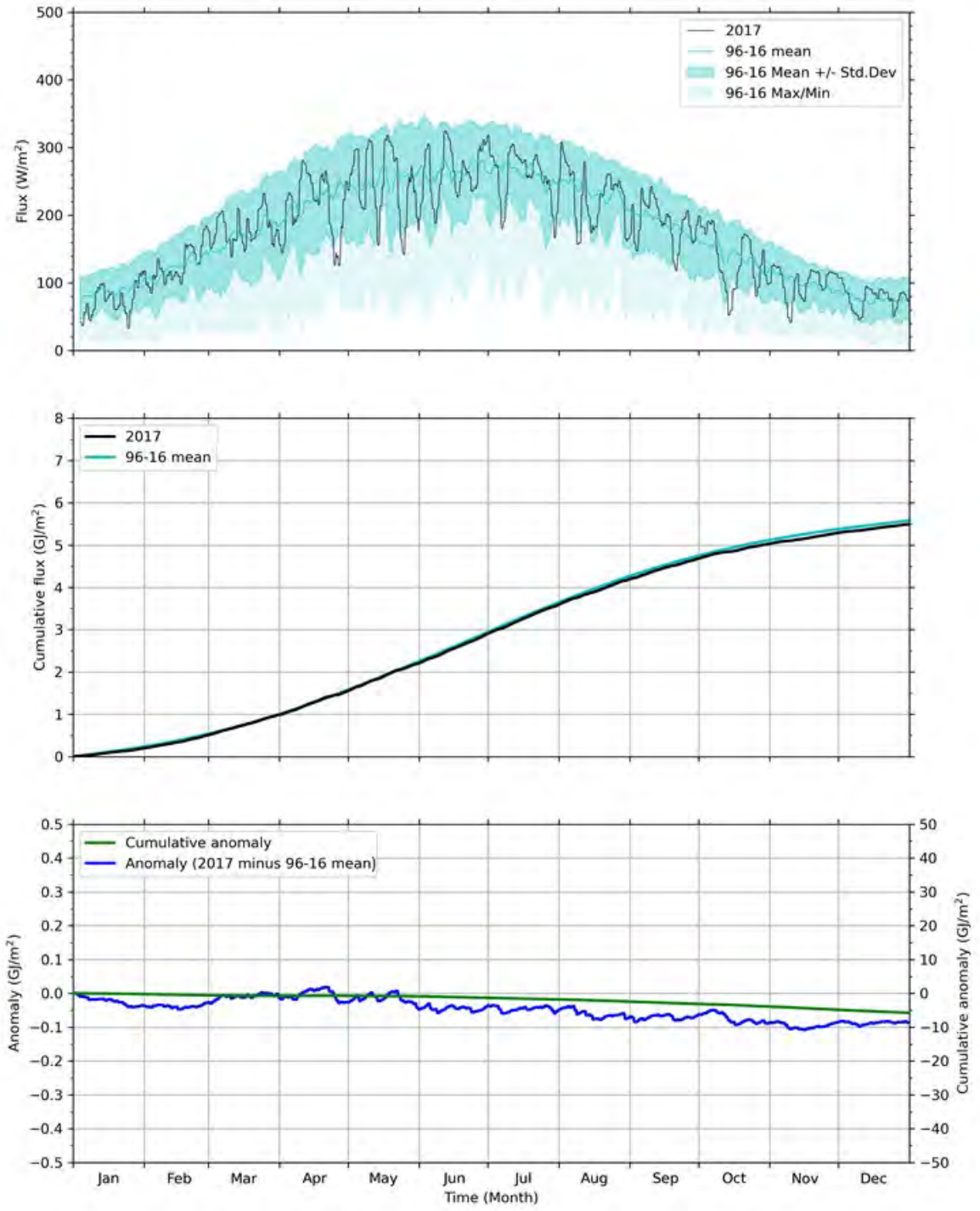

Figure 3-3 Solar radiation.

Top frame: Solar radiation into ocean. Middle frame: Cumulative solar radiation starting from January 1. Bottom frame: Anomaly and cumulative anomaly (=cumulative sum of daily mean anomaly) of 2017 cumulative solar radiation relative to 1996-2016 average.

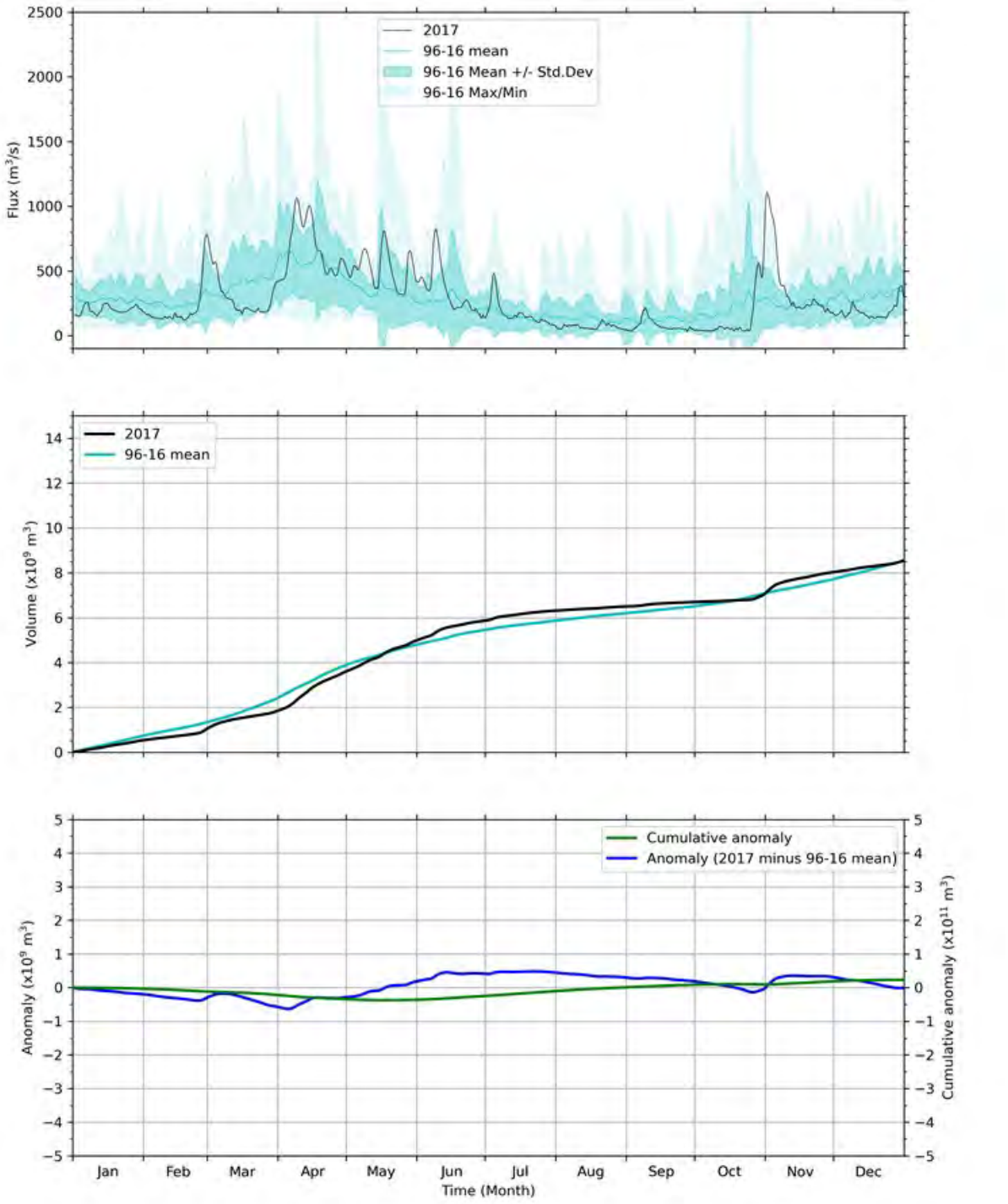

Figure 3-4 Merrimack River daily/cumulative flux and anomaly relative to previous 20 years

Top frame: Merrimack River volume flux. Middle frame: Cumulative flux relative to January 1. Bottom frame: Anomaly and cumulative anomaly (cumulative sum of daily mean anomaly) of flux in 2017 relative to 1996-2016 average.

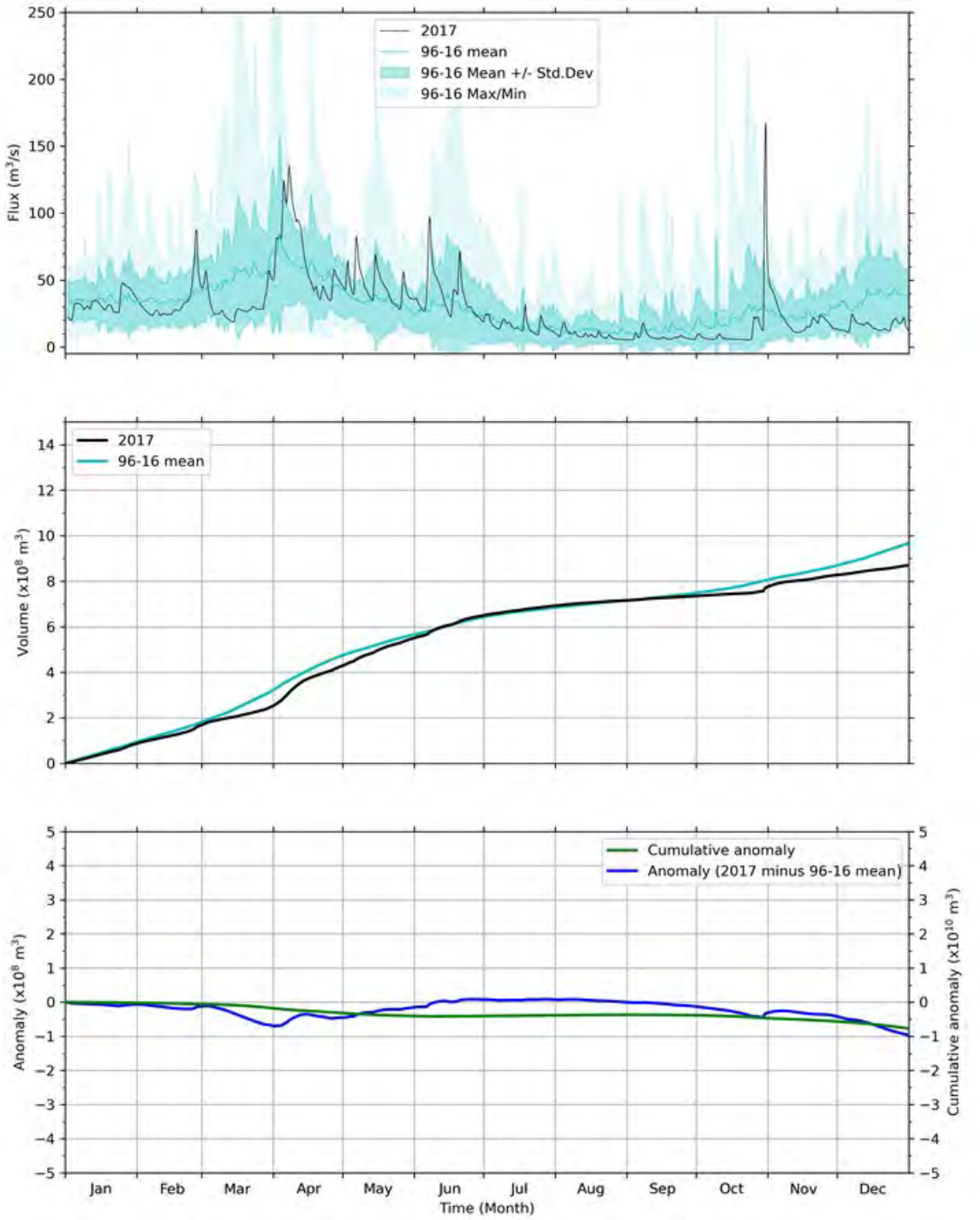

Figure 3-5 Summed discharge of all modeled rivers flowing in to Massachusetts and Cape Cod Bays.

Presented as in Figure 3-4.

3.2 Loading of organic carbon, nitrogen, and phosphorous

3.2.1 Rivers, MWRA effluent, and atmospheric sources

Modeled loads directly entering Massachusetts and Cape Cod Bays from rivers, the Deer Island treatment plant, and the atmosphere are shown in Figure 3-6. Loads entering the system through its offshore boundary are “oceanic input”, for example originating from rivers to the north including the Merrimack.

Model results show that oceanic input was the dominant source of organic carbon (OC), nitrogen and phosphorus (both in organic and inorganic forms), accounting for 99%, 92% and 96% of their total inputs, respectively (Figure 3-6). The simulated oceanic input of total nitrogen (TN) was comparable to the estimates based on the simulation of 1992 conditions from Hunt et al. (1999), reported by Zhao et al. (2017). The latter indicated that 93% of the TN entering the Mass Bay originated from the Gulf of Maine.

Further model results are as follows. Rivers were the second largest source of OC, accounting for roughly 4/5 of the non-oceanic input. MWRA loads constitute the main non-oceanic source of TN and total phosphorus (TP). These occur mainly in the inorganic form for nitrogen and in the organic form for phosphorus. Atmospheric deposition accounted for approximately 11% of the non-oceanic TN inputs. Finally, rivers are the smallest source of TN and TP to Massachusetts and Cape Cod Bays, representing less than 7% and 4% of their non-oceanic inputs, respectively.

Modeled 2017 OC loads from the MWRA effluent were comparable to and slightly higher than the highest years in the prior five-year period. TN and TP loads from the effluent for the year 2017 were in the middle of the range of loads from the prior five-year period.

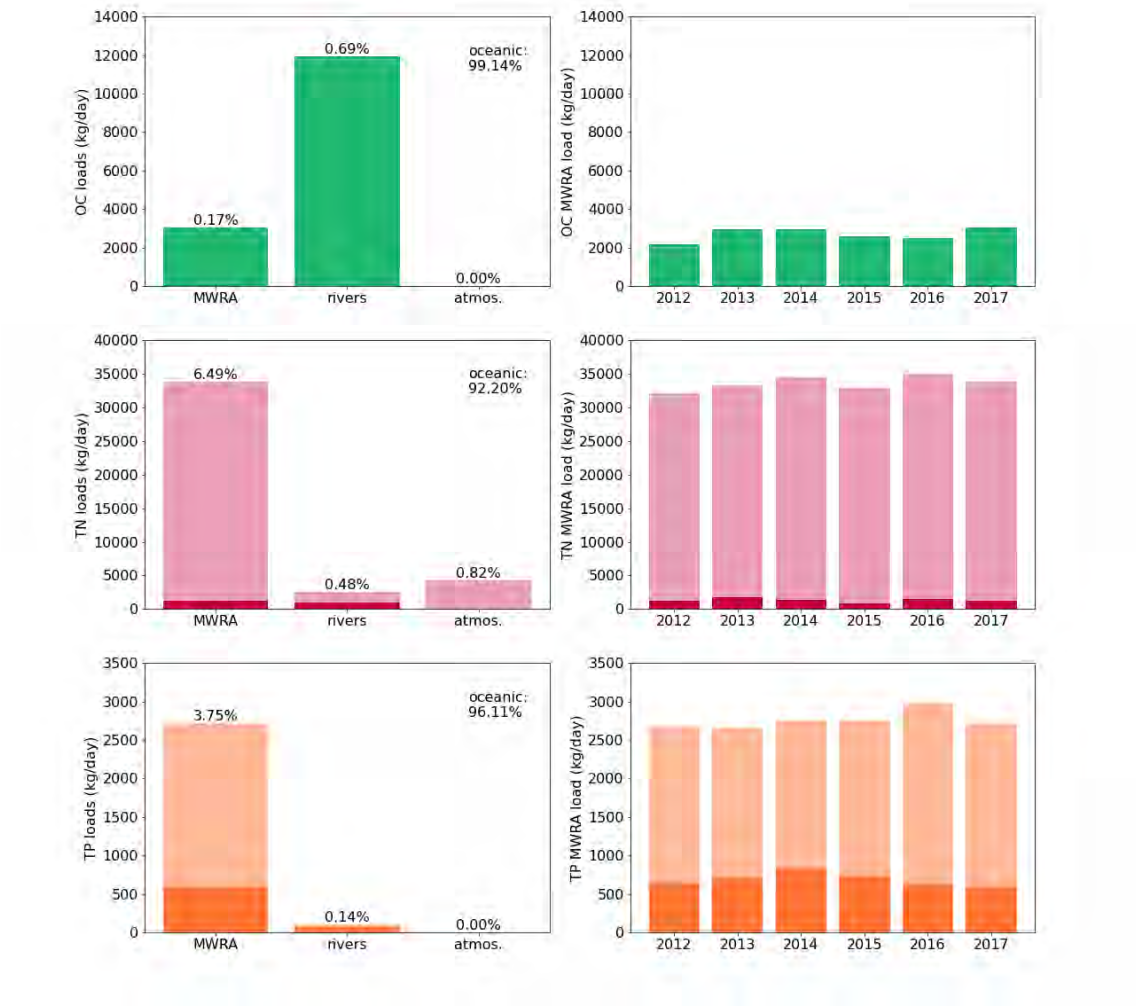

Figure 3-6: Organic Carbon (OC), Total Nitrogen (TN) and Total Phosphorus (TP) loads to Massachusetts and Cape Cod Bays. In the TN and TP plots, the darker sections of the bars represent the organic fractions. Left: 2017 loads from non-oceanic sources; percent of total is shown at top of each bar, and percent oceanic input (offshore boundary) shown at upper right. (Percentages correspond to summed organic and inorganic fractions.) Right: Deer Island Treatment Plant loads since 2012. OC=organic carbon; TN=total nitrogen; TP=total phosphorus.

3.2.2 Background information about nitrogen loads from non-MWRA dischargers

Because the focus of this model is potential effects from the MWRA effluent, it does not include loads from non-MWRA dischargers. To provide context for the potential role in bay processes of effluent discharges from non-MWRA sources (which, again, are not treated by the model) the magnitudes of their loads were estimated and shown to be a relatively small fraction of the MWRA load, as follows.

Average loads of total nitrogen (TN) from outfalls of non-MWRA dischargers to Massachusetts waters within and north of Massachusetts Bay and Cape Cod Bay were estimated. Figure 3-7 shows approximate locations of all outfalls examined. Three outfalls have very small flows, so loads were not estimated: USCG Eastern Point (Gloucester), Shore Cliff Retirement Home (Gloucester), and USCG Little Brewster. Table 3-1 lists the outfalls for which load estimates were made, from north to south.

Flow and concentration data were obtained from EPA's Enforcement and Compliance History Online (ECHO) database (https://echo.epa.gov/) for the 5-year period from mid-2017 to mid-2021. Average TN load was estimated as the product of average TN concentration and average plant flow, each averaged over this period. For the outfalls of South Essex Sewage District, Lynn, and Marshfield, TN measurements were not available, and the average TN was estimated as the sum of the averages of the measured NO3, NO2 and TKN. For Rockport, Gloucester, and Hull, concentration data are not collected, as there is no reporting requirement and no permit limit. For Rockport and Hull, the value used was that of Deer Island effluent, which was taken to be representative of effluent from these secondary-treated dischargers; for Gloucester, which currently provides primary treatment, the average concentration of Deer Island primary-treated wastewater was used. Manchester concentrations were calculated from data reported in May 2020 – June 2021, after the new permit requiring monthly reporting of TN went into effect; measurements from earlier times are not available. The MWRA outfall load used 32,000 kg/day, which is representative of the past several years (e.g. Werme et al, 2021).

The collective load from all non-MWRA outfalls was about 14.5% of the MWRA load (Table 3-1). The two individual outfalls that have the largest loads were South Essex Sewerage District and Lynn, at about 7% and 5% of the MWRA load respectively. All other dischargers together contributed a load that is about 2.5% as large as the MWRA load.

Figure 3-7 Approximate locations of non-MWRA dischargers listed in Table 3-1.

Table 3-1 Non-MWRA dischargers nitrogen load estimates.

Region	Discharger/Outfall	Average flow [MGD]	Average TN concentration [mg/L]	Average N load [kg/day]	Percent of MWRA outfall[3]
Outside bays, north of Cape Ann	Ipswich	0.8	8.2	25	0.08
	Rockport	0.7	27.8[1]	74	0.23
In Massachusetts Bay, north of Boston Harbor	Gloucester	3.2	37.0[1]	448	1.40
	Manchester-by-the-Sea	0.4	9.5[2]	14	0.04
	South Essex Sewerage District	26.2	23.0	2,281	7.13
	Lynn	21.5	18.8	1,530	4.78
In Massachusetts or Cape Cod Bays, south of Boston Harbor	Hull	1.5	27.8[1]	158	0.49
	Cohasset	0.3	12.9	15	0.05
	Scituate	1.4	2.1	11	0.03
	Marshfield	1.4	13.9	74	0.23
	Plymouth	1.5	5.5	31	0.10
All regions	Sum, all above	N/A[4]	N/A	4,660	14.56

1. *For Rockport, Gloucester, and Hull, concentration data are not collected, as there is no reporting requirement and no permit limit. For Rockport and Hull, the value used was that of Deer Island effluent, which was taken to be representative of effluent from these secondary-treated dischargers; for Gloucester, which currently provides primary treatment, the average concentration of Deer Island primary-treated wastewater was used.*
2. *Manchester-by-the-Sea concentrations were calculated from data reported in May 2020 – June 2021, after the new permit requiring monthly reporting of TN went into effect. Measurements from earlier times are not available.*
3. *The MWRA outfall load used 32,000 kg/day, which is representative of the past several years (e.g. Werme et al, 2021).*
4. *Not applicable.*

4 Hydrodynamic Model

In this section the performance of the hydrodynamic model is discussed, and model results are compared to measurements.

4.1 Verification of model performance

The model skill was assessed for surface and bottom temperature and salinity by means of a statistical analysis. Three quantitative skill measures (correlation, normalized standard deviation Std*, and normalized unbiased root mean square error uRMSE*) were determined, based on simulation results and vessel-based observations by MWRA surveys. The result is presented in four sets of Taylor diagrams in Figure 4-1. The left column shows the 2012-2016 validation period (Deltares, 2021) and the right column shows the 2017 simulation. See also the box below for further details and an explanation of the statistics in the diagrams.

Temperatures had correlation of over 0.95 and 0.90, Std* of 1.0-1.2 and 0.7-1.3, and uRMSE* of under 0.35 and 0.60, at the surface and bottom respectively. In general, the performance at the surface was similar to the validation result, with a slightly larger spread. At the bottom, the performance deviates more from the validation result. This was visible in some increases in bottom temperature that were not captured by the model, for example near the end of July for station F06 (Figure 4-2 below).

The skill of simulated salinity varied more per observation station. This ranged from a correlation of 0.55 or greater and 0.35 or greater, a Std* of 0.45-1.20 and 0.75-1.25, and a uRMSE* of up to 0.85 and 1.05, at the surface and bottom respectively. The performance at the surface slightly improved compared to the validation result. At the bottom, the improvement was a bit larger.

Overall, the figures presented here serve to verify that the performance of the hydrodynamic model in the simulations of 2017 did not deviate substantially from its performance during the prior 5-year period. For completeness, Taylor diagrams broken out for individual years 2012-2016, are presented in Appendix A to facilitate comparisons to 2017.

How to read a Taylor diagram

A Taylor diagram consists of a combination of three quantitative skill measures:

- Correlation Coefficient, represented in the plot by the azimuthal angle or blue lines.
- Normalized Standard Deviation (Std*), the Standard Deviation of the model results, normalized (*) by the standard deviation of the corresponding measurements. This ratio represents the relative amplitude of the modeled and observed variations, with a value of less than one indicating less modeled variability. It is represented in the plot by the radial distance from the origin (0,0).
- Unbiased Root-Mean-Square Error or standard deviation of the error, normalized with the standard deviation of the corresponding measurements (uRMSE*). It is represented in the plot by the grey contours, whose values are proportional to the radial distance from the target (black star), which represents perfect model-observation agreement.

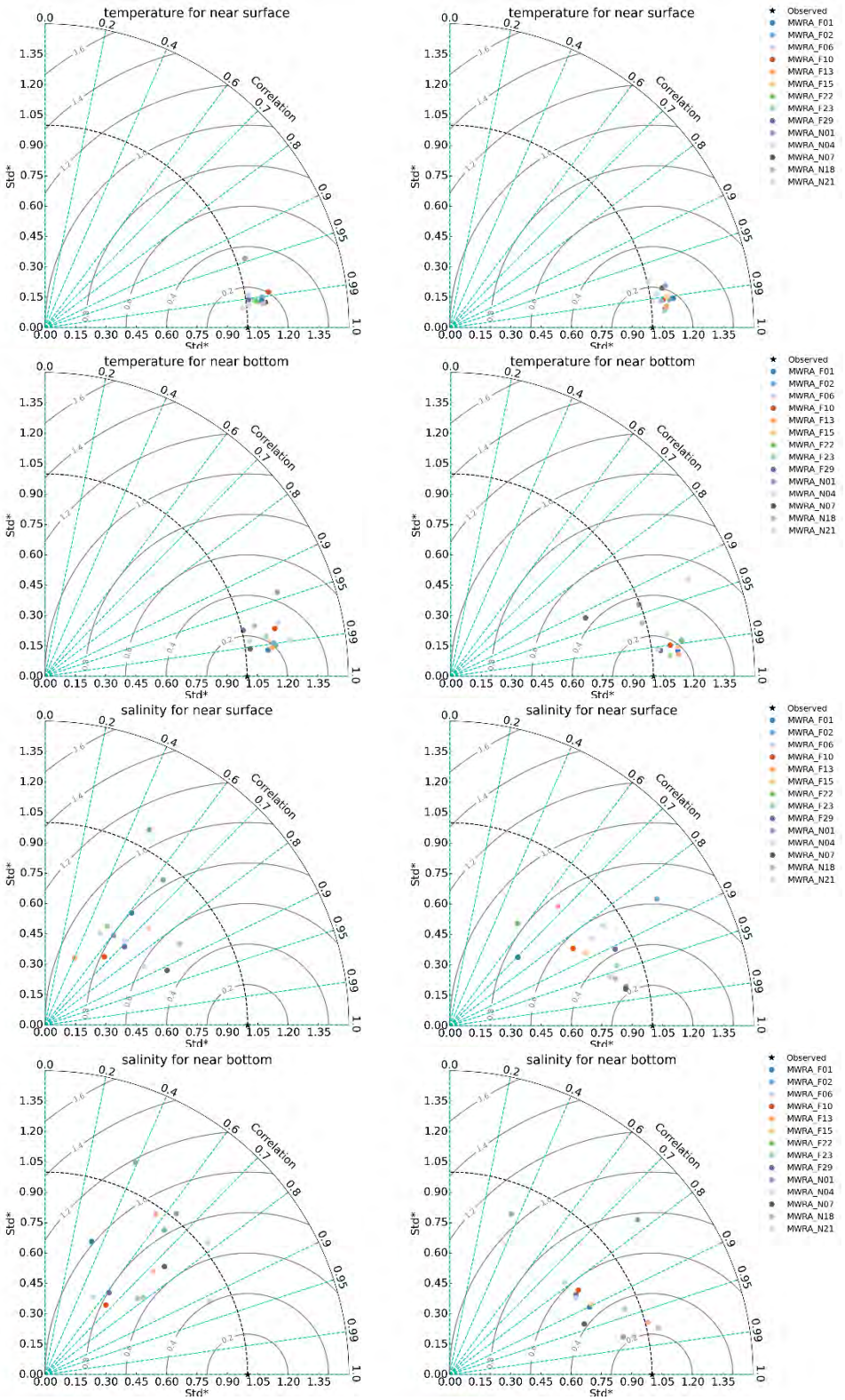

Figure 4-1 Taylor diagrams of hydrodynamic model for MWRA vessel-based survey observations.

Temperature (upper frames), salinity (lower frames); 2012-2016 validation period (left column) and 2017 simulation (right column).

4.2 Model-observation comparisons

The simulation for 2017 was compared to observations to assess the level of agreement between them for temperature and salinity, both in time and space.

4.2.1 Time series of temperature and salinity

For eight observation stations in the Massachusetts Bay and Cape Cod Bay, simulation timeseries of the surface (less than 5 m deep) and bottom (within 5 m of seafloor) temperature and salinity are presented in Figure 4-2 and Figure 4-4. Additionally, a comparison at three levels within the water column, between the surface and seafloor, is given in Figure 4-3 and Figure 4-5 (described below).

In these figures, vessel-based observations by MWRA surveys are included as individual symbols. The locations of the observation stations are given on a bathymetric map in the upper left frame. They include four stations generally surrounding the outfall (N01, N07, N18, and F13), one to the south (F06), one farther offshore (F22), one at the mouth of Boston Harbor (F23), and one in central Cape Cod Bay (F02).

In Figure 4-3 and Figure 4-5. showing results from within the water column, the depths vary from station to station and survey to survey but are nominally at 25%, 50%, and 75% of the water depth. The model output between surveys is not shown on these figures because the depths used, set by the observations, differ from survey to survey.

Overall, the seasonal cycle and most events were well captured by the model. Simulated stratification was in line with observations. At most stations, the onset of stratification was in April with a maximum in July and August. The water column started to become mixed again over the course of November. In the first half of September, stations in the shallower parts of Massachusetts Bay and Cape Cod Bay (N01, N18, F02, F06 and F13) were suddenly mixed after which the previous stratification level partially returned. This can be attributed to a storm event, visible in the timeseries of wind velocities in Figure 4-12. Furthermore, a peak in bottom temperature (and temporary drop in surface temperature) by the end of July was well represented by the model, with the exception of station F06, where the peak in bottom temperature was about 3°C too low. In the deeper parts of Massachusetts Bay (N06, N18, F06 and F22), simulated bottom temperatures were about 1°C too cold at the end of August and beginning of September. Simulated salinity showed a slight bias of about 0.25-0.50psu (as discussed in Deltares, 2021), but because this bias was present throughout the water column, salinity stratification was well represented. This also holds for the seasonal pattern in both surface and bottom salinity.

4.2.2 Spatial representation of temperature and salinity

To assess the simulation spatially, maps have been plotted with the mean of the modeled results at the surface and the bottom, averaged over a period of 5 days centered on the observation dates in Massachusetts Bay and Cape Cod Bay. The five presented periods span the seasonal cycle of stratification. This is given in Figure 4-6 and Figure 4-7 for temperature and in Figure 4-8 and Figure 4-9 for salinity. For the model-observation comparison, the available observations are plotted over the simulation fields as colored symbols.

These figures show a good agreement between the simulation and observations. The spatial variation at both the surface and bottom was comparable, with near-shore temperatures warmer in summer and colder in winter. At both depths, salinities were generally fresher near the coast.

Model-observation differences for temperature were largest in the months July and August with about 2°C at the surface. For salinity, model-observation differences were largest in May with up to 1.5 PSU at the surface.

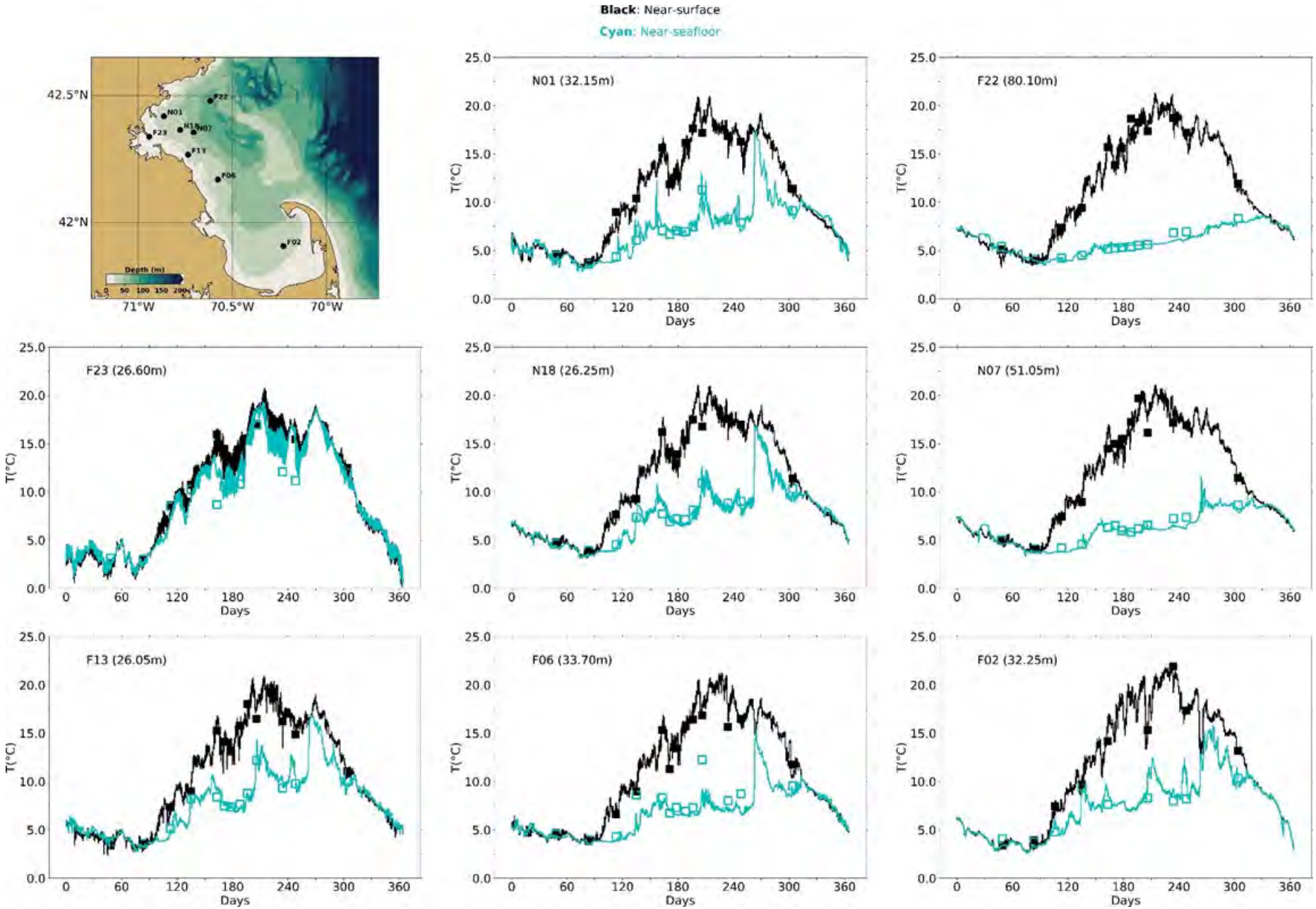

Figure 4-2 Temperature time series, model-observation comparison near surface (black) and seafloor (cyan). Model results: lines. MWRA vessel-based survey observations: symbols.

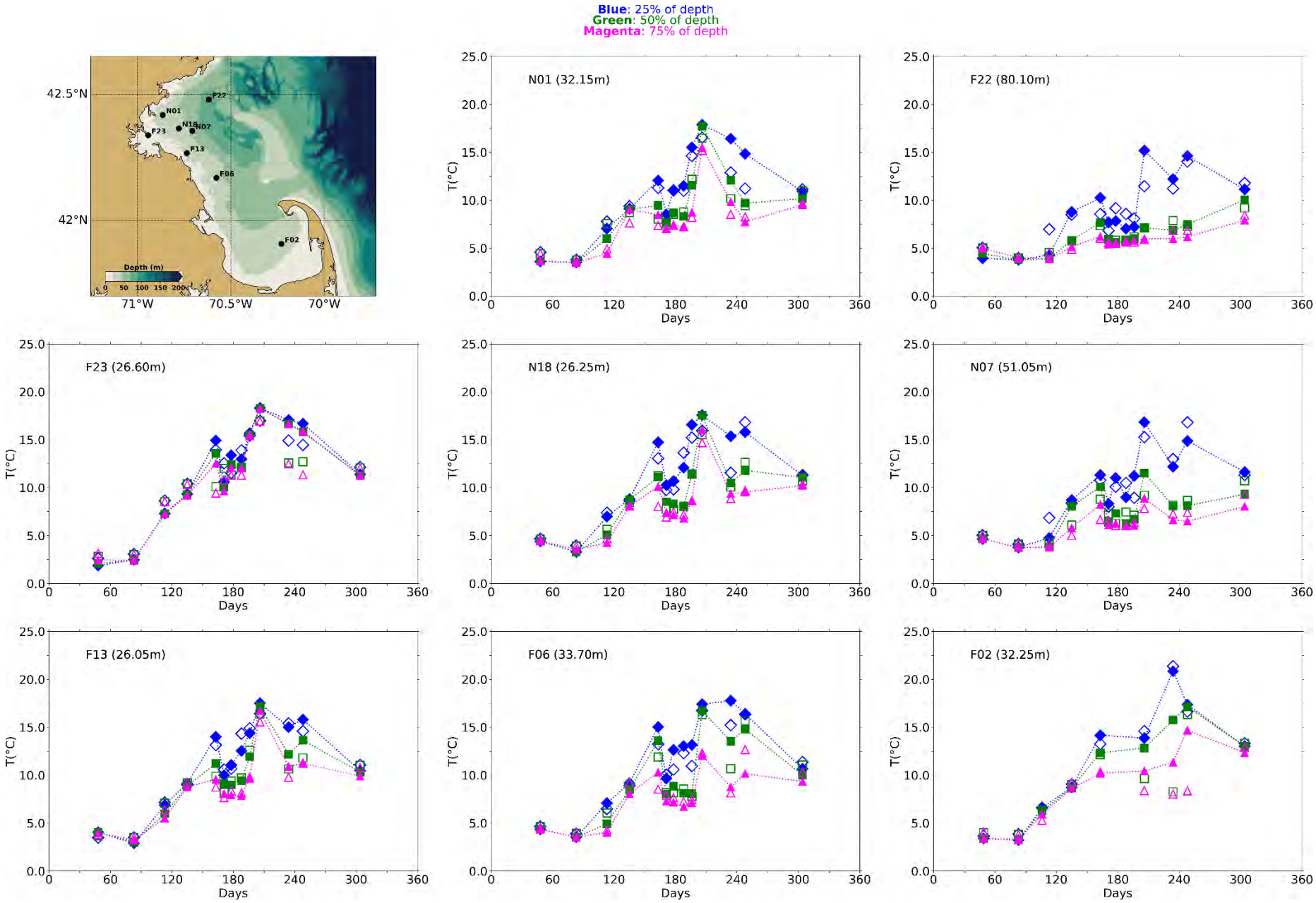

Figure 4-3 Temperature time series, model-observation comparison within water column (between surface and seafloor). Model results: lines with filled symbols. MWRA vessel-based survey observations: open symbols.

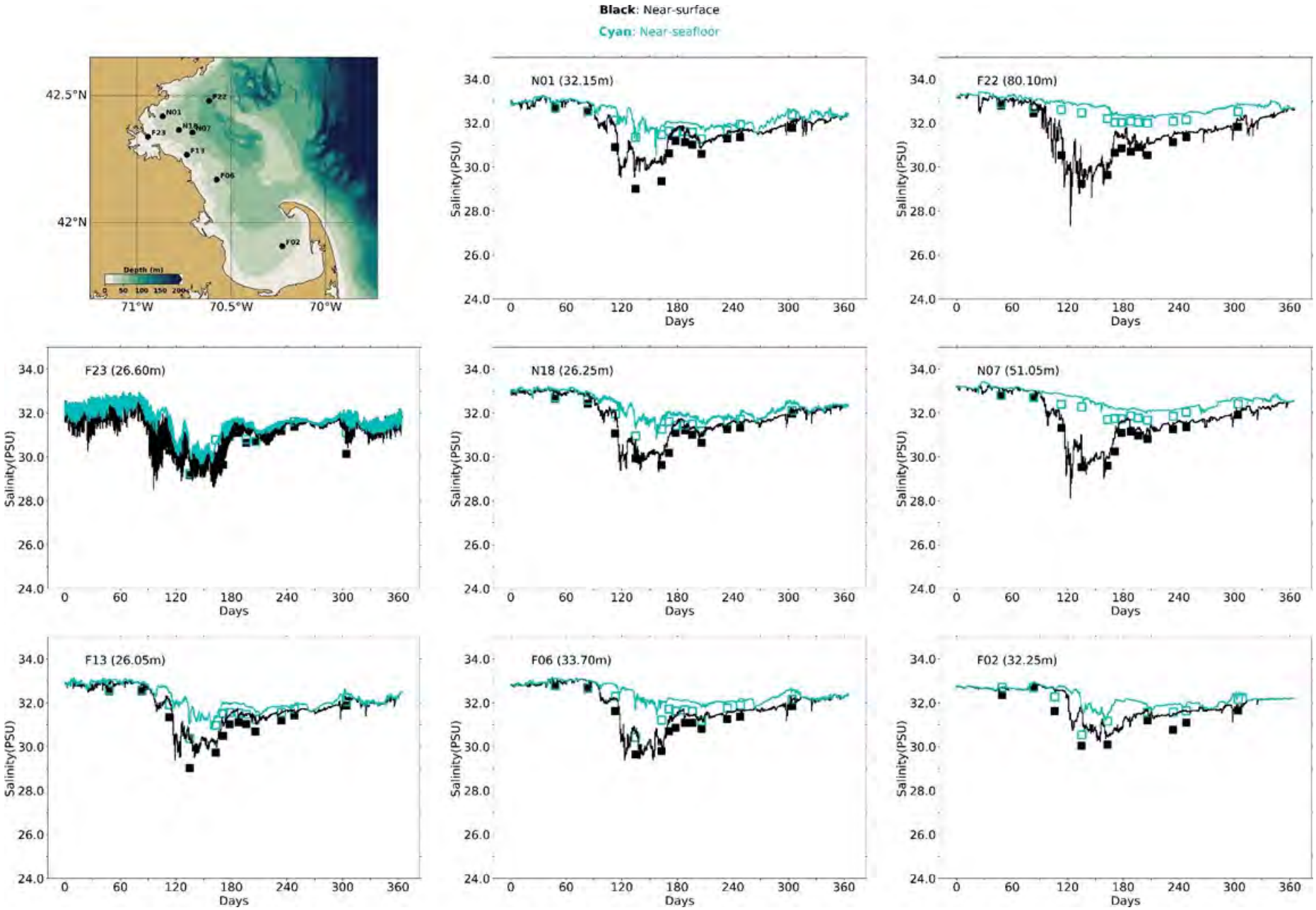

Figure 4-4 Salinity time series, model-observation comparison near surface (black) and seafloor (cyan).
Model results: lines. MWRA vessel-based survey observations: symbols.

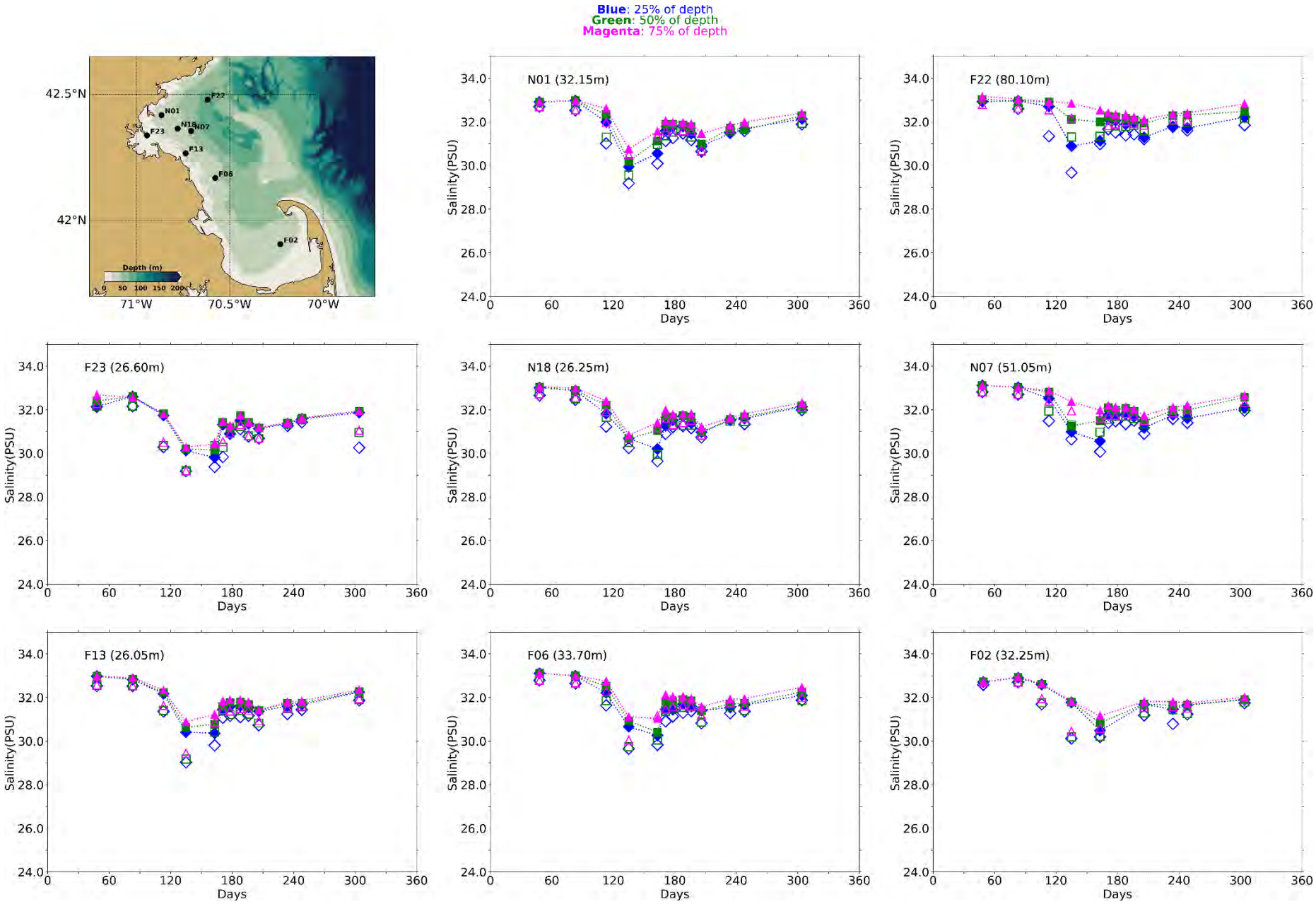

Figure 4-5 Salinity time series, model-observation comparison within water column (between surface and seafloor). Model results: lines with filled symbols. MWRA vessel-based survey observations: open symbols.

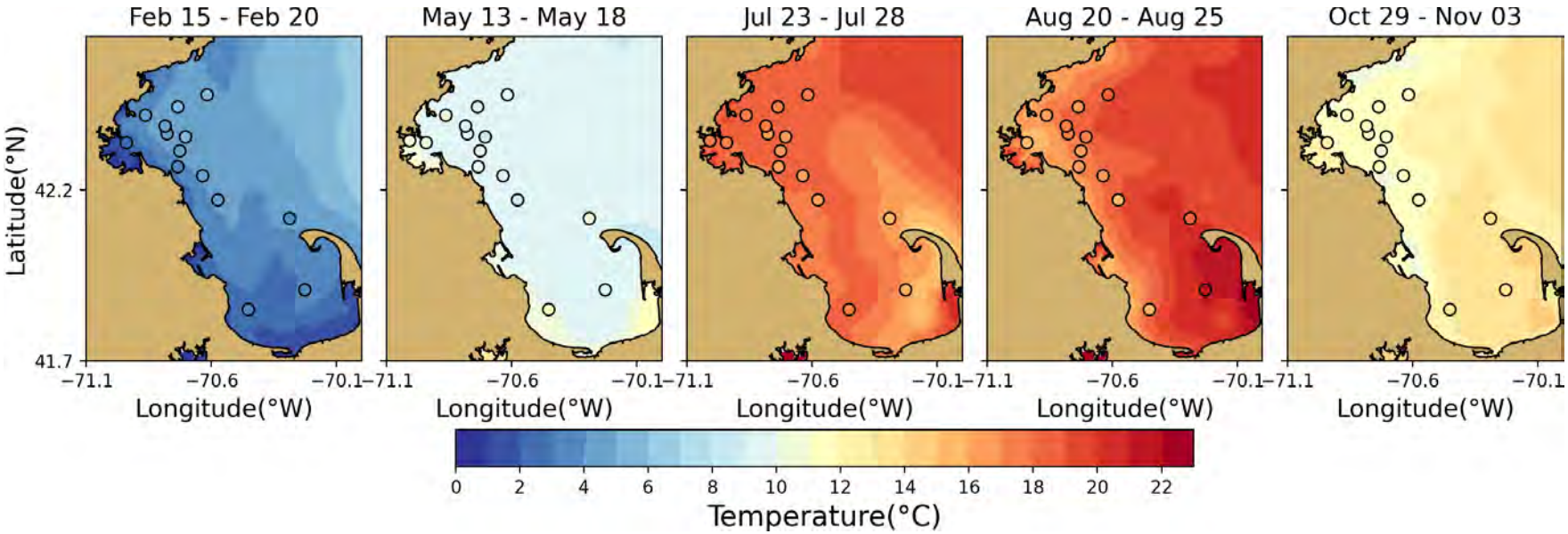

Figure 4-6 Temperature spatial structure, at/near sea surface, model-observation comparison.
Model results: background. MWRA vessel-based survey observations: symbols. Model results are averaged over the 5-day period centered on the measurement date.

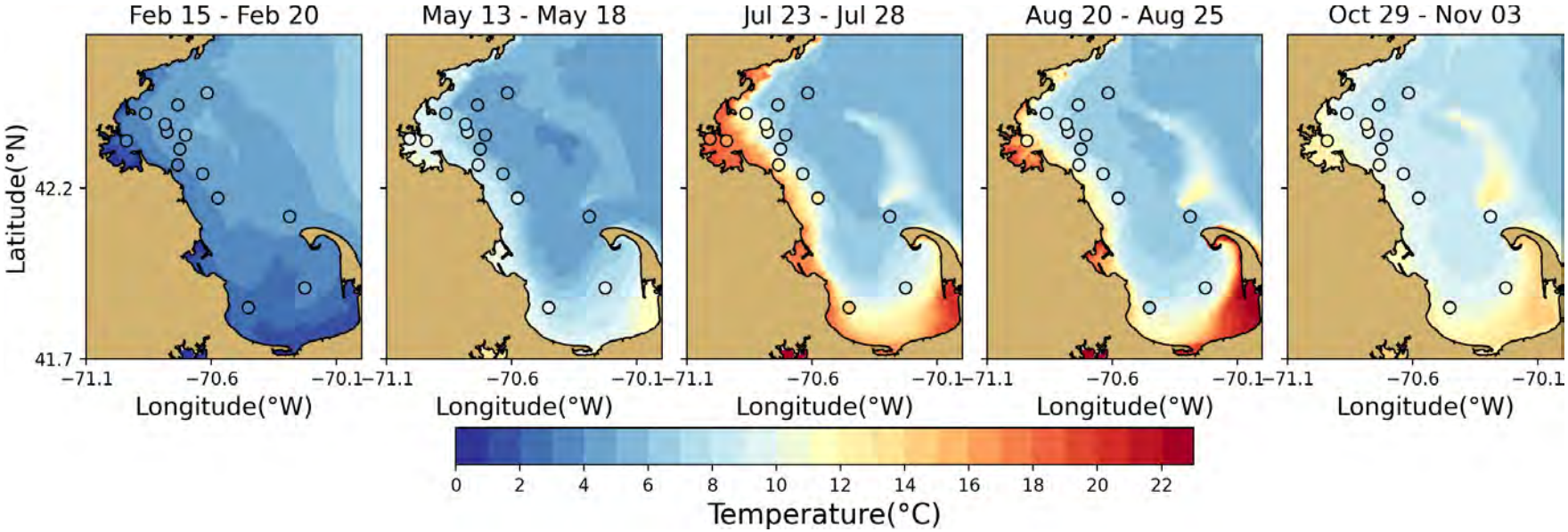

Figure 4-7 Temperature spatial structure, at/near seafloor, model-observation comparison.
Model results: background. MWRA vessel-based survey observations: symbols. Model results are averaged over the 5-day period centered on the measurement date.

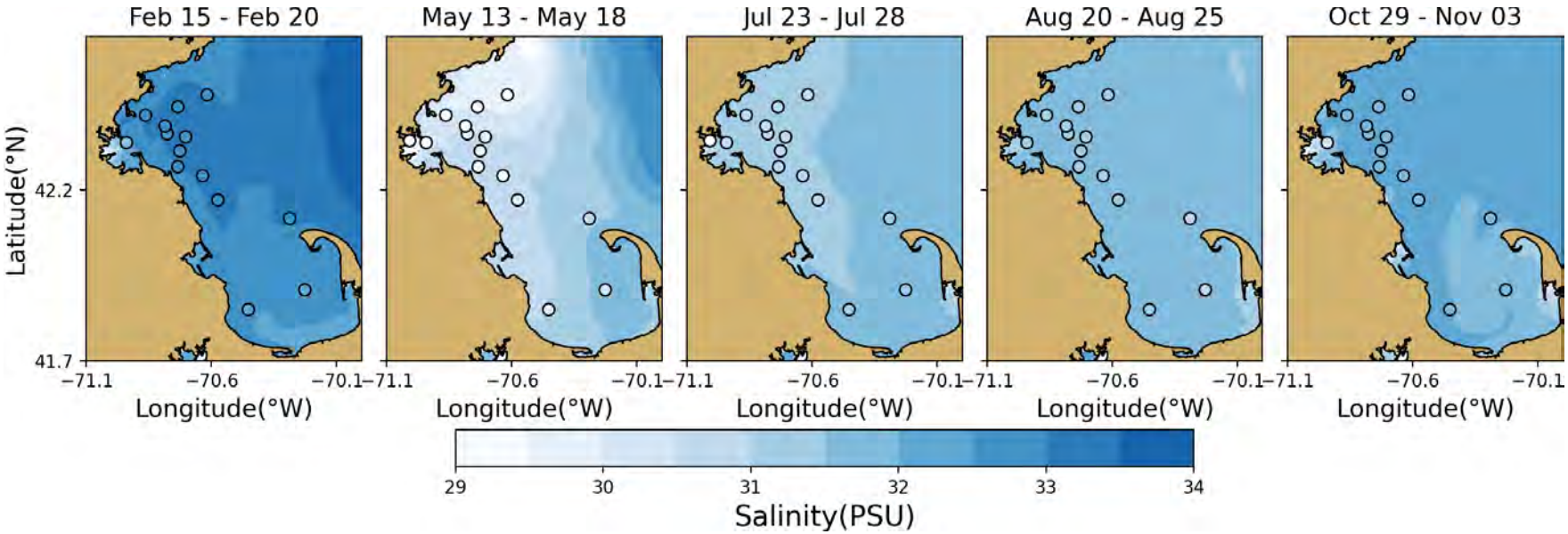

Figure 4-8 Salinity spatial structure, at/near sea surface, model-observation comparison.
Model results: background. MWRA vessel-based survey observations: symbols. Model results are averaged over the 5-day period centered on the measurement date.

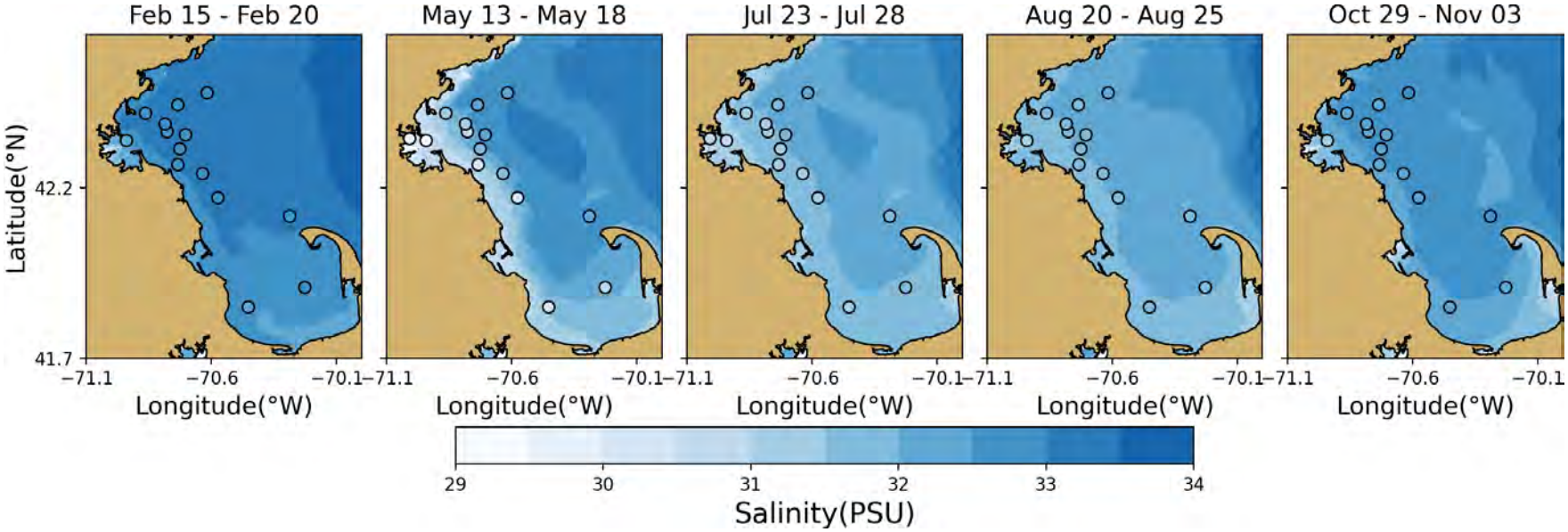

Figure 4-9 Salinity spatial structure, at/near seafloor, model-observation comparison.
Model results: background. MWRA vessel-based survey observations: symbols. Model results are averaged over the 5-day period centered on the measurement date.

4.2.3 Continuous measurements of temperature and salinity

Continuous hourly measurements were available from Mooring A01 at multiple depths. This station is located south of Cape Ann, northeast from MWRA station F22. It is operated by the University of Maine as part of the Northeast Regional Association of Coastal and Ocean Observing Systems (NERACOOS). For a more complete assessment of the model-observation comparison in time, timeseries for this station are presented in Figure 4-10. For three depths (1m, 20m and 50m) the simulated and observed temperature and salinity are given. This is also done for the vertical temperature and salinity difference between 1m and 20 m as well as 1m and 50 m, which can be seen as a measure of stratification. In the measurements some outliers were present, visible as spikes in the salinity and bottom temperature.

The time series compare well, showing that the model captured the strength and timing of the seasonal cycle of temperature and salinity, as well as the stratification of these quantities. Furthermore, event-based changes in stratification on timescales of days to weeks were picked up by the model. The simulated stratification was a bit better represented for temperature than for salinity, where a bias of 0.25-0.5PSU more saline water in the simulation was visible (although crucially, no such bias existed for the salinity stratification, which governs vertical transport).

4.2.4 Continuous measurements of non-tidal currents

For Mooring A01 observed currents were available as well. In Figure 4-11 and Figure 4-12 a model-observations comparison is presented for the first and the second half of the year. In the top frame, time series of wind from the ERA5 reanalysis dataset, used to force the model, is given for context. In the frames below, simulated and observed time series of non-tidal currents are given alternately at four depths (2m, 10m, 22m and 50m). To remove the tidal variability, timeseries have been filtered using a low-pass filter with a 33h filter half amplitude (PL33: Alessi, 1985). The resulting signal then consists mainly of weather-related and seasonal changes. For plotting this has been subsampled to a 6h resolution.

The time series of the filtered wind showed wind in all directions. Winds were generally changing on timescales of multiple days. In general, the wind speeds were lower during the calmer summer months. Winds included a dominantly eastward component year-round, with a dominant southward component in winter and a dominant northward component in summer.

The simulated and observed non-tidal currents showed a similar pattern with a prevailing direction to the south and west. The simulated currents showed less variability in direction. The order of magnitude was similar, but slightly smaller in the top of the water column (2m and 10m deep). At 22m deep the simulated currents were slightly larger than the observations in July and in October. Individual storm events were mostly picked up by the model with a similar timing, direction and magnitude as observed. An exception was a large surface current in the first days of February, which was not present in the simulation result. This model-observation comparison at a specific location is a challenging test of the hydrodynamic simulation performance. The agreement between the two was sufficient to conclude that the representation of processes in the hydrodynamic model was adequate to support water quality modeling.

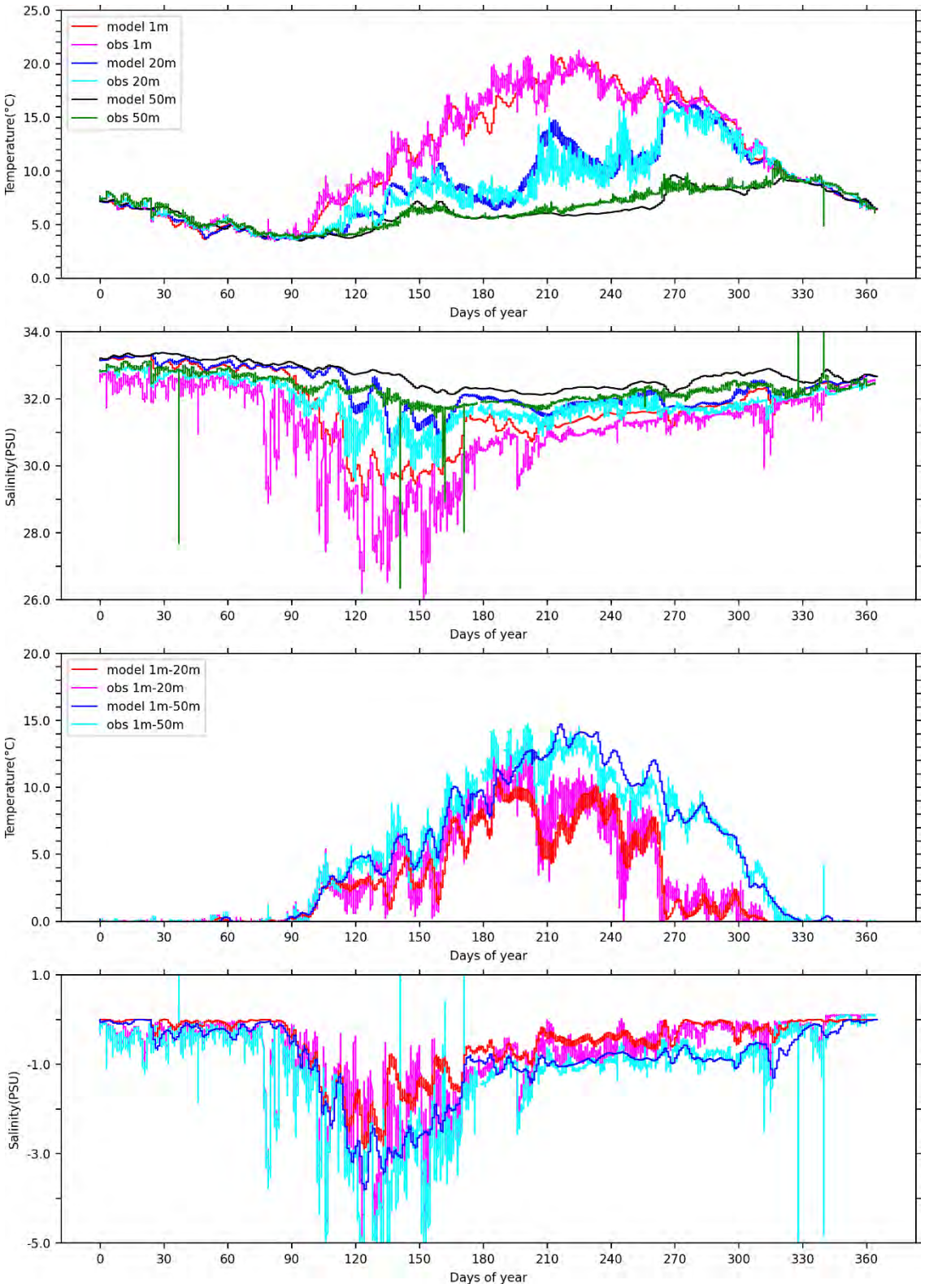

Figure 4-10 Time series Mooring A01 temperature/salinity model-observation comparison (3-day means), three depths and two stratification levels.

Temperature (upper frames), salinity (lower frames).

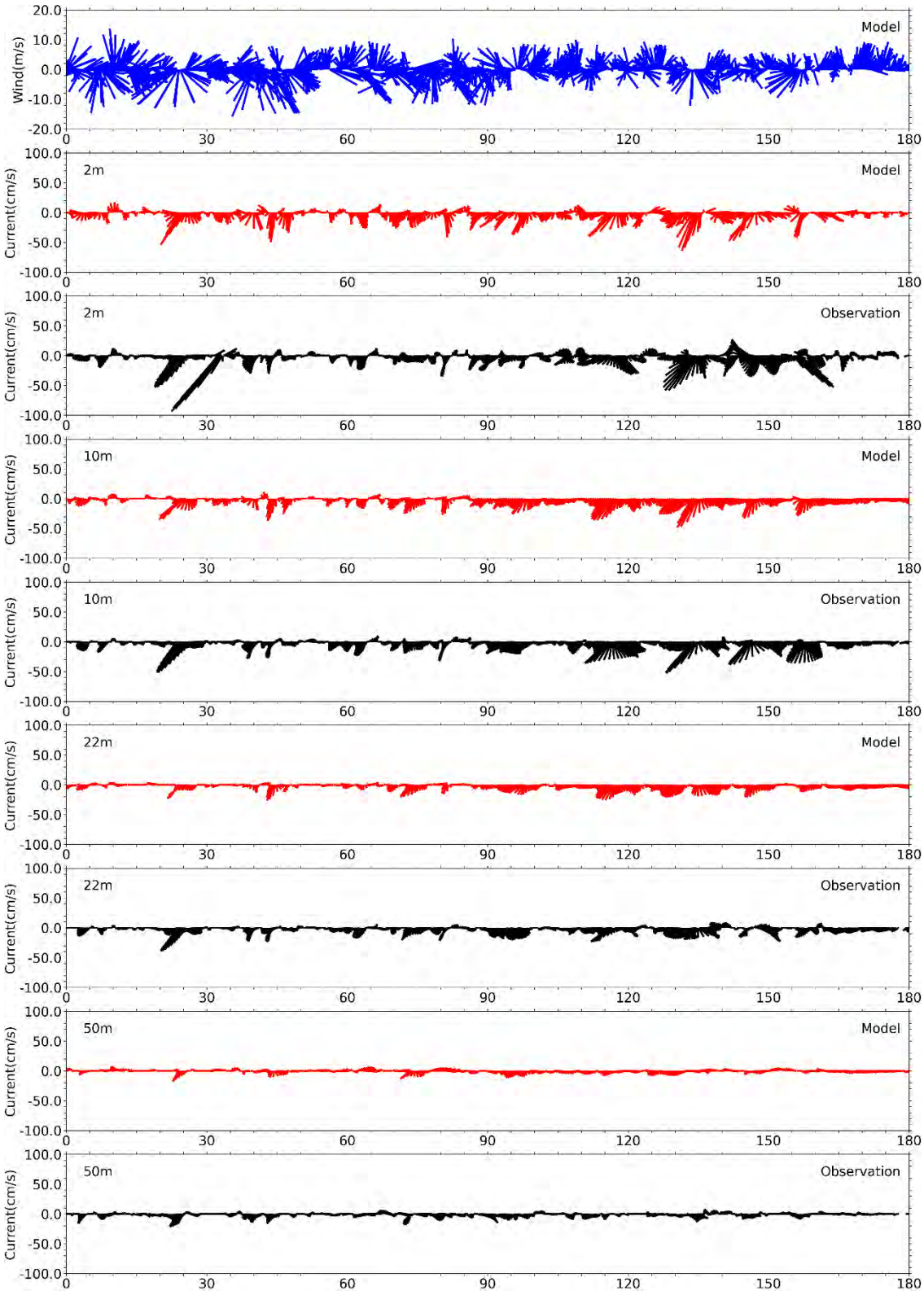

Figure 4-11 Currents time series model-observation comparison, Jan – Jun.

Sticks point in the direction of flow, away from zero line; north/eastward flow up/rightward.

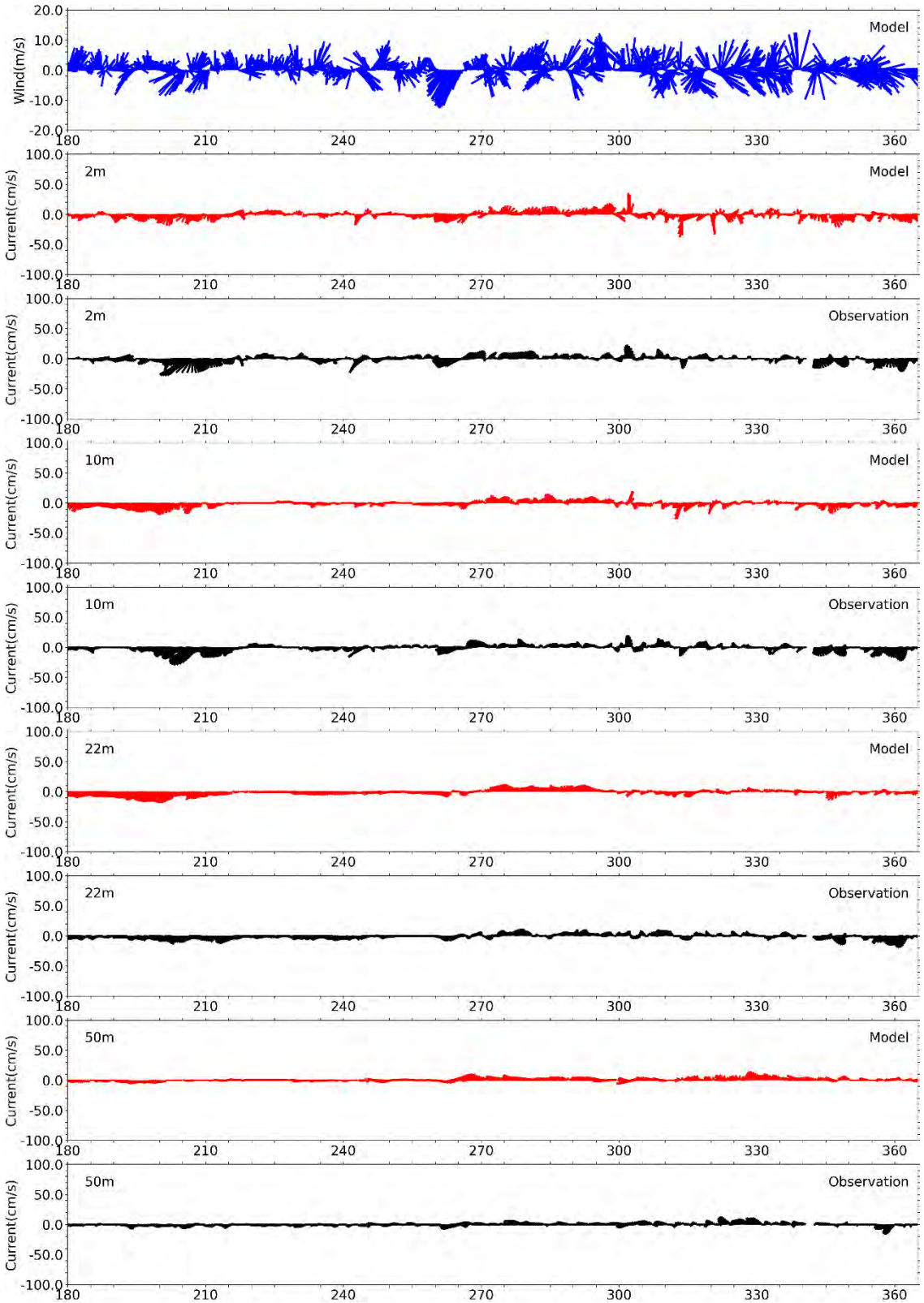

Figure 4-12 Currents time series model-observation comparison, Jul – Dec.

Sticks point in the direction of flow, away from zero line; north/eastward flow up/rightward.

4.3 Model monthly-mean circulation

Figure 4-13 and Figure 4-14 present the simulated monthly-mean currents at the surface and at a depth of 15m. Flow was largely consistent with the general circulation pattern recognized to hold (Figure 1-1).

This schematic pattern was most apparent in spring and early summer. Later in the year, the WMCC was located further offshore with smaller magnitudes, and flow was sometimes northeastward in Massachusetts Bay. Surface currents were largest off Cape Ann and Cape Cod with largest magnitudes in March to June, reaching up to 0.35-0.45m/s in May. In this month, the residual currents within Massachusetts Bay were the strongest as well, with magnitudes up to 0.20m/s near North Passage and South Passage. In October surface currents were directed to the north with a magnitude up to 0.15m/s. During the rest of the year surface currents were calmer and did not exceed 0.10m/s.

The circulation pattern at 15m deep (Figure 4-14) showed less influence of the surface forcing. In general, the expected general circulation pattern was more distinguishable. Current magnitudes were lower with maxima in May of up to 0.30m/s in North Passage and of up to 0.10m/s in the central Massachusetts Bay. In Cape Cod Bay residual current magnitudes at this level were weaker, due to its limited depth and sheltered geometry.

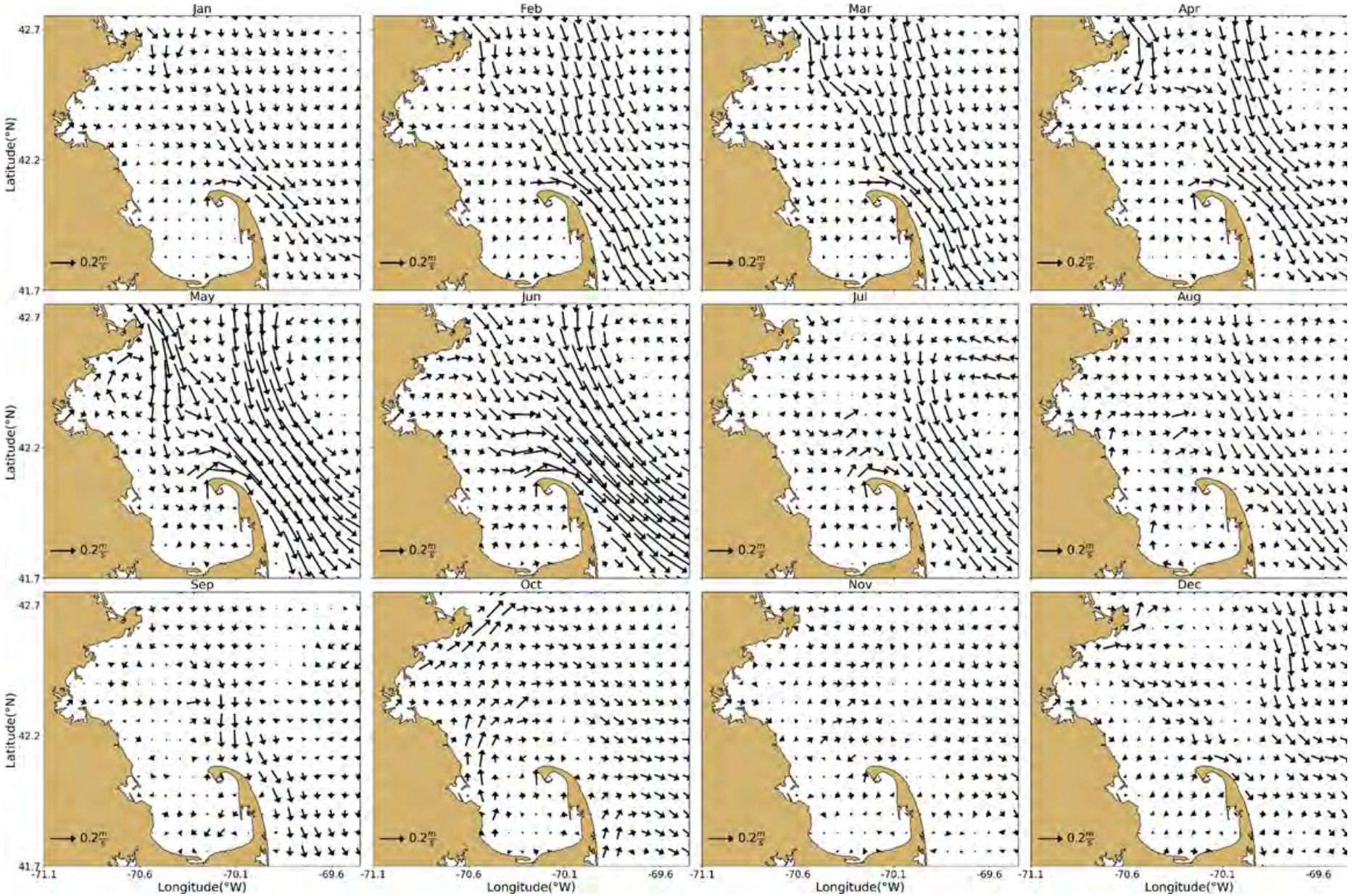

Figure 4-13 Model currents, monthly-mean spatial structure, at sea surface.

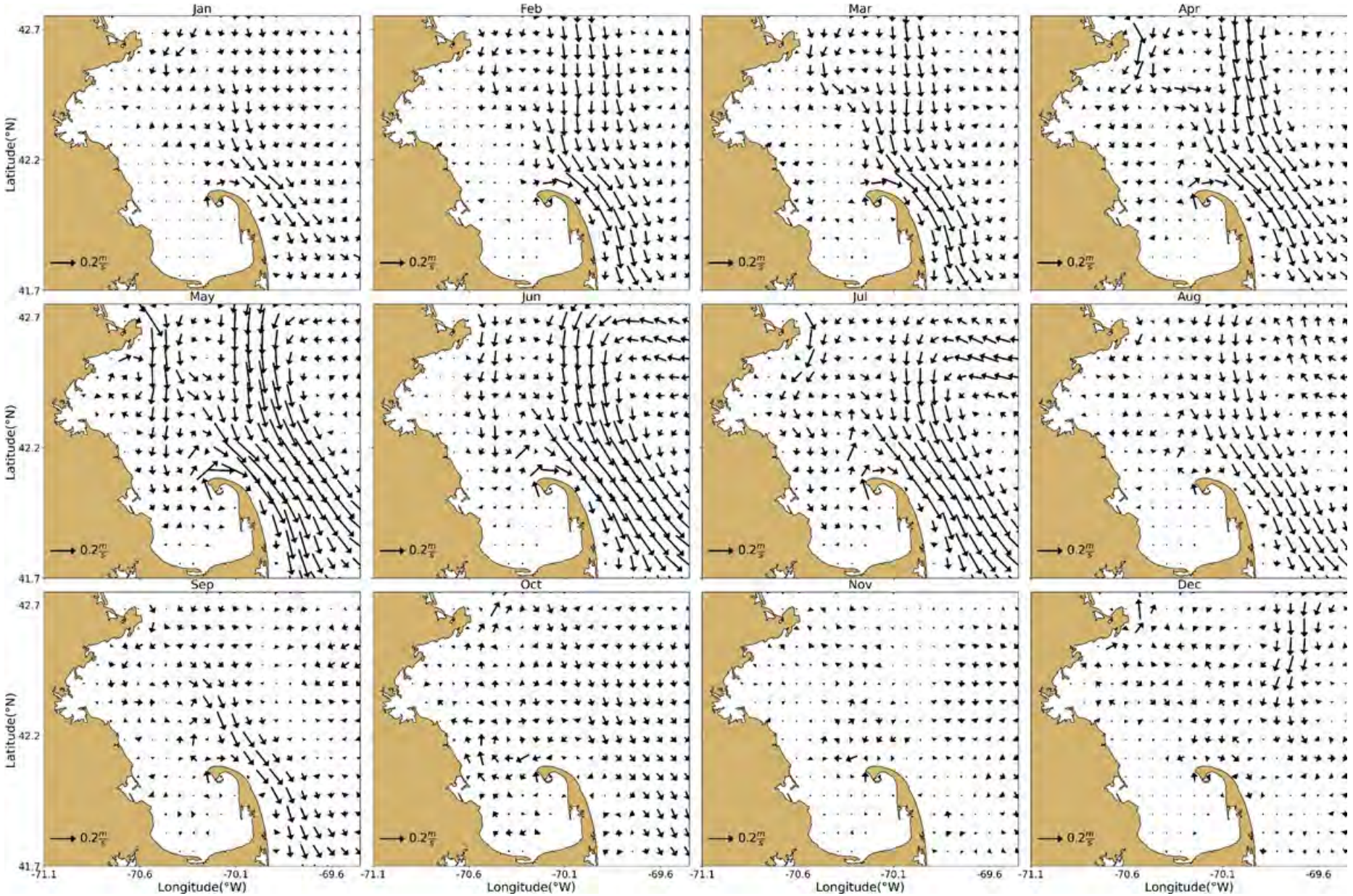

Figure 4-14 Model currents, monthly-mean spatial structure, 15 m deep.

5 Water Quality Model

In this section the performance of the water quality model is discussed, and its results are compared to measurements.

5.1 Verification of model performance

To demonstrate that the model performance during 2017 was comparable to the period 2012-2016, skill metrics were calculated and plotted on Taylor diagrams as in Section 4. Station N21 directly on top of the outfall was excluded, as a comparison to field data is of limited value for this station (reference is made to Deltares (2021) for a discussion). Information on how to interpret Taylor diagrams can be found in section 4.1 (box “How to read a Taylor diagram”).

Taylor diagrams are plotted for light extinction coefficient and DIN in Figure 5-1, and for Chl and DO in Figure 5-2. These parameters were selected because they are key drivers of ecosystem functioning. Statistics for the complete period 2012-2016 are plotted on the left side and statistics for 2017 on the right side. For reference, Appendix A provides similar diagrams for the individual years 2012 to 2016. The plots show statistics for three clusters of monitoring stations: Northern Bay stations (F22, N01, N04, N07, F10, N18, F15, F13 and F23), Southern Bay and Cape Cod stations (F06, F29, F01 and F02) and harbor stations (024, 140, 142, 139 and 124).

As described in Section 2.1, for the 2017 BEM run, the representation of effluent nutrient concentrations has been corrected compared to the runs for 2012-2016 (Deltares, 2021). An analysis of the effect of this correction upon the results in 2016 has shown that the effects of correcting the loads effects are minor and localized in the direct vicinity of the outfall (Section 2.1). The effect of the correction of the loads upon the Taylor diagrams and statistics for the period 2012-2016 used here is negligible.

Extinction skill metrics (Figure 5-1) lay in the same range as those estimated for 2012-2016. Compared to 2012-2016, the correlation between model results and observations was slightly better.

Skill metrics for DIN (Figure 5-1) were overall comparable to previous years but tended to show more station-to-station variability. Correlation between model and observations was relatively high in the surface layer stations, and relatively low near the seafloor and in the harbor area. On average, the variability of the field data was well represented by the model compared to previous years.

Skill metrics for chlorophyll a (Figure 5-2) were partly comparable to previous years: modeled and measured chlorophyll a concentrations showed little correlation, and correlation coefficients differed from one station to another. The number of stations with correlation >0.5 was higher than for previous years (Appendix A). Contrary to 2012-2016, Chlorophyll a variability was overall underestimated by the model (Std*<1), both near the surface and the seafloor. This was diagnosed to be a co-incidental consequence of the low sampling frequency relative to the high temporal variability of chlorophyll a. See the end of this section for a further discussion.

DO skill metrics were similar to those from 2012-2016 (Figure 5-2). Correlation between modeled and observed concentrations near the seafloor was excellent and the variability of DO was very well reproduced.

Overall, the figures presented here serve to verify that the performance of the water quality model in the simulations of 2017 does not deviate substantially from its performance during the prior five-year period.

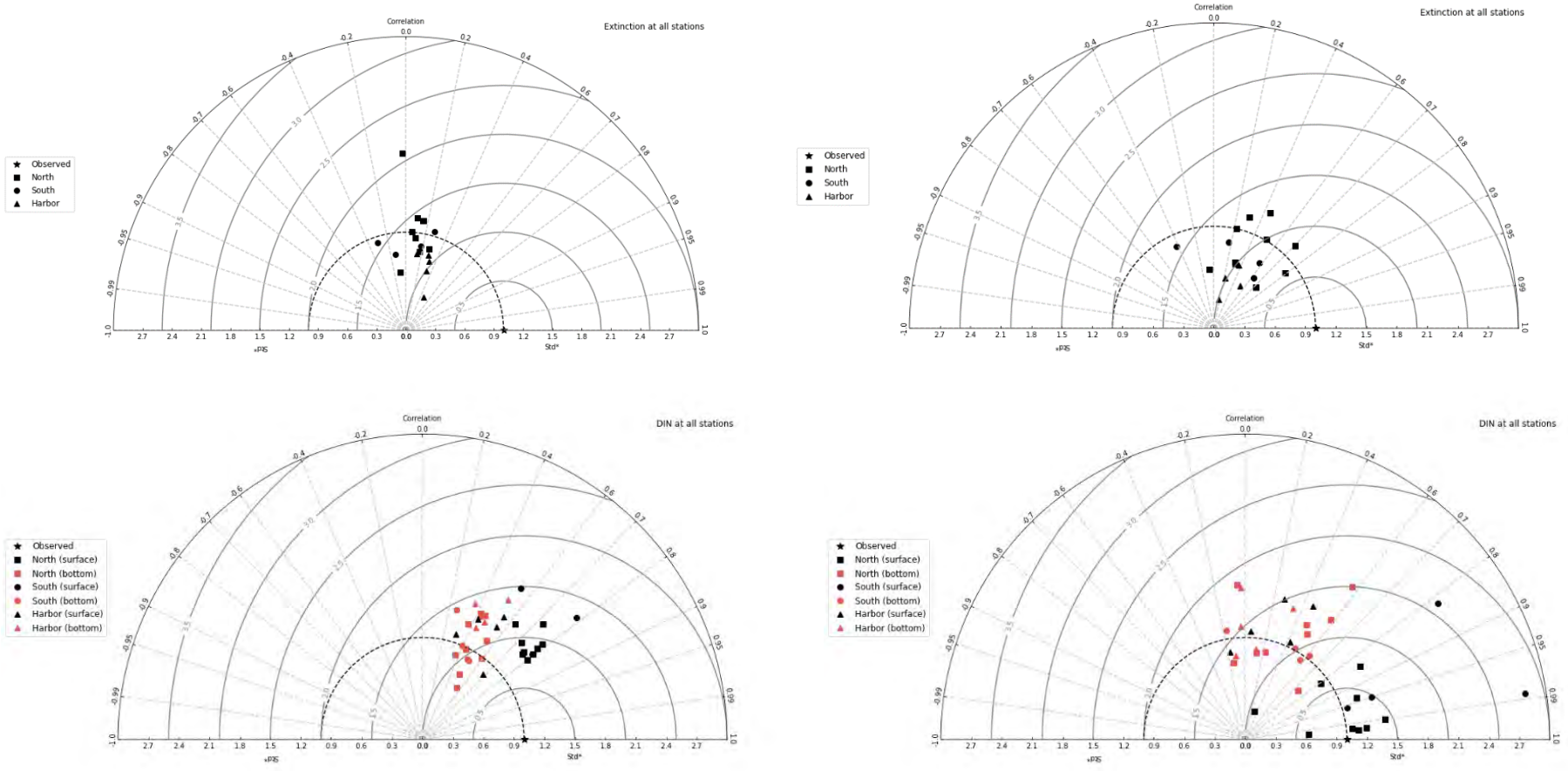

Figure 5-1: Taylor diagrams for MWRA vessel-based survey observations. Top panels show the parameter Extinction and bottom panels Dissolved Inorganic Nitrogen. Left panels show results for the simulation period 2012-2016 and right panels for the year 2017.

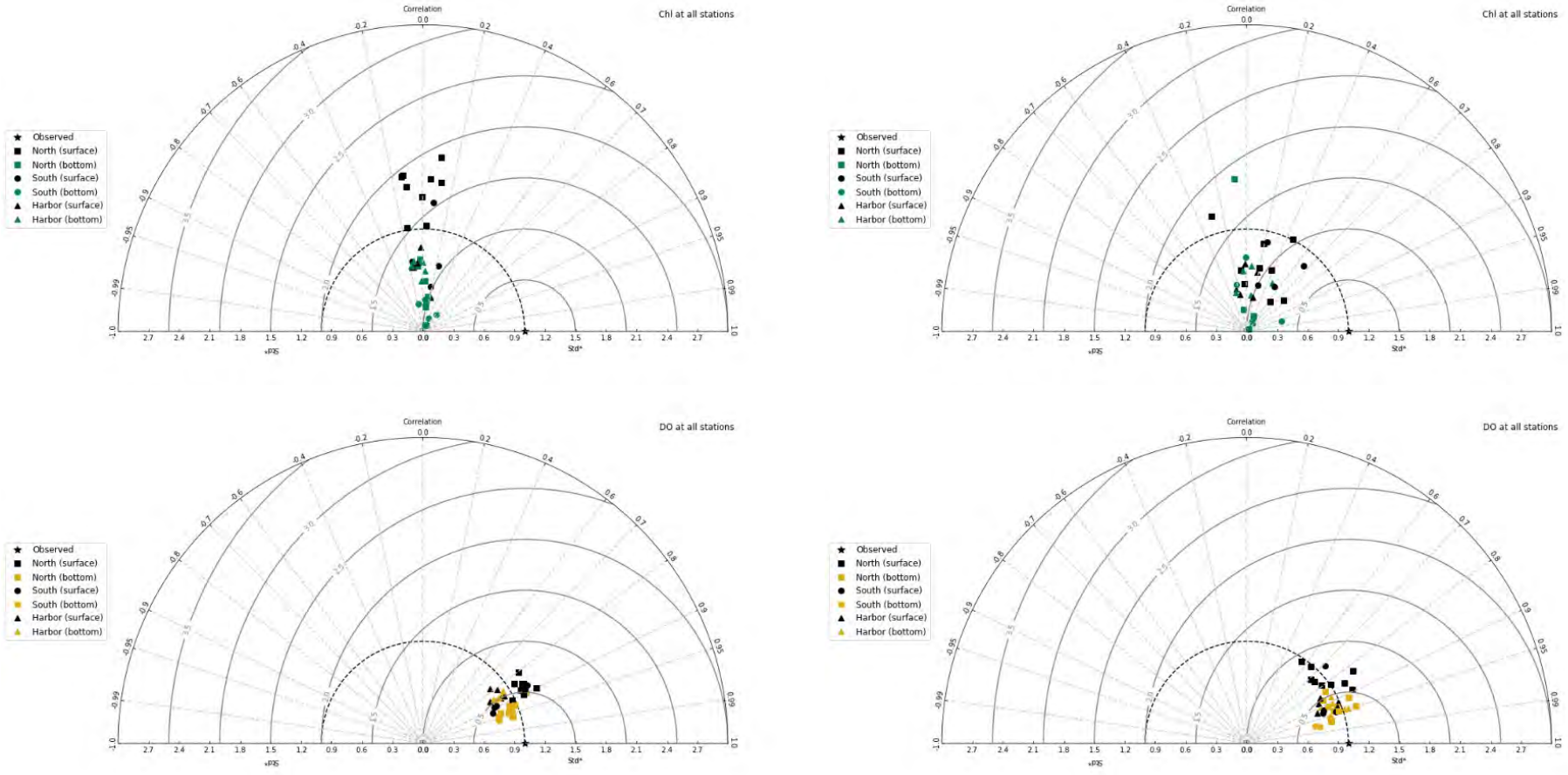

Figure 5-2: Taylor diagrams forfor MWRA vessel-based survey observations. Top panels show the parameter Chlorophyll-a and bottom panels Dissolved Oxygen. Left panels show results for the simulation period 2012-2016 and right panels for the year 2017.

The apparent underestimation of chlorophyll a variability in 2017 was further investigated (see Table 5-1). The 2017 simulation results do not appear to be less variable than those of previous years (yearly standard deviation in the range of those calculate for 2012-2016). Moreover, the simulated time-series for 2017 does not consistently show lower standard deviations than the observations as the Taylor diagram suggests. The underestimation of variability seems to result from the low sampling frequency. Due to the highly transient character of algae blooms, this low frequency makes it difficult to ensure that all peaks are captured. Moreover, if the sampling captures one of these peaks, while the simulated peak occurs too early or late in the model, the value of Std* is pulled down and simulated variability found underestimated. This seems to be what happened for 2017, where observed and simulated chlorophyll peaks did not exactly coincide, while the overall behavior of observed and simulated time-series did not greatly differ from previous years (see example station N18, Figure 5-3).

Table 5-1: Summary statistics of near-surface chlorophyll a concentrations for 2017 and 2012-2016.

	2017					**2012-2016**			
Station	N_{obs}	Std_{obs} (ug/L)	m_{obs} (ug/L)	Std_{sim} (ug/L)	m_{sim} (ug/L)	Std_{sim} range (ug/L)	Std_{sim} average (ug/L)	m_{sim} range (ug/L)	m_{sim} average (ug/L)
N01	9	2.65	4.39	2.01	2.20	1.52-2.22	1.84	1.41-2.11	1.72
F22	13	2.06	2.59	1.44	1.26	1.31-1.65	1.49	1.02-1.24	1.16
F23	9	1.95	3.89	1.68	3.18	1.47-2.43	1.85	2.12-3.35	2.67
N18	13	1.34	2.55	1.72	1.87	1.40-1.88	1.63	1.11-1.84	1.46
N07	8	1.25	2.38	1.52	1.29	1.34-1.77	1.51	0.97-1.33	1.15
F13	13	1.79	3.28	1.69	2.06	1.40-1.93	1.64	1.33-2.11	1.67
F06	9	1.04	2.79	1.34	1.19	1.19-1.78	1.42	1.00-1.30	1.14
F02	9	2.33	2.73	0.78	0.76	0.71-1.30	1.02	0.70-0.84	0.76

Nobs=number of observations, StdX=time-series standard deviation, mX=time-series mean (X=obs or sim, e.g. observations or simulation). Simulation statistics are calculated on full daily outputs. Range and average values of yearly statistics are provided for the period 2012-2016.

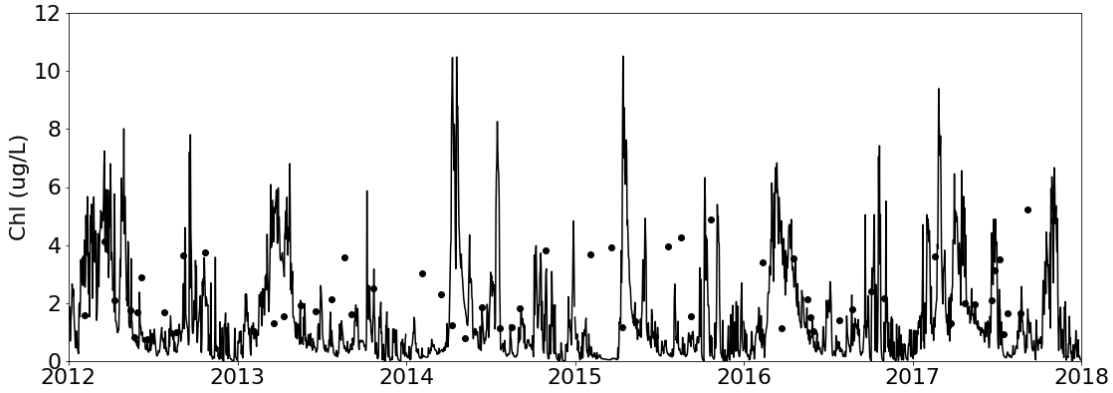

Figure 5-3: Multi-annual simulated (line) and observed (dots) near-surface chlorophyll a concentrations at station N18

5.2 Model-observation comparisons

In this section model-observation comparisons in the same format as for the hydrodynamic model (Section 4) are provided. For time series plots, a 3-day moving average is applied to the model outputs to smoothen high-frequency variability that was not captured by the field measurements.

To assess the simulation spatially, vertical transects have been plotted along North-South (N-S) and West-East (W-E) transects (Figure 2-4). Model results in these figures are 5-day averages centered around the sampling date sampling date indicated in each plot.

5.2.1 Light extinction

Extinction measurements for the year 2017 (Figure 5-4) ranged from 0.1 to 0.4 at all stations, except at F23, near the harbor, where it was slightly higher and more variable. This was similar to previous years for which higher and more variable extinction was observed at harbor stations (e.g. Zhao et al., 2017). At stations F23, F06 and F13, measured extinction had a slight peak in spring, likely due to phytoplankton.

The model reproduced extinction range and variability well at most plotted stations. Extinction was however underestimated at station F23, especially at the sampling dates in winter and spring. The high observed concentrations at this station could be due to storm resuspension of sediment inside the harbor. The small peak in extinction during the spring bloom at stations F23, F06 and F13 was furthermore not captured by the model.

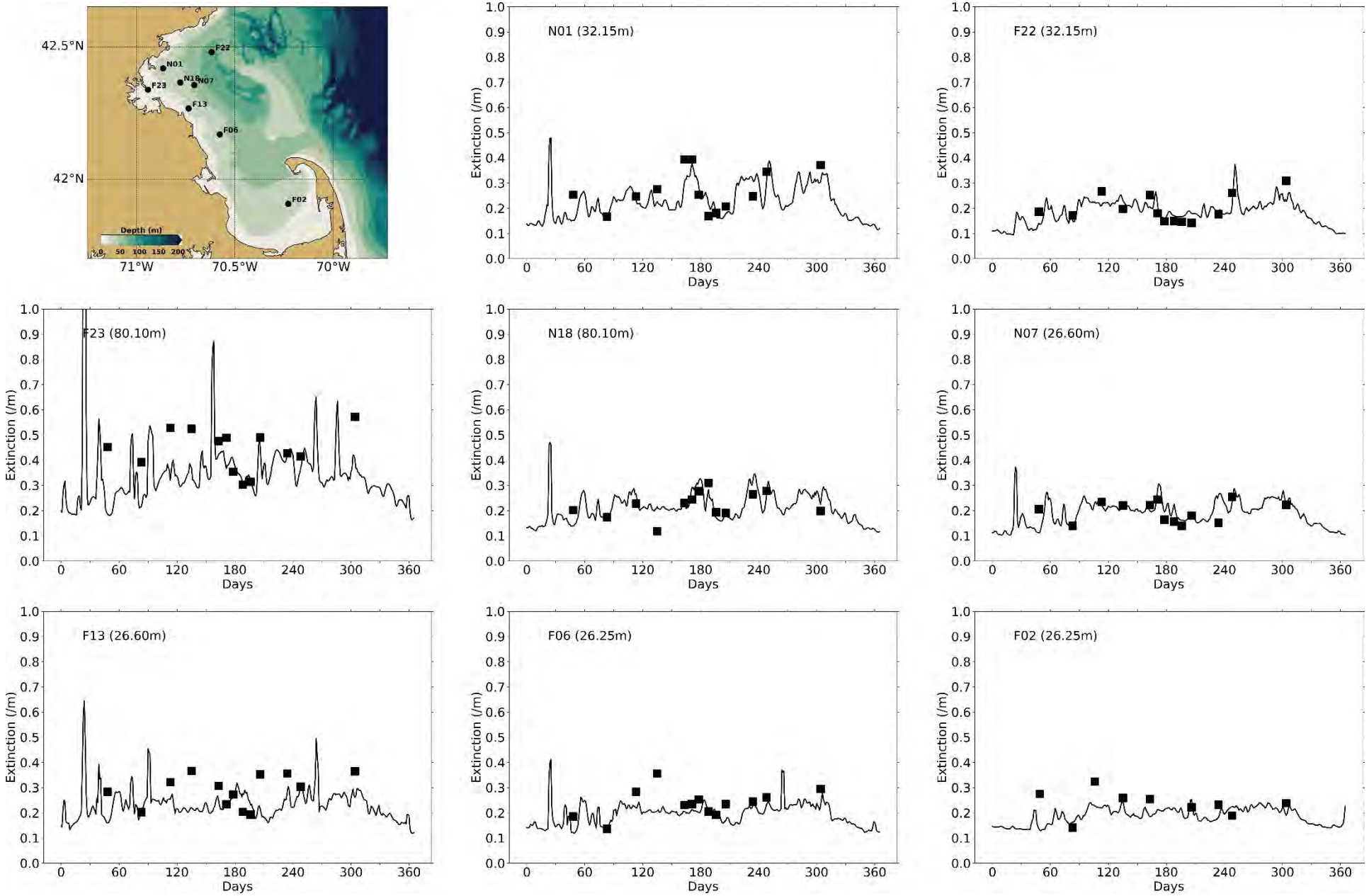

Figure 5-4: Extinction time series, model-observation comparison. Model: lines. MWRA vessel-based survey observations: symbols.

5.2.2 Dissolved inorganic nitrogen

Seasonal variations of surface and bottom DIN concentrations in 2017 were similar to those observed and simulated for previous years (Figure 5-5). Surface and bottom were comparable in winter, when the water column was well mixed. Surface DIN concentrations declined in April and were depleted throughout the rest of spring and summer, before increasing again in autumn. Bottom concentrations declined to a much lesser degree in spring and summer. The model generally reproduced these observed seasonal variations and vertical differences, including the timing of the decline in observed concentrations in spring. DIN was however slightly overestimated at stations F06, N01 and N18 at the end of the summer.

Observed variations at intermediate depths in the water column were also generally reproduced by the model (Figure 5-6). At stations N01 and N18, where the model overestimated bottom DIN at the end of summer, concentrations were overestimated at intermediate depths as well.

According to the model results, the signature of the outfall in terms of DIN concentrations was visible all year round, leading to increased concentrations up to a distance of ~10 km or more (Figure 5-7). The extra DIN load remained in the lower layers of the water column during the period of stratification (April-October). During the other months, the effluent led to an increase in DIN concentrations throughout the water column on top of the outfall (station N21). This was similar to what was simulated for previous years. While in the model for periods of stratification, the highest concentrations at N21 (outfall) were always simulated at the bottom of the water column, these were sometimes measured higher up in the water column (e.g., April 24th and June 13th).

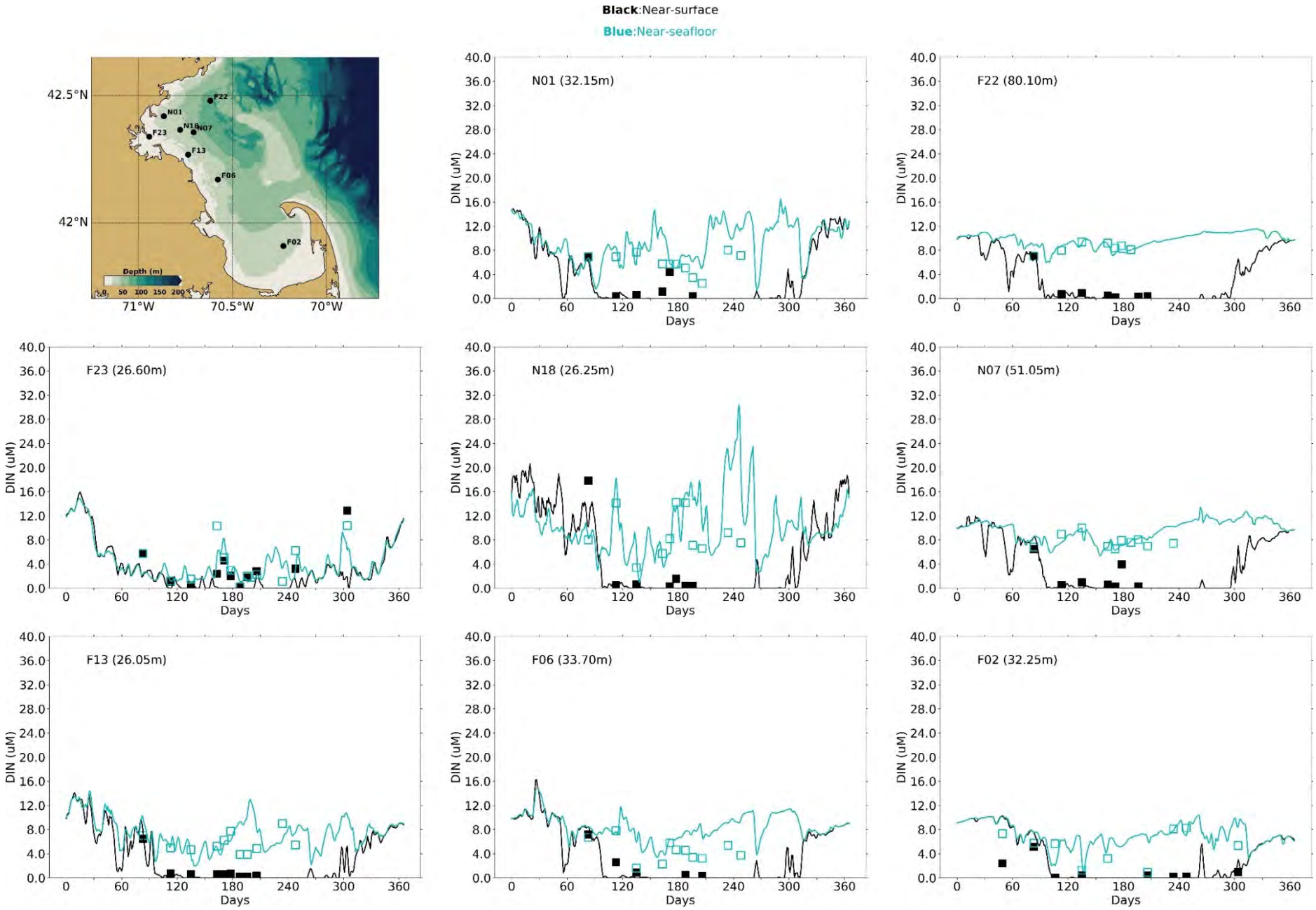

Figure 5-5: Dissolved Inorganic Nitrogen time series, model-observation comparison near surface (black) and seafloor (cyan). Model results: lines. MWRA vessel-based survey observations: symbols.

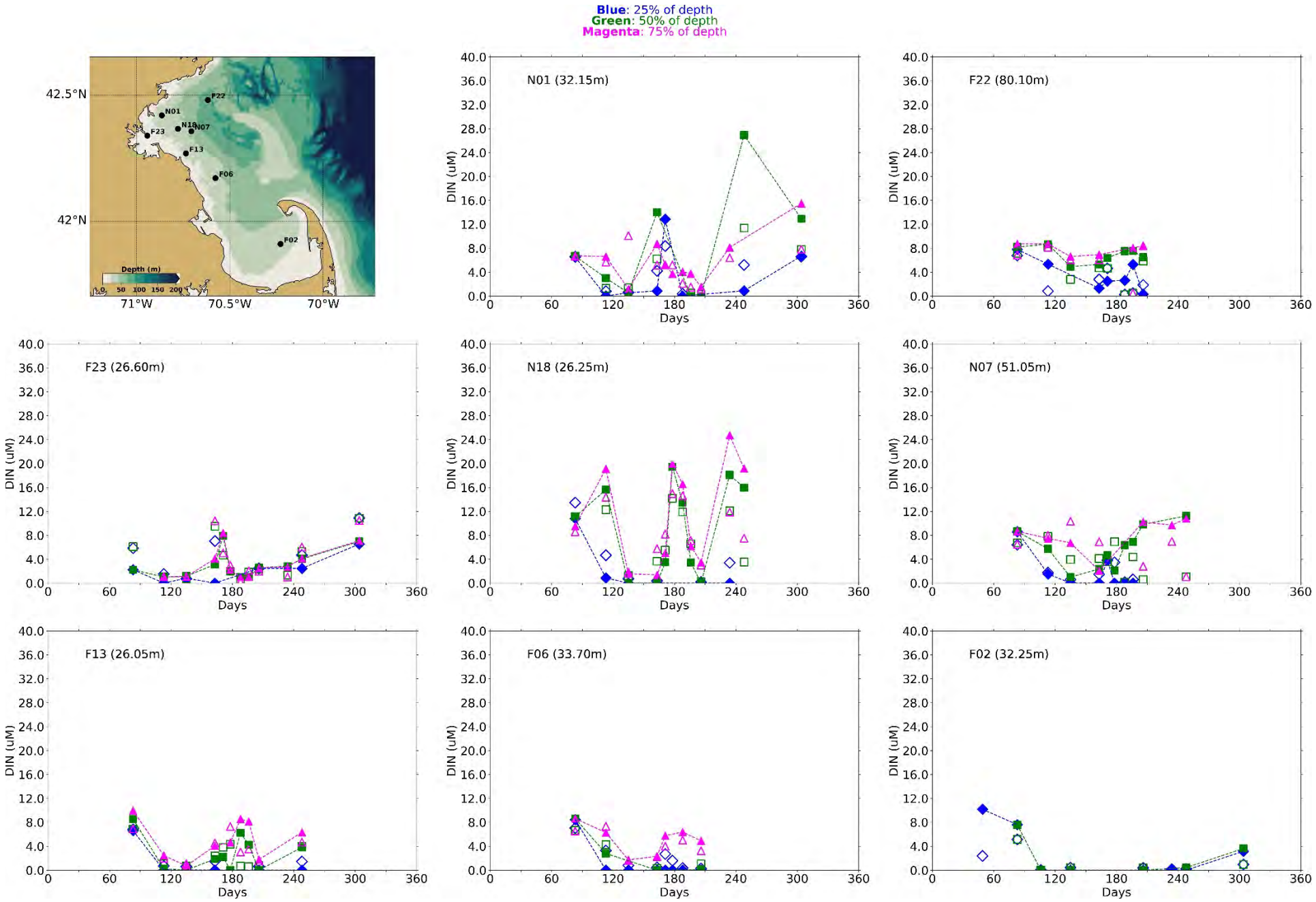

Figure 5-6: Dissolved Inorganic Nitrogen time series, model-observation comparison within water column (between surface and seafloor). Model results: lines and full symbols. MWRA vessel-based survey observations: open symbols.

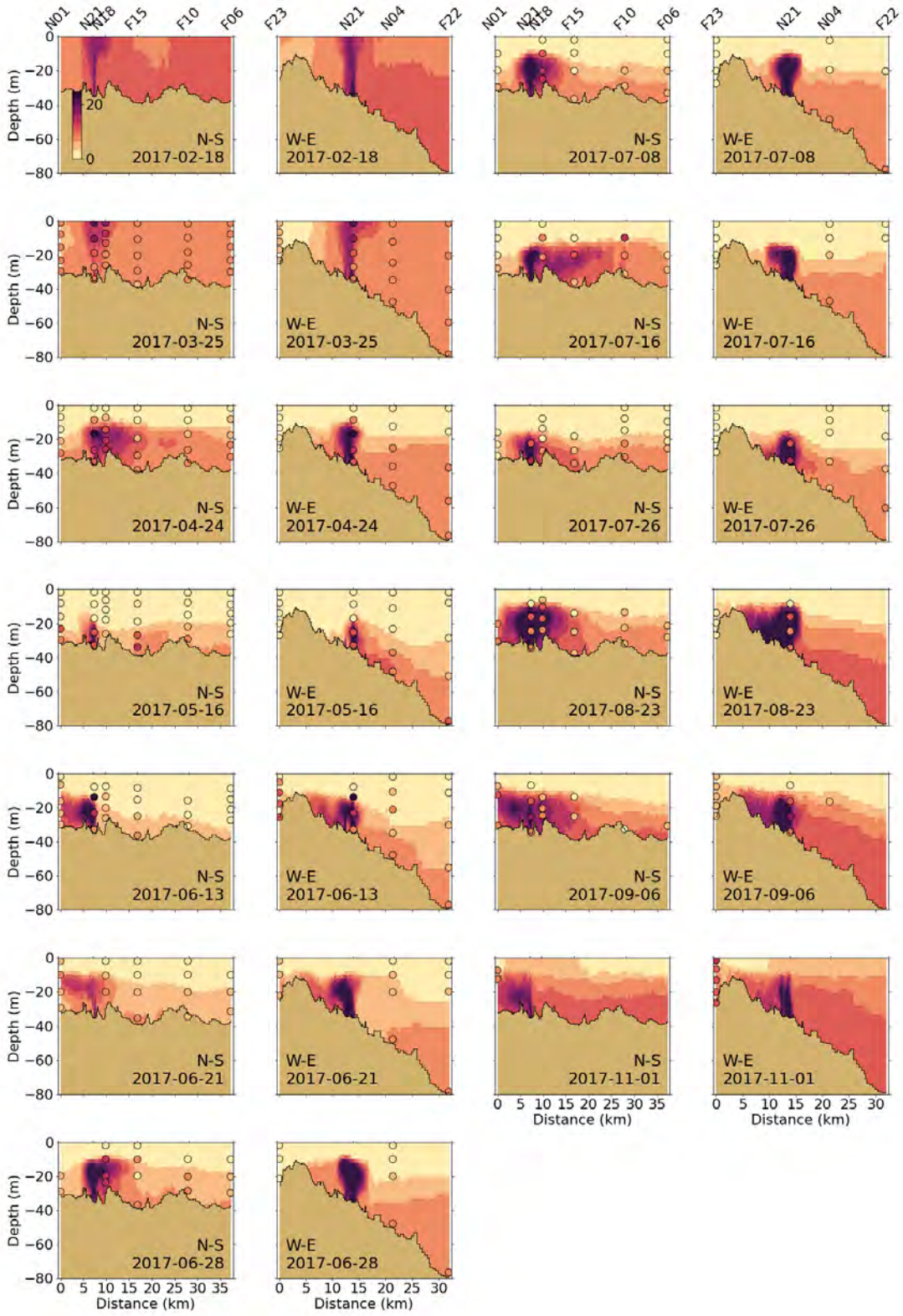

Figure 5-7: Dissolved Inorganic Nitrogen (µM) for 2017 along North-South (N-S) and West-East (W-E) transects (Figure 2-4). MWRA measurements are plotted with round symbols. Model results are 5-day averages around sampling date.

5.2.3 Chlorophyll a

Seasonal variations of chlorophyll a observations in 2017 were not very marked (Figure 5-8). No clear bloom was visible at the sampling frequency of the MWRA observations. While chlorophyll a seemed to peak in summer closer to the Massachusetts Bay coast (F23, N01 and F13), highest concentrations were observed in fall closer to the outfall (N07 and N18) and in spring in Cape Cod Bay (F02). While bottom chlorophyll a concentrations were very small at the deeper F22 station, these were in the same range as surface concentrations at stations F23, N18 and F02.

The model simulated two modest chlorophyll a blooms, in spring and at the end of fall (Figure 5-8). It simulated small chlorophyll a summer peaks at stations F23, N01 and F13. As in the simulations for previous years, near surface simulated concentrations were in the same range as observations, while the temporal variability was not always reproduced. This was to some extent related to the relatively low sampling frequency and the high temporal variability. As in the simulations for previous years, simulated bottom chlorophyll a was underestimated at many stations. Chlorophyll a concentrations in summer and in the beginning of fall were underestimated at the observation stations at intermediate depths as well (Figure 5-8 and Figure 5-9).

Simulated chlorophyll a concentrations decreased eastward from the coast (Figure 5-10). In the model, the highest concentrations occurred from February to April. Since the water column was relatively well mixed, these higher concentrations also occurred deeper in the water column. During the more stratified months, simulated bottom chlorophyll a remained low and highest values occurred in the subsurface. The observations tended to show that chlorophyll a concentrations actually declined in March (both along the North-South and West-East transects) before increasing again in April. Highest observed concentrations occurred in September and were observed from the surface to depths of ~30 m, which was not captured by the model.

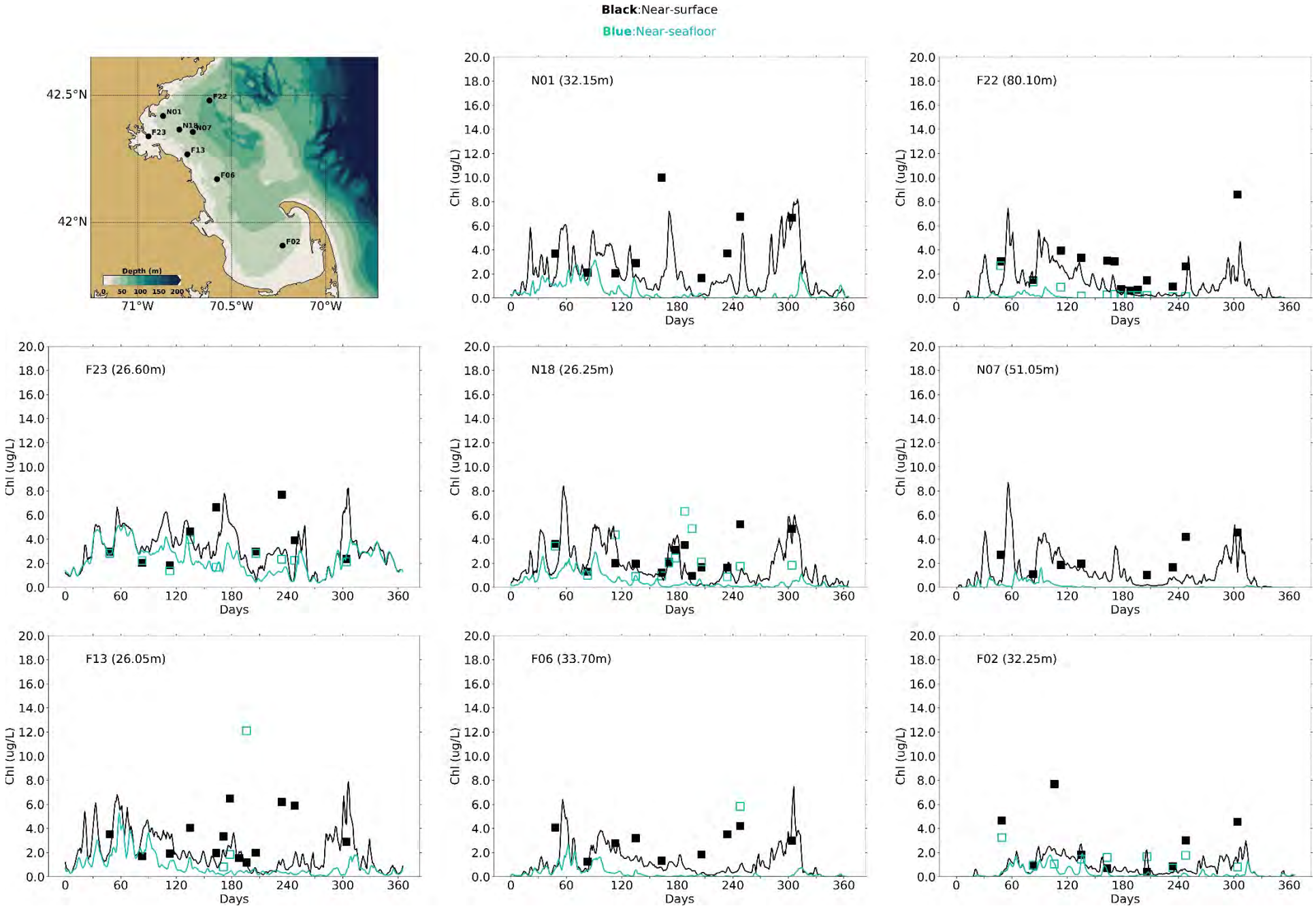

Figure 5-8: Chlorophyll a time series, model-observation comparison near surface and seafloor. Model results: lines. MWRA vessel-based survey observations: symbols.

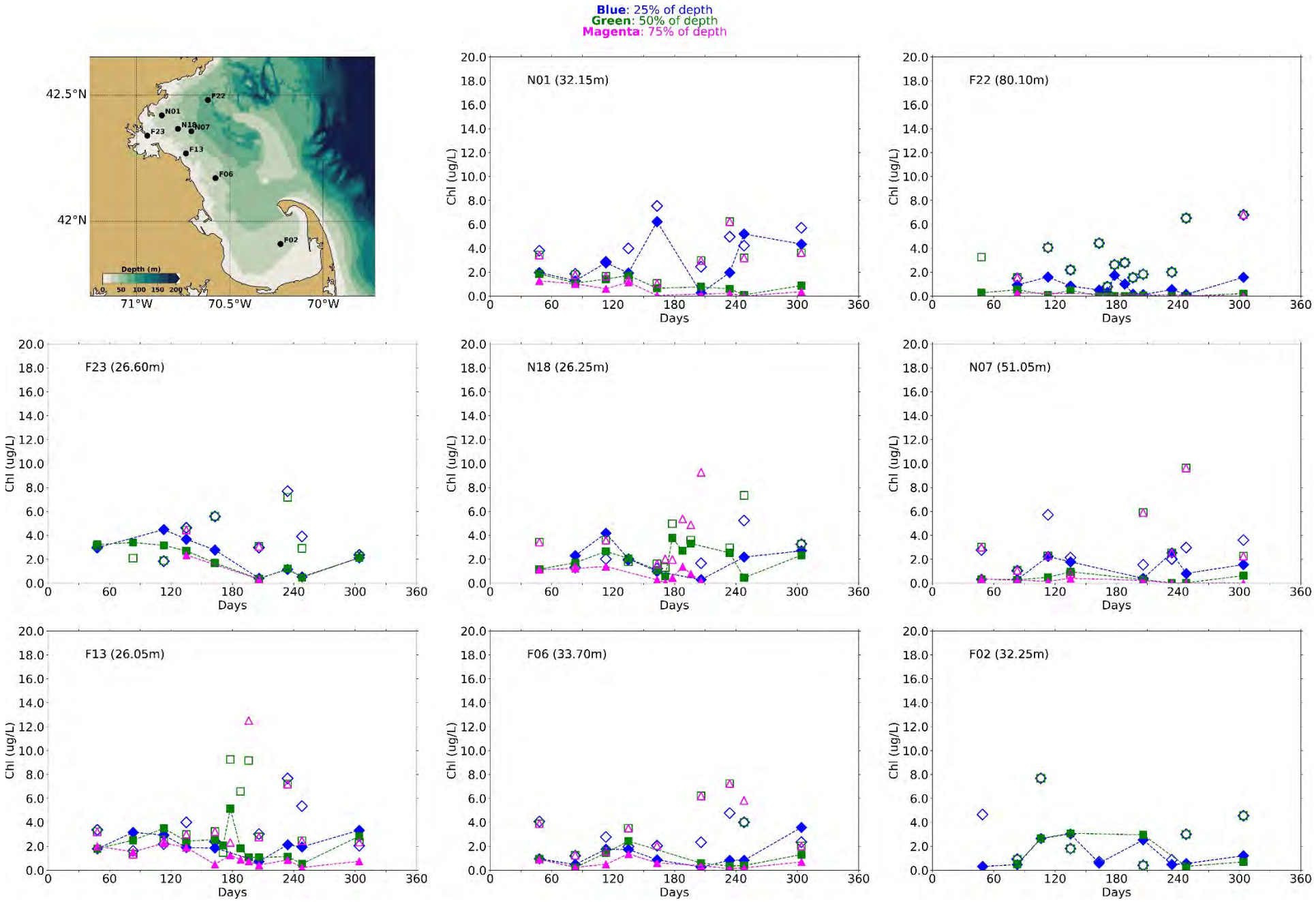

Figure 5-9: Chlorophyll a time series, model-observation comparison within water column (between surface and seafloor). Model results: lines and full symbols. MWRA vessel-based survey observations: empty symbols.

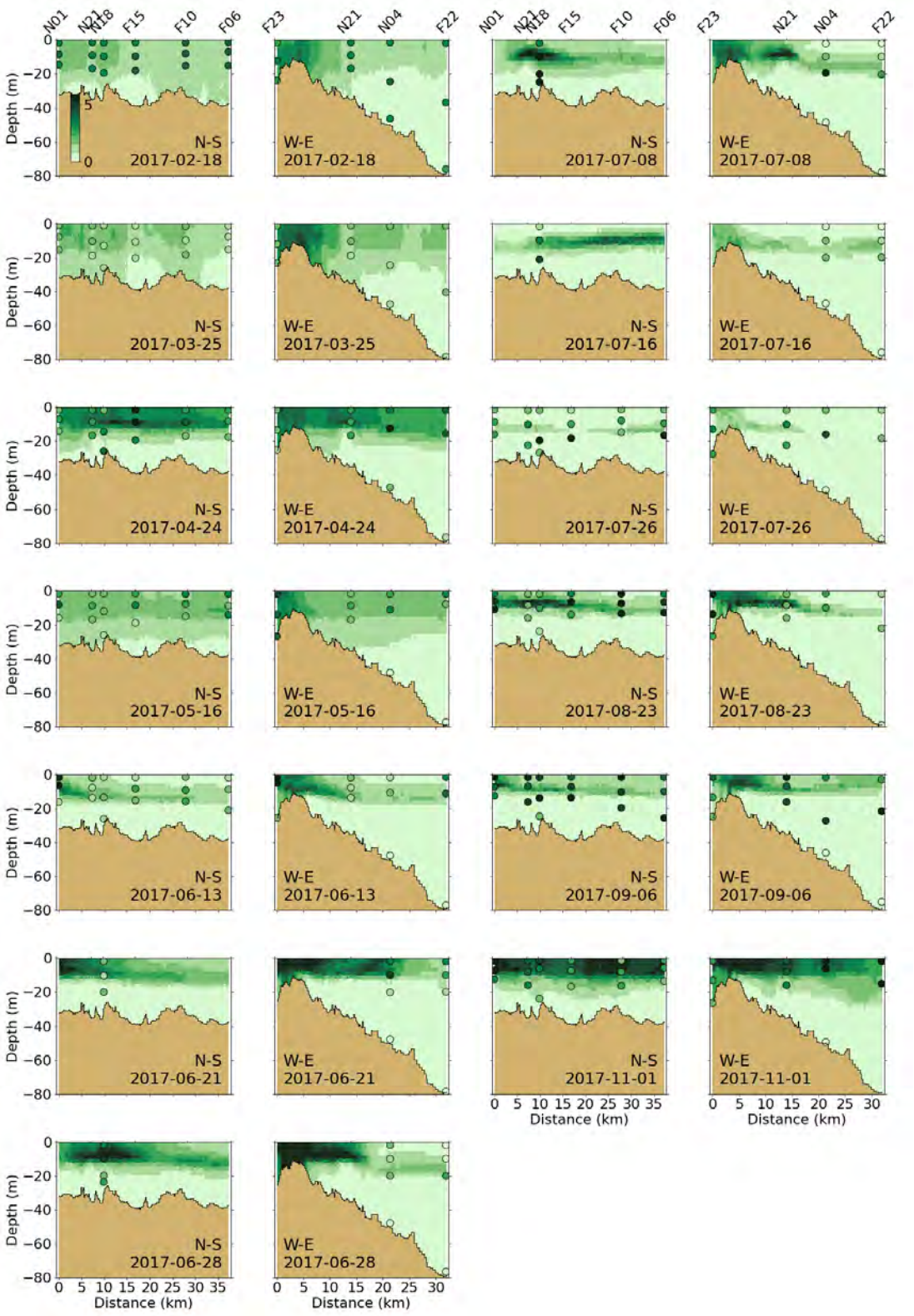

Figure 5-10: Chlorophyll a (µg/L) for 2017 along North-South (N-S) and West-East (W-E) transects (Figure 2-4). MWRA measurements are plotted with round symbols. Model results are 5-day averages around the sampling date.

5.2.4 Particulate organic carbon

POC concentrations at the observation stations were extremely variable and it was difficult to identify any clear seasonal pattern (Figure 5-11). Concentrations were however slightly lower in winter and early spring than the rest of the year. Among the plotted stations, POC concentrations were highest at F23, closer to the harbor, likely due to the high river POC inputs (see Figure 3-6). Concentrations were slightly lower near the bottom than at the surface.

The model generally captured POC concentration ranges, variability and vertical gradients at the plotted locations (Figure 5-11). POC concentrations were however overestimated at F23, closer to the harbor, and underestimated at some stations further away from the major local POC sources (F22 and F06). Given the high variability of POC and the low frequency of the sampling campaigns it was difficult to further interpret the model-observation comparisons for intermediate depths (Figure 5-12).

According to the model results, POC concentrations increased from the coast eastward (Figure 5-13). The signature of the outfall was not visible along neither the North-South nor the West-East transects. This was consistent with the fact that the MWRA outfall only represented about 1/5 of the total non-oceanic OC inputs to the study area (Figure 3-6). Highest simulated concentrations occurred in April, in the subsurface along the entire transects and in August, closer to the coast. High concentrations were measured in September 2017 along both transects and quite deep throughout the water column (~30 m). This was not fully captured by the model and was most likely due to the underestimation of phytoplankton biomass (chlorophyll a) for that period.

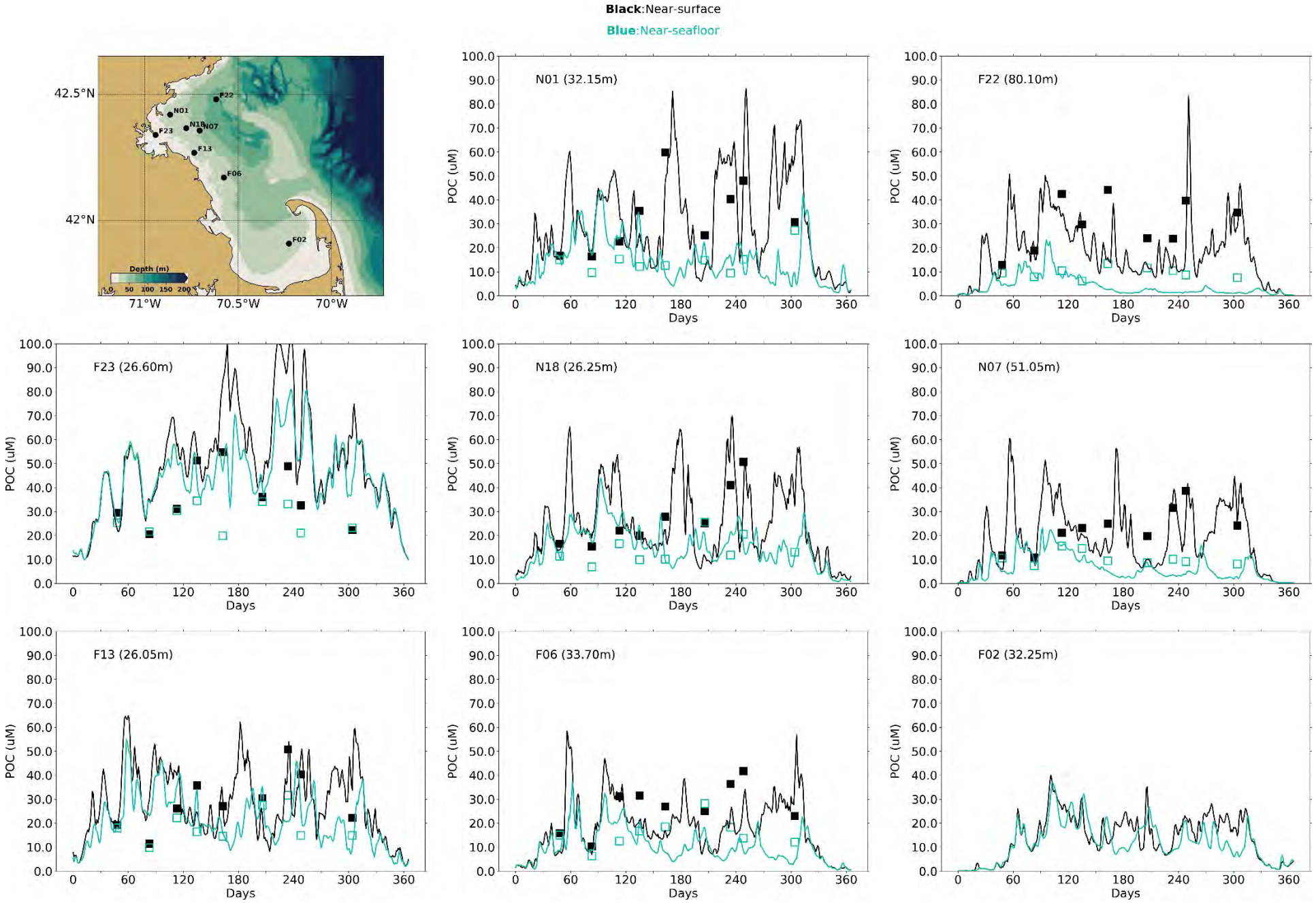

Figure 5-11: Particulate Organic Carbon time series, model-observation comparison near surface and seafloor. Model results: lines. MWRA vessel-based survey observations: symbols.

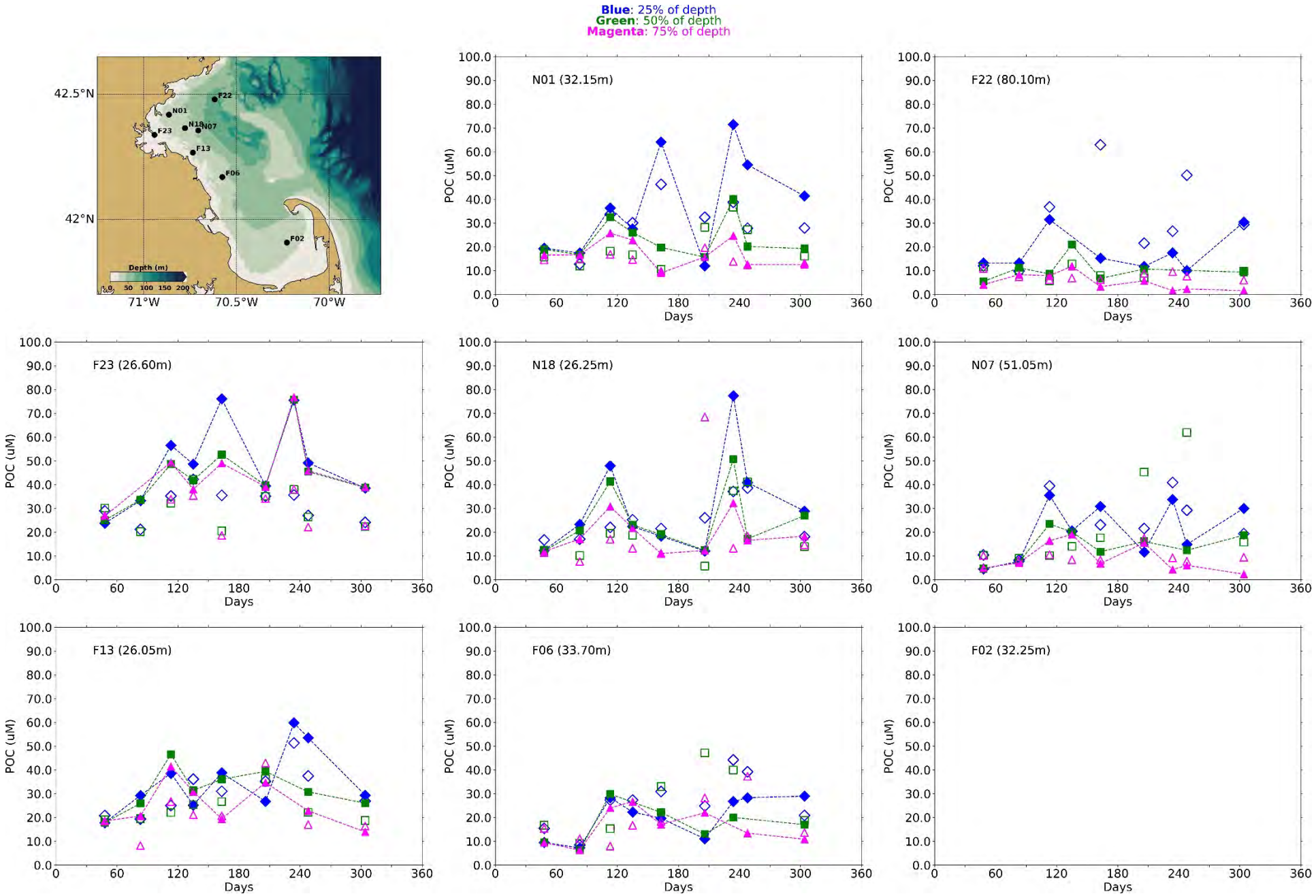

Figure 5-12: Particulate Organic Carbon time series, model-observation comparison within water column (between surface and seafloor). Model results: lines and full symbols. MWRA vessel-based survey observations: empty symbols.

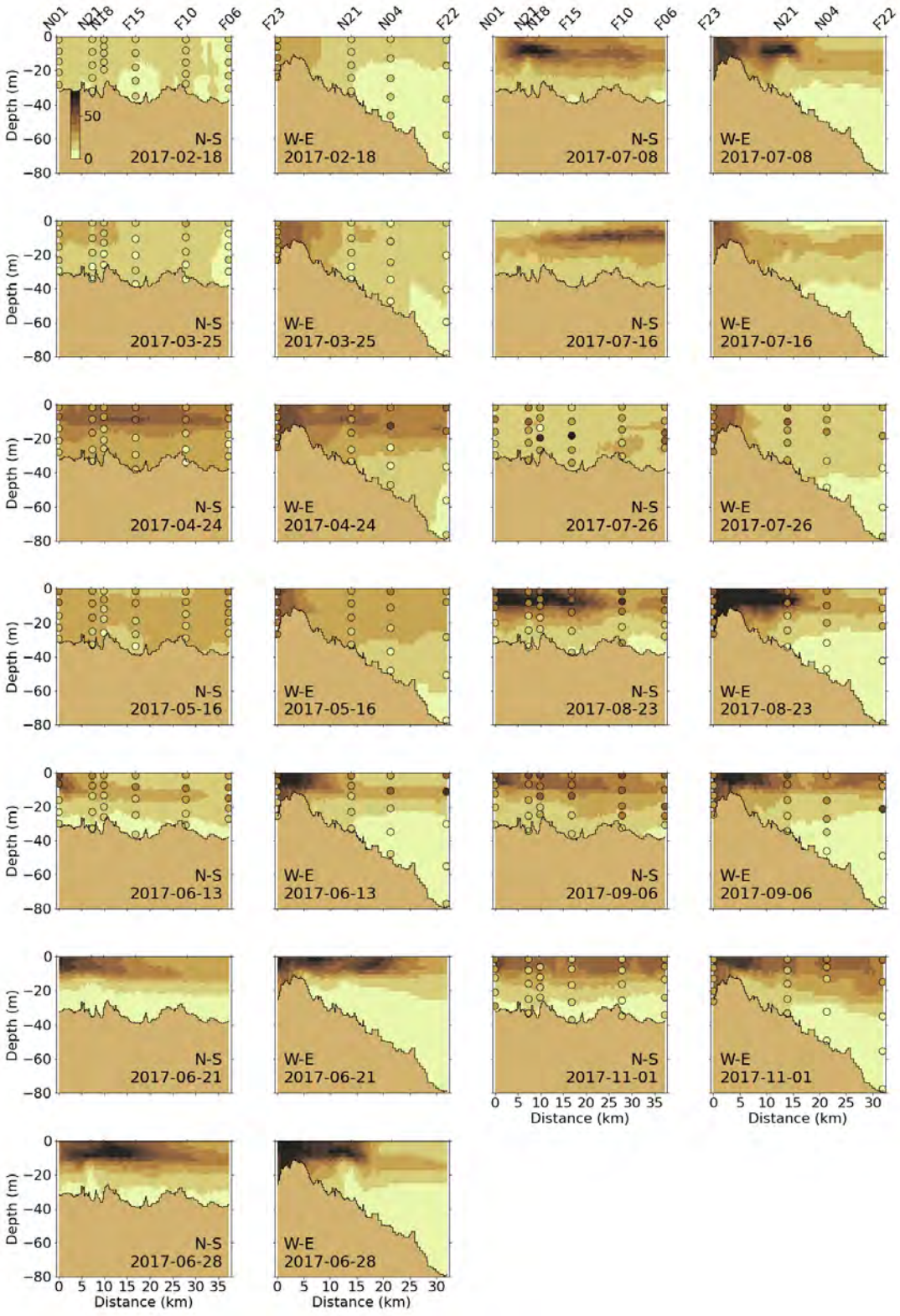

Figure 5-13: Particulate Organic Carbon (µM) for 2017 along North-South (N-S) and West-East (W-E) transects (Figure 2-4). MWRA measurements are plotted with round symbols. Model results are 5-day averages around the sampling date.

5.2.5 Dissolved oxygen

The 2017 seasonal variations of DO concentrations were well reproduced, with maximum concentrations observed at the end of winter/beginning of spring and decreasing until fall before rising again (Figure 5-14). While winter concentrations at the surface and the bottom were comparable, bottom concentrations dropped lower at the end of the summer and beginning of fall. Differences between top and bottom concentrations reached ~2 mg/L at the end of October at several stations. As for previous years, the model underestimated this drop of DO in the bottom layer in the Southern Massachusetts Bay and Cape Cod Bay (e.g. F06 and F02). Observed peaks in summer DO concentrations (e.g. at station N01) were not fully captured by the model, likely due to the underestimation of phytoplankton biomass in that period. The model-observation comparison at intermediate water depths showed similar behavior: summer concentrations at smaller depths and the drop of DO in fall deeper in the water column were usually slightly underestimated (Figure 5-15).

At the A01 mooring station, the model reproduced the seasonal pattern in the observed DO very well, though it again somewhat overestimated the end of autumn minimum (Figure 5-16).

The North-South and West-East cross-section plots show that DO generally had weak vertical gradients (Figure 5-17). Concentrations were higher at the end of winter and beginning of spring, and decreased until fall, which showed the high control by temperature. Higher concentrations were observed and simulated in the subsurface in periods with higher primary production (e.g. April-July). In months with visible vertical gradients in DO concentrations, the model captured these well (e.g. highest concentrations in the subsurface in June and July).

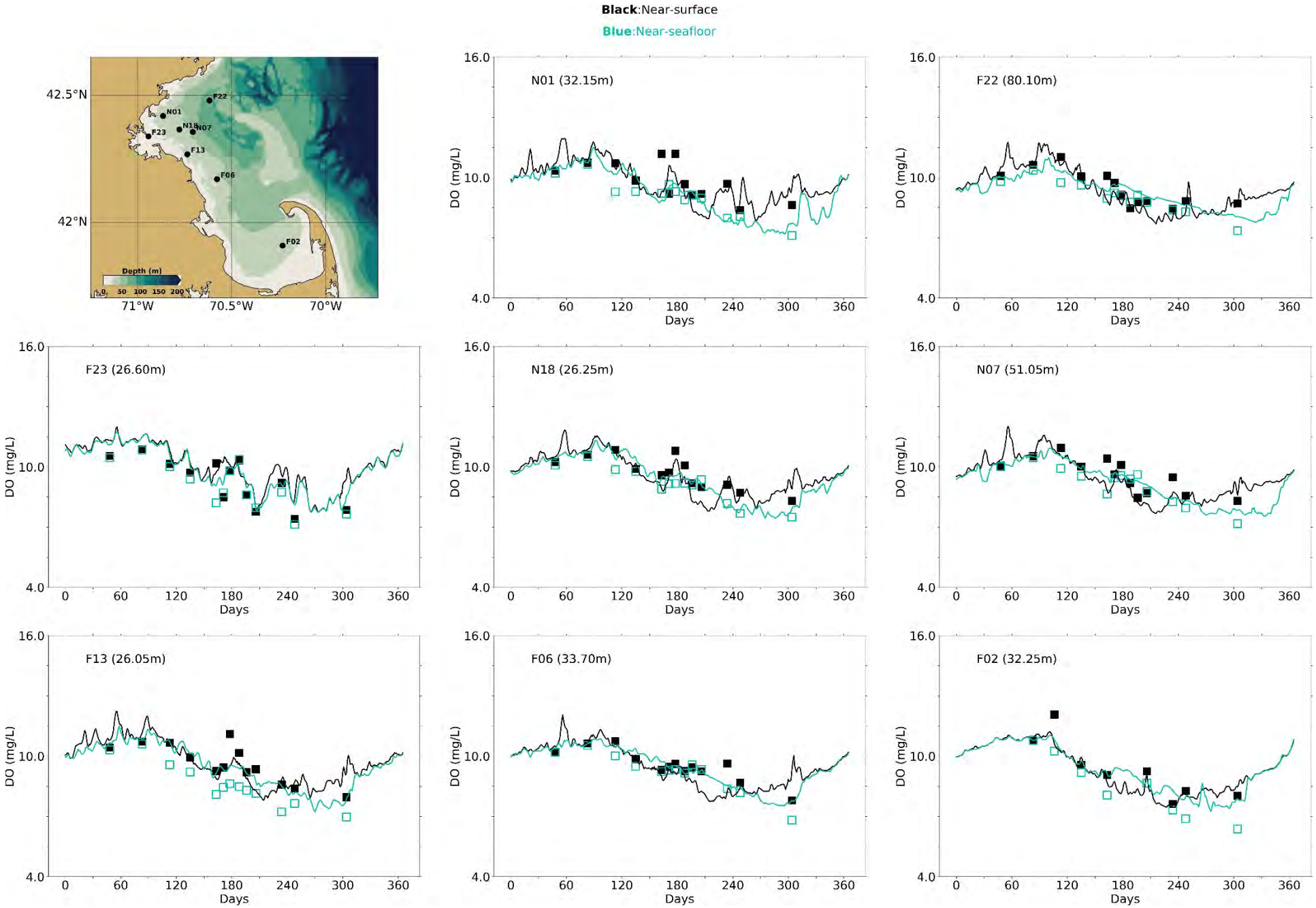

Figure 5-14: Dissolved Oxygen time series, model-observation comparison near surface and seafloor. Model results: lines. MWRA vessel-based survey observations: symbols.

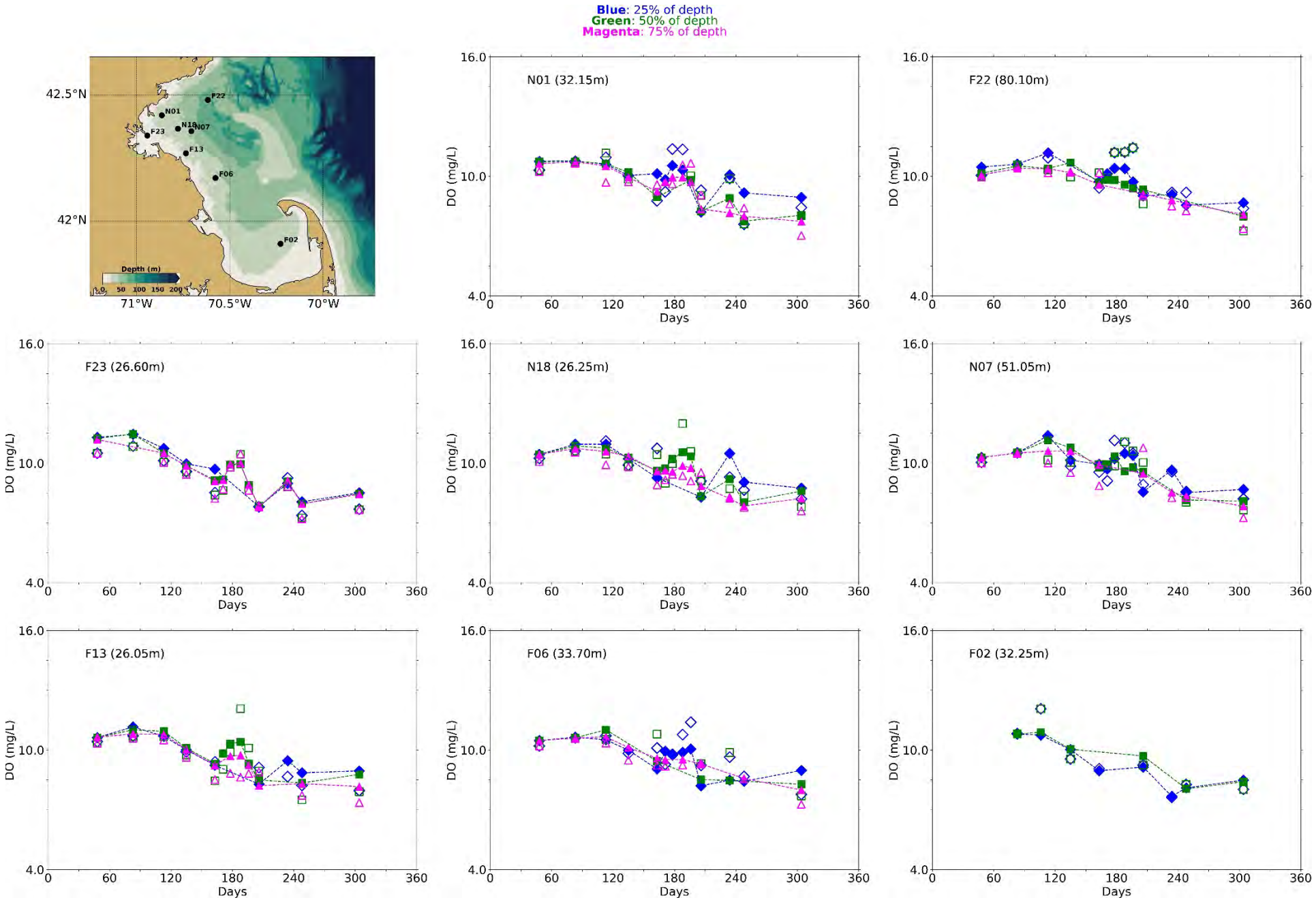

Figure 5-15: Dissolved Oxygen time series, model-observation comparison in water column. Model results: lines and full symbols. MWRA vessel-based survey observations: open symbols.

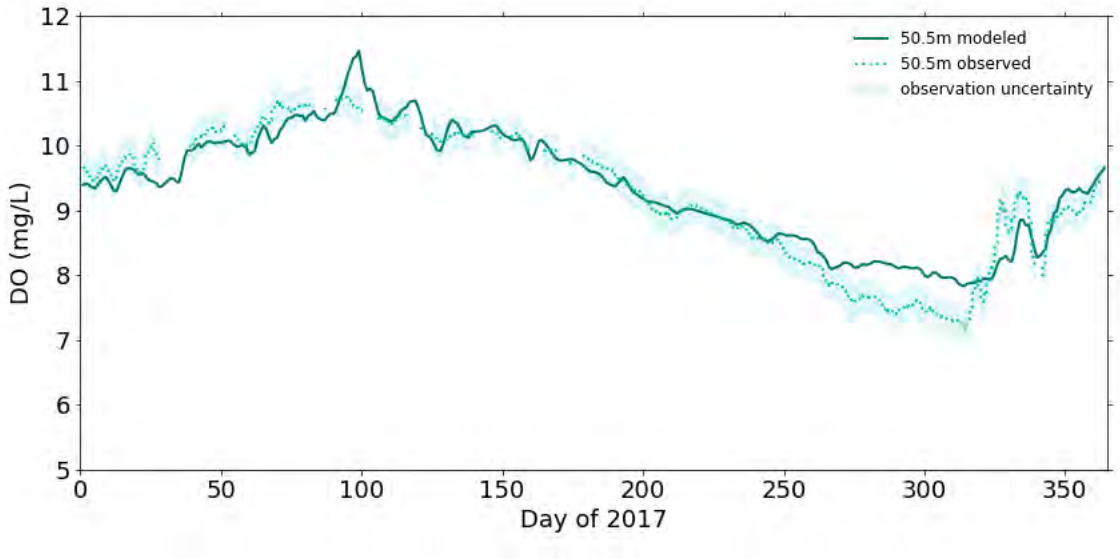

Figure 5-16: Dissolved Oxygen time series 50.5m deep at A01 mooring site, model-observation comparison for 2017.

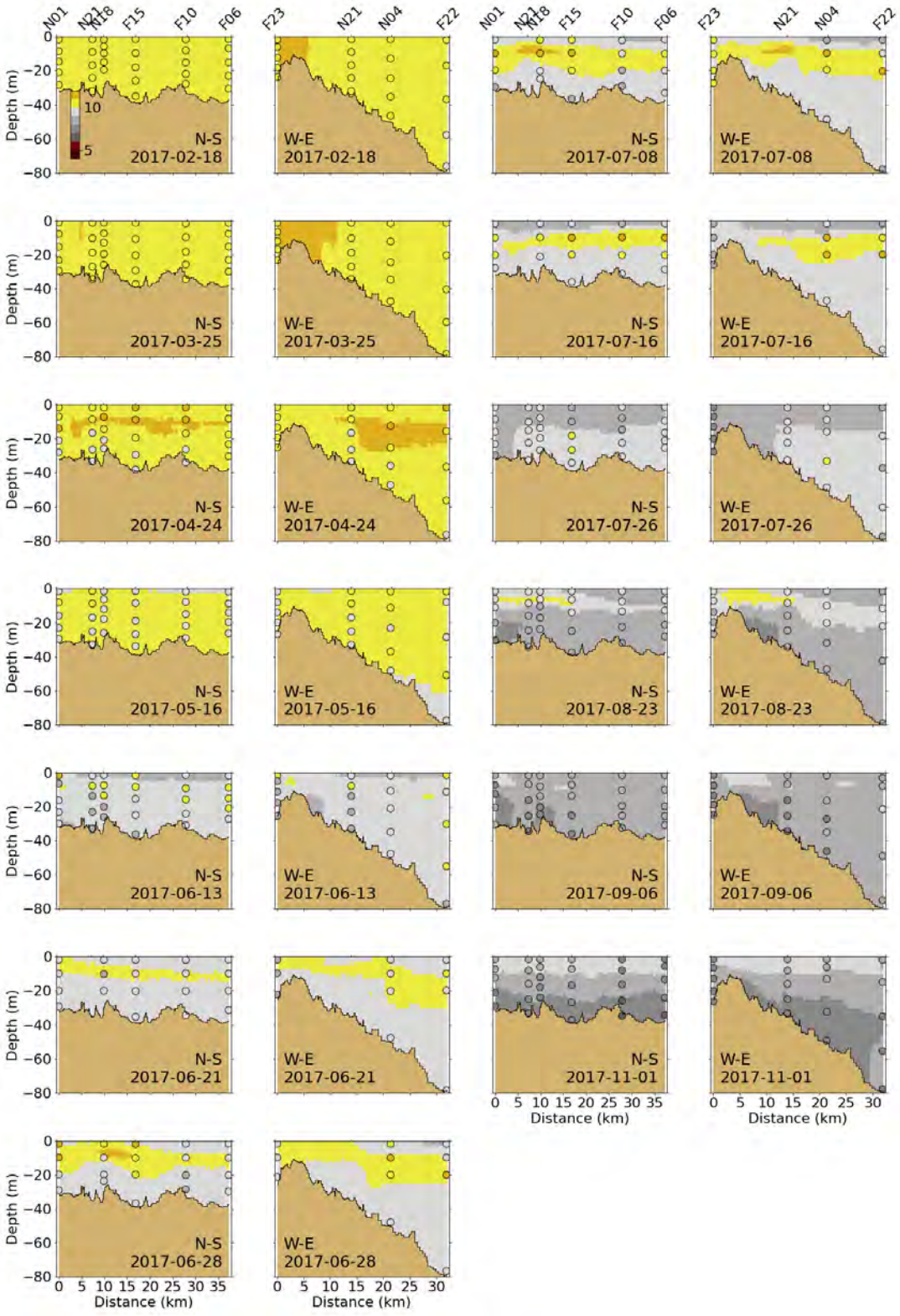

Figure 5-17: Dissolved Oxygen (mg/L) for 2017 along North-South (N-S) and West-East (W-E) transects (Figure 2-4). MWRA measurements are plotted with round symbols. Model results are 5-day averages around the sampling date.

5.2.6 Primary production

Simulated primary production was compared to historical measurements at three monitoring locations (Figure 5-18). Box whiskers represent the 9th, 25th, 50th, 75th and 91st percentiles of primary productions observations over the period 1995-2010 (Keay et al., 2012). Primary production in 2017 was in the range of historical measurements for the entire year 2017 at F23, N04, N18. It was also quite typical in comparison to the years 2012 to 2016, with no exceptional peaks (such as in 2012 and 2014 at F23; see Deltares 2021) nor prolonged periods of exceptionally low production.

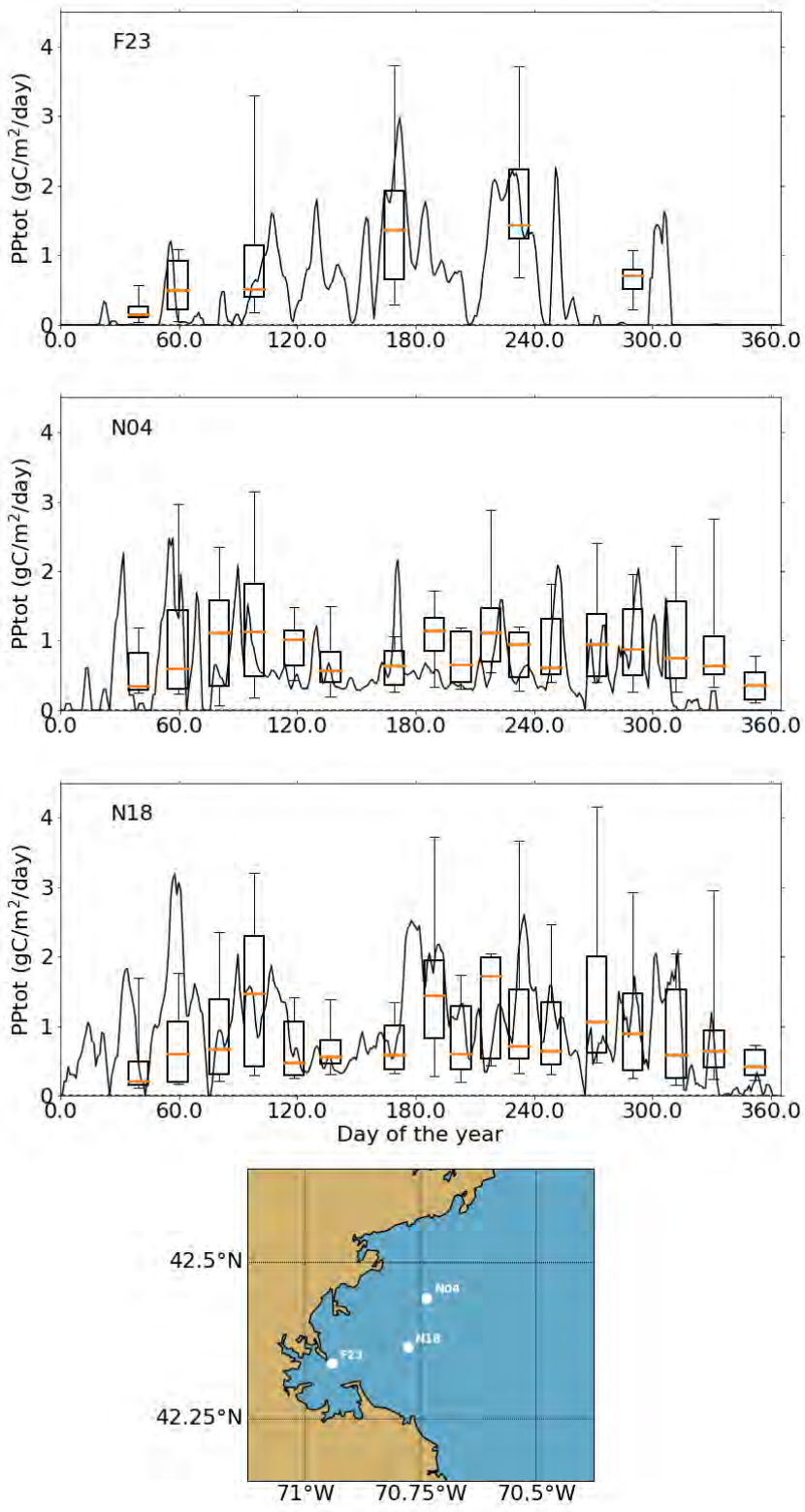

Figure 5-18: Simulated (lines; 2017) and observed (box-whiskers; 1995-2010) primary production.

5.2.7 Sediment fluxes

Sediment NH4 fluxes (Figure 5-19) and sediment oxygen demand (Figure 5-20) outputs from the model were compared to measurements from the 2001-2010 period from Tucker et al. (2010) at stations located in Boston Harbor and Massachusetts Bay using plots in the same format as Figure 5-18.

Simulated sediment fluxes were low in winter and peaked in the summer due to higher temperatures, favorable to biogeochemical activity (mineralization of organic matter in the sediment). Sediment fluxes were higher in the harbor area than in Massachusetts Bay, which was captured by the model. Results for the year 2017 were similar to those from the individual years 2012 to 2016. These were mostly in the range of historical measurements, except for NH4 sediment fluxes at the Mass Bay stations (MB01, MB03 and MB05). This discrepancy is related to the simplified representation of sediment biogeochemical processes (see Deltares, 2021).

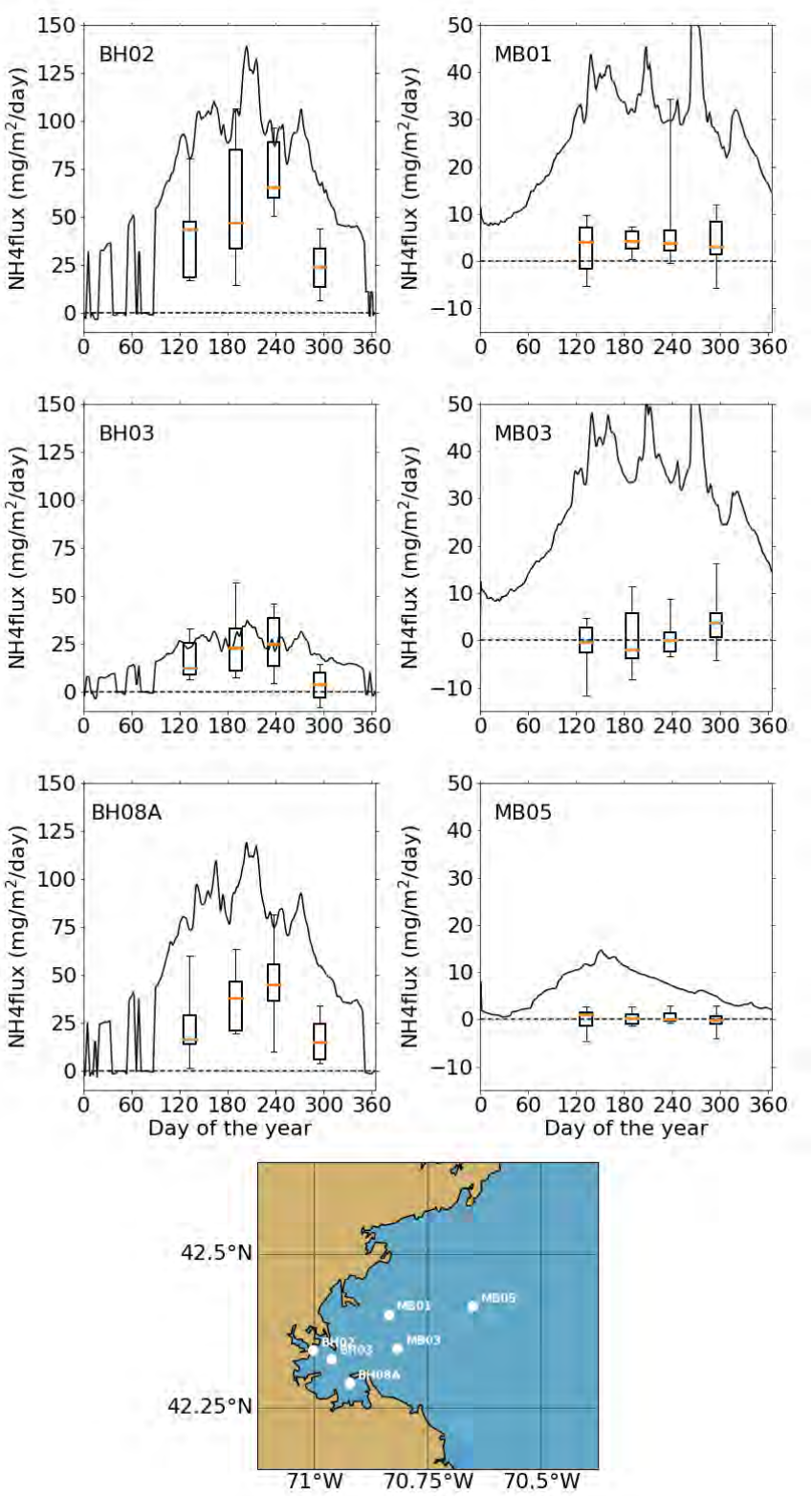

Figure 5-19: Simulated (line; 2017) and observed (box-whiskers; 2001-2010) sediment flux of ammonium. Note change of scale between the Boston Harbor stations (left) and Mass Bay stations (right).

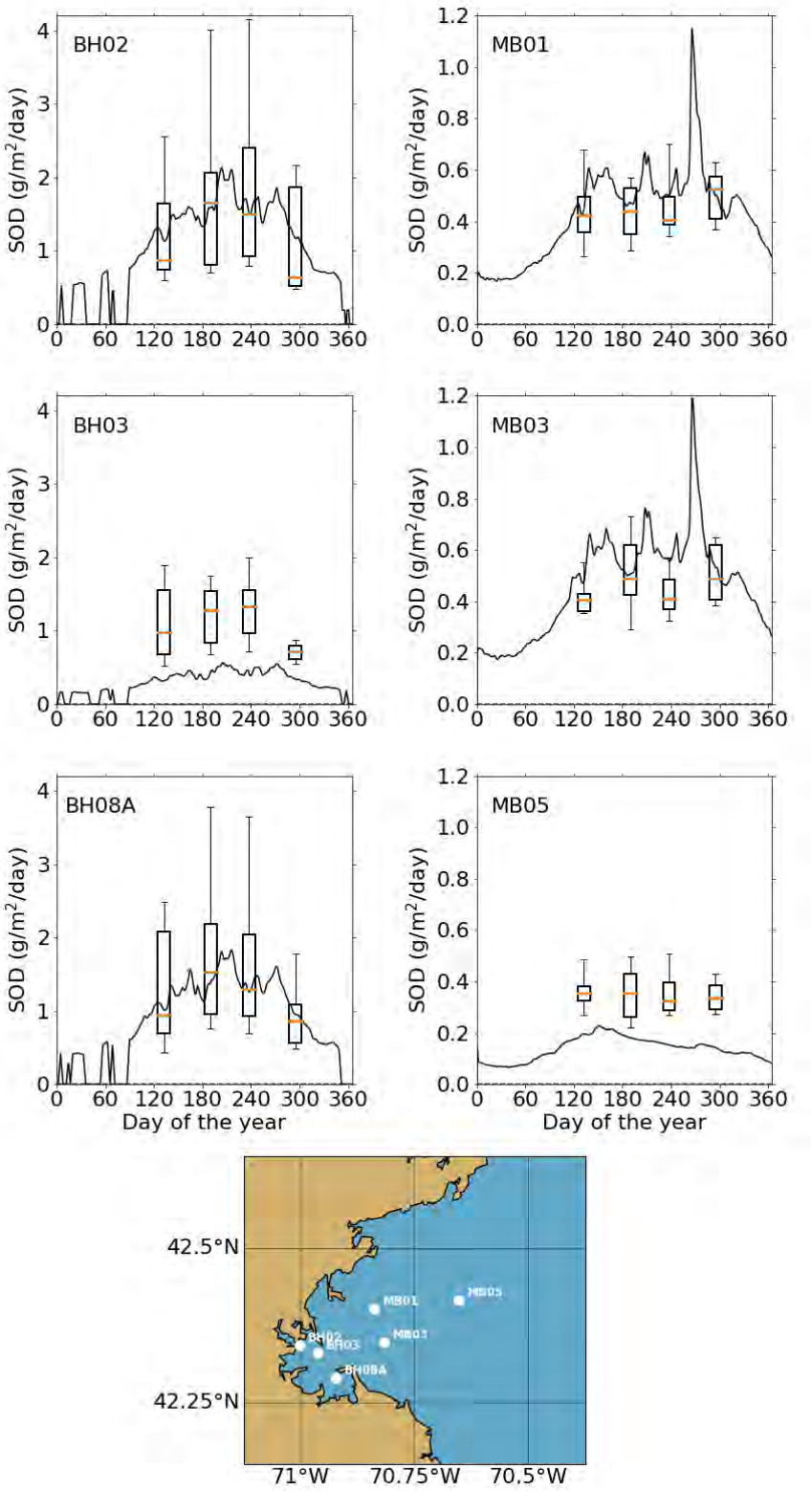

Figure 5-20: Simulated (line; 2017) and observed (box-whiskers; 2001-2010) sediment oxygen demand. Note change of scale between the Boston Harbor stations (left) and Mass Bay stations (right).

5.3 Phytoplankton community composition

Model phytoplankton community/species composition was not validated against field observations during model setup and calibration/validation. However, it is of interest to verify that its main characteristics in the model are not inconsistent with general patterns known to characterize the bays, based on monitoring observations.

The phytoplankton sub-module (BLOOM) simulated the dynamics of 4 functional groups and their adaptation to changing environmental conditions (i.e. light and nutrient limitation). BLOOM simulates the rapid shifts in phytoplankton communities due to these changes, using linear programming to optimize whole-community net primary production (Los, 2009). Simulated phytoplankton groups include: diatoms, dinoflagellates, other marine flagellates, and *Phaeocystis*. Their parameterization was initially based on that used in the North Sea eutrophication model (Blauw et al., 2009) and tuned during the BEM calibration process to better represent chlorophyll a as well as observed PON:POC ratios at MWRA monitoring locations (see Appendix B of Deltares, 2021).

Figure 5-21 shows the share of the different simulated phytoplankton groups in the total phytoplankton biomass near the water surface. Although total phytoplankton biomass temporal dynamics differed from station to station for the year 2017, phytoplankton composition showed similar temporal patterns. Marine diatoms dominated in the winter period and were succeeded in spring by marine flagellates. Dinoflagellates clearly dominated from June to the end of October. These were typical characteristics of community composition seen in monitoring observations.

Phaeocystis biomass in the model remained extremely low at all stations throughout the year 2017. Observations from the routine monthly surveys in 2017 did not capture a large *Phaeocystis* bloom. High chlorophyll levels were seen in satellite images of ocean color and in time series measurements at the A01 mooring in April and May. Although some aspects of changes in nutrient concentrations at about the same time suggest these peaks might possibly have been due a *Phaeocystis* bloom, this cannot be confirmed. The 2017 model results for *Phaeocystis* were therefore not consistent with available observations.

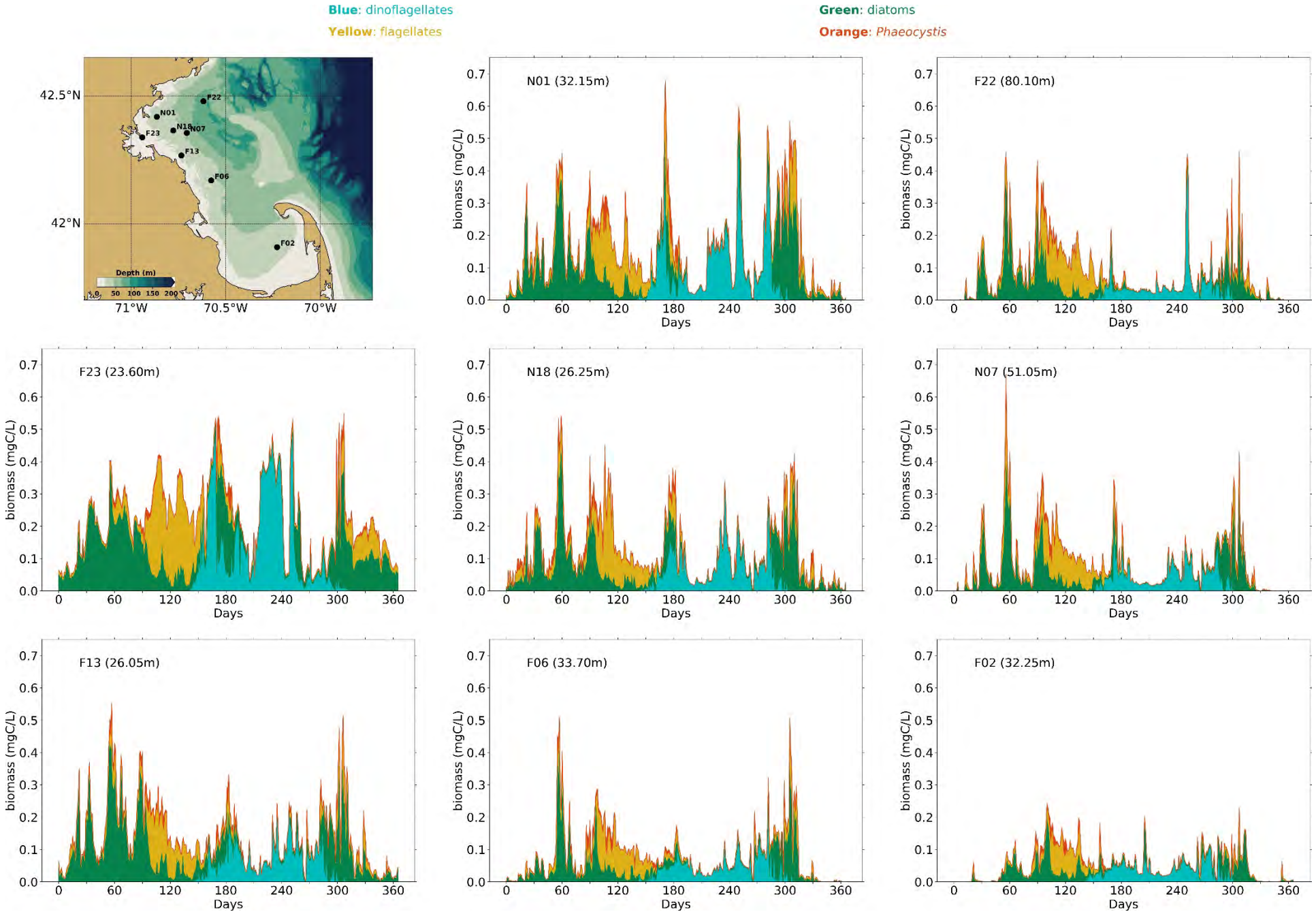

Figure 5-21: Simulated phytoplankton biomass time-series. Biomasses of the 4 simulated species groups (dinoflagellates, other flagellates, diatoms and Phaeocystis) are stacked.

5.4 Conditions on East-West transect through outfall

The signature of the outfall in terms of DIN concentrations was visible all year round, with increased concentrations up to a distance of about 10 km (Figure 5-22). The extra DIN load was “trapped” in the lower layers of the water column in the period of stratification (April-October). During the other months, the effluent led to an increase in surface DIN concentrations as well. These temporal patterns were similar to those observed in previous years.

All year round, chlorophyll a concentrations were higher nearshore (Figure 5-23). This was most likely due to the nutrient inputs from rivers to the harbor area, promoting algal growth. Further offshore, highest chlorophyll a concentrations were simulated in spring and, during the summer months, maximum chlorophyll a concentrations occurred at a depth of ~15 m. As for DIN, these patterns were similar to those simulated for previous years. Any effect of the outfall on chlorophyll a concentrations was difficult to detect.

The vertical cross-sections of DO concentrations for 2017 showed similar temporal and spatial patterns as for previous years (Figure 5-24), with the highest concentrations occurring near the surface between February and May. The highest concentrations occurred slightly under the surface between April and July, which corresponded to the depths at which chlorophyll a was the highest. As for chlorophyll a, no effect of the outfall on DO concentrations was visible in the plotted cross sections.

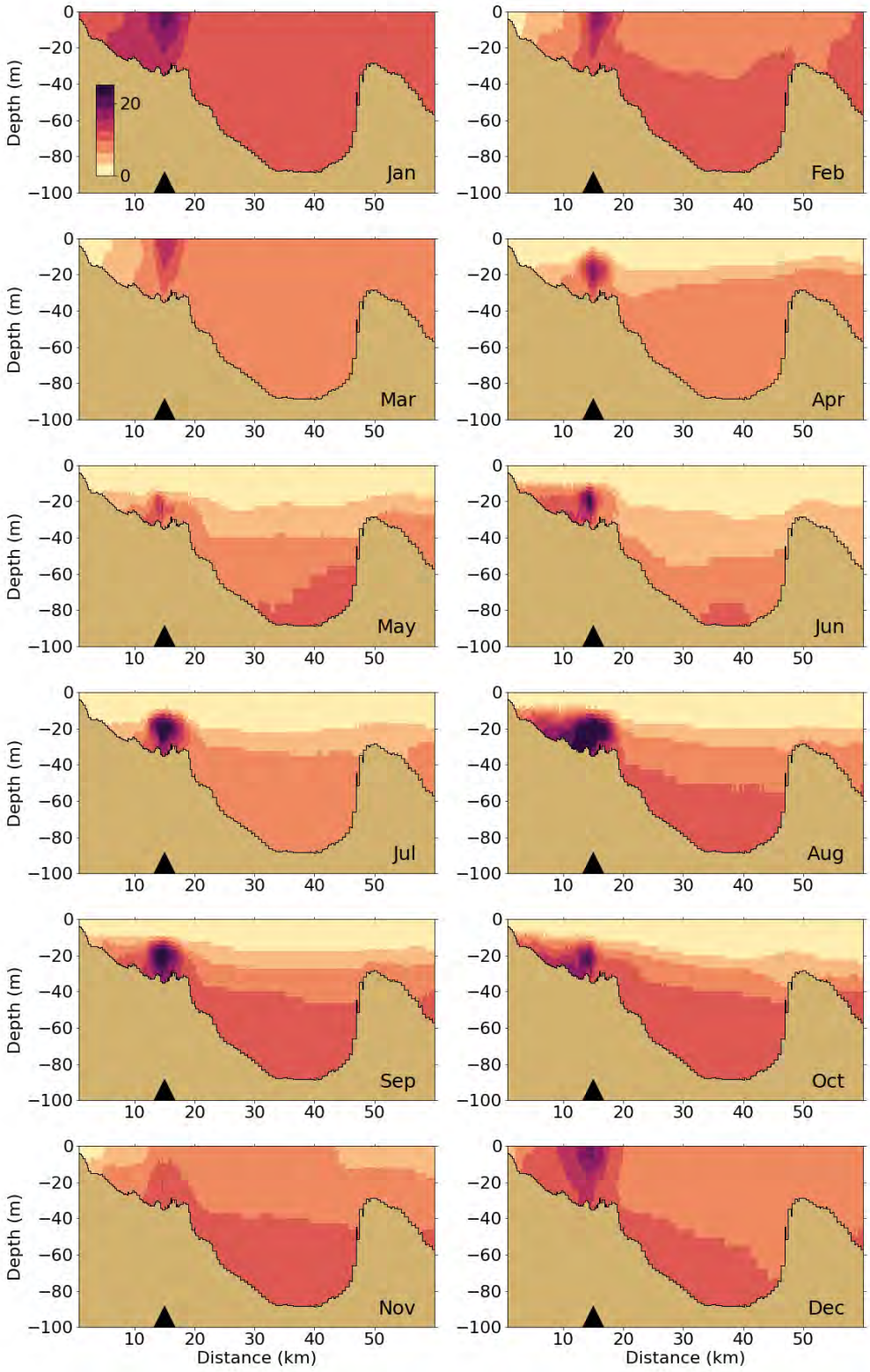

Figure 5-22: Dissolved Inorganic Nitrogen (µM) for 2017 along east-west transect (Figure 2-4). Horizontal axis is distance eastward from coast; black triangle indicates the location of the outfall on the seafloor.

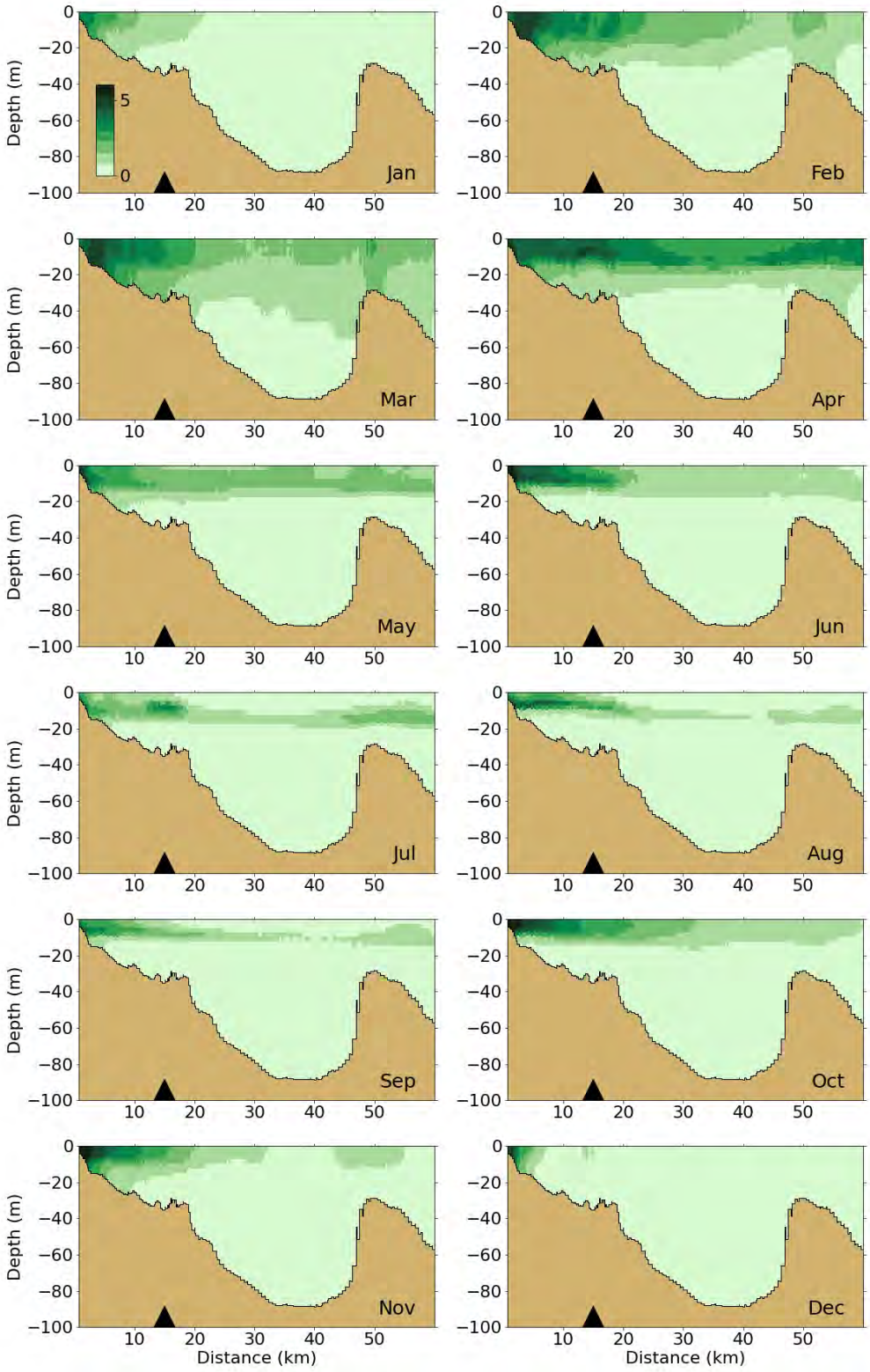

Figure 5-23: Chlorophyll a (µg/L) for 2017 along east-west transect (Figure 2-4). Horizontal axis is distance eastward from coast; black triangle indicates the location of the outfall on the seafloor.

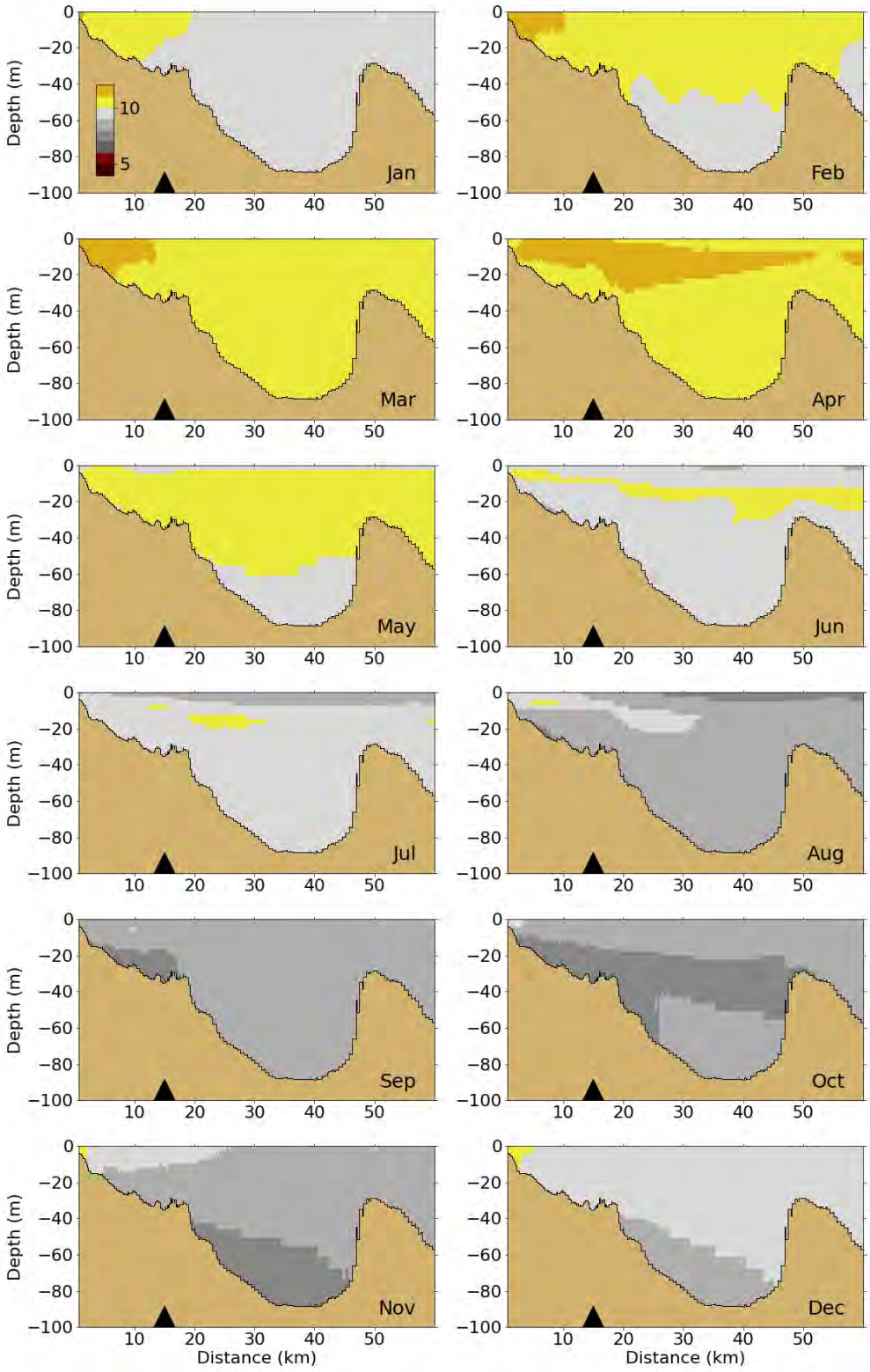

Figure 5-24: Dissolved Oxygen for 2017 along east-west transect (Figure 2-4). Horizontal axis is distance eastward from coast; black triangle indicates the location of the outfall on the seafloor.

6 Synthesis/Application

There are no synthesis/application simulations focused on the year 2017.

7 Summary

The meteorological and hydrological forcing conditions in the year 2017 were not substantially different from the long-term mean over the previous 20 years. Wind speeds, heat fluxes and discharges showed no large deviation. However, the effect of a large storm event in September 2017 was visible in the wind speed and mainly in the North-South wind stress. Furthermore, the total discharged volume from the rivers in Massachusetts Bay and Cape Cod Bay was slightly below the long-term mean.

Loading of organic carbon (OC), total nitrogen (TN) and total phosphorus (TP) originated mainly (>90%) from oceanic input outside of Massachusetts Bay and Cape Cod Bay. The remaining OC load originated mostly (about 4/5th) from rivers, while the non-oceanic TN and TP loads originated mostly from the MWRA outfall. OC loads for the year 2017 from the MWRA effluent were slightly higher than in the period 2012-2016. TN and TP loads from the effluent were well within the range of loads from previous years.

The performance of the hydrodynamic model was in line with the previous years. Temperatures were reproduced accurately, especially at the surface. Model salinity performed slightly better than in previous years, although a small overall bias remained. At most stations, temperature and salinity stratification was present from April until November with its maximum in July and August. Due to the storm event in the first half of September 2017, sudden mixing occurred at the shallower stations. Furthermore, a sudden peak in bottom temperature (and a minor drop in surface temperature) was visible in both the observations and the model at the end of July.

Modeled non-tidal current patterns were in line with observations, but the magnitudes in the top of the water column, and the temporal variability, were slightly smaller. Looking at a larger scale, the expected circulation pattern driven by the Western Maine Coastal Current was visible in the model. In general, the agreement between the hydrodynamic model and the observations was sufficient to conclude that the representation of processes was adequate to support water quality modeling.

In terms of water quality, conditions in 2017 could also be considered typical compared to previous years, in terms of nutrient and oxygen concentrations and seasonal patterns. Overall, the water quality model accurately represented temporal dynamics and vertical gradients of the different water quality variables, e.g. DIN, POC, DO and light conditions. Skill metrics were mostly comparable to previous years. The model captured the observed timing and amplitude of DIN decline in spring and replenishment in fall, as well as stratification in the summer months. During late spring and summer, the model underestimated some chlorophyll a peaks, which occasionally led to an underestimation of surface DO during this time as well. Seasonal variations of DO concentrations were well reproduced, with a decrease in summer and minimum concentrations reached in fall. This drop was steeper for bottom concentrations than at the surface. The model tended to underestimate the drop in bottom DO concentrations in southern Massachusetts Bay and Cape Cod Bay, as it did for previous years. Chlorophyll a concentrations in 2017 were modest, with no clear bloom captured at the sampling frequency of the MWRA observations. The model overall underestimated chlorophyll a variability at the sampling dates, which was most likely due to the mismatch between sampling frequency and the high temporal variability of chlorophyll. The overall behavior of observed and simulated chlorophyll a

concentration time-series however did not greatly differ from previous years. Modeled primary production in 2017 was in the range of historical measurements and modeled estimates for 2012 to 2016, with no exceptional peaks nor prolonged periods of exceptionally low production. The model showed that the phytoplankton biomass was composed of a succession of diatoms and flagellate species, *Phaeocystis* biomass remaining extremely low throughout 2017.

According to the model results, the MWRA outfall did not have visible effects on ecosystem functioning at the Massachusetts Bay scale. The outfall led to a local increase in DIN concentrations all year round, up to a distance of about 10 km from the outfall. The DIN from the outfall was “trapped” in the lower layers of the water column during the period of stratification (April-October), and led to an increase in winter concentrations throughout the entire water column. Other water quality variables, such as phytoplankton biomass and oxygen concentration were not visibly affected by the effluent.

References

Alessi, Carol A., Beardsley, Robert C., Limeburner, Richard, Rosenfeld, Leslie K., Lentz, Steven J., Send, Uwe, Winant, Clinton D., Allen, John S., Halliwell, George R., Brown, Wendell S., lrish, James D.,1985. "CODE-2: moored array and large-scale data report", Woods Hole Oceanographic Institution Technical Report 85-35, DOI:10.1575/1912/1641. (https://hdl.handle.net/1912/1641)

Blauw AN, HFJ Los, M Bokhorst and PLA Erftemeijer, 2009. GEM: a Generic Ecological Model for estuaries and coastal waters. Hydrobiologia 618: 175-198.

Deltares, 2019a. D-Flow Flexible Mesh, Technical Reference Manual. Released for: Delft3D FM Suite 2020. Version: 1.1.0 SVN Revision: 63652. December 4, 2019.

Deltares. 2019b. Delft3D Flexible Mesh Suite, D-Flow FM in Delta Shell, User Manual, Version 1.5.0, December 5, 2019 (https://content.oss.deltares.nl/delft3d/manuals/DFlow_FM_User_Manual.pdf)

Deltares, 2021. Demonstration of the updated Bays Eutrophication Model. Boston: Massachusetts Water Resources Authority. Report 2021-02. 138 p. plus appendices. (www.mwra.com/harbor/enquad/pdf/2021-02.pdf)

Hunt CD, RK Kropp, JJ Fitzpatrick, P Yodzis, and RE Ulanowicz, 1999. A Review of Issues Related to the Development of a Food Web Model for Important Prey of Endangered Species in Massachusetts and Cape Cod Bays. Boston: Massachusetts Water Resources Authority. Report ENQUAD 99-14. 62 p. (http://www.mwra.state.ma.us/harbor/enquad/pdf/1999-14.pdf)

Keay KE, WS Leo, and PS Libby, 2012. Comparisons of Model-Predicted and Measured Productivity in Massachusetts Bay. Boston: Massachusetts Water Resources Authority. Report 2012-03. 11 p. plus Appendix. (http://www.mwra.state.ma.us/harbor/enquad/pdf/2012-03.pdf)

Libby PS, Borkman DG, Geyer WR, Turner JT, Costa AS, Wang J, Codiga D. 2018. 2017 Water column monitoring results. Boston: Massachusetts Water Resources Authority. Report 2018-04. 59 p. (https://www.mwra.com/harbor/enquad/pdf/2018-04.pdf)

Los, FJ, 2009. Eco-hydrodynamic modeling of primary production in coastal waters and lakes using BLOOM. Ph.D. Thesis, Wageningen University, 2009.

Tucker J, S Kelsey, and AE Giblin, 2010. 2009 benthic nutrient flux annual report. Boston: Massachusetts Water Resources Authority. Report 2010-10. 27 p. (http://www.mwra.state.ma.us/harbor/enquad/pdf/2010-10.pdf)

Werme C, Codiga DL, Libby PS, Carroll SR, Charlestra L, Keay KE., 2021. 2020 Outfall monitoring overview. Boston: Massachusetts Water Resources Authority. Report 2021-10. 55 p. (https://www.mwra.com/harbor/enquad/pdf/2021-10.pdf)

Xue, P, C Chen, J Qi, RC Beardsley, R Tian, L Zhao, and H Lin, 2014. Mechanism studies of seasonal variability of dissolved oxygen in Mass Bay: A multi-scale FVCOM/UG-RCA application. Journal of Marine Systems. 131, 102-119.

Zhao L, Beardsley RC, Chen C, Codiga DL, Wang L, 2017. Simulations of 2016 Hydrodynamics and Water Quality in the Massachusetts Bay System using the Bays Eutrophication Model. Boston: Massachusetts Water Resources Authority. Report 2017-13. 111p. (https://www.mwra.com/harbor/enquad/pdf/2017-13.pdf)

A Statistical assessment of model performance for years 2012-2016

A.1 Hydrodynamics

In the following figures, Taylor diagrams of the individual years of the validation simulation are presented. These can be consulted in addition to the combined Taylor plots for the years 2012-2016 in Figure 4-1.

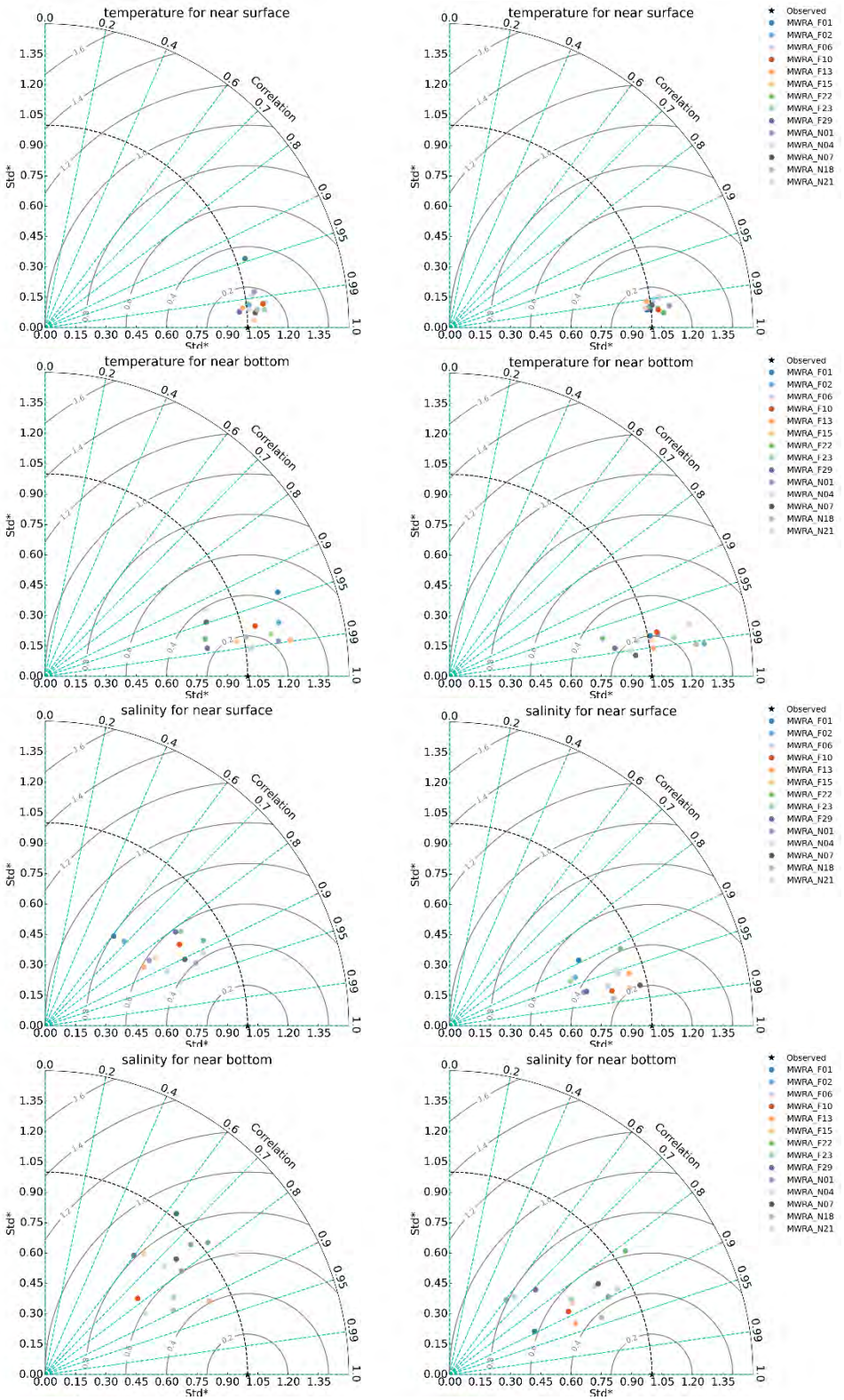

Fig. A-1 Taylor diagrams of hydrodynamic model for MWRA vessel-based survey observations. Temperature (upper frames), salinity (lower frames); 2012 (left column) and 2013 (right column).

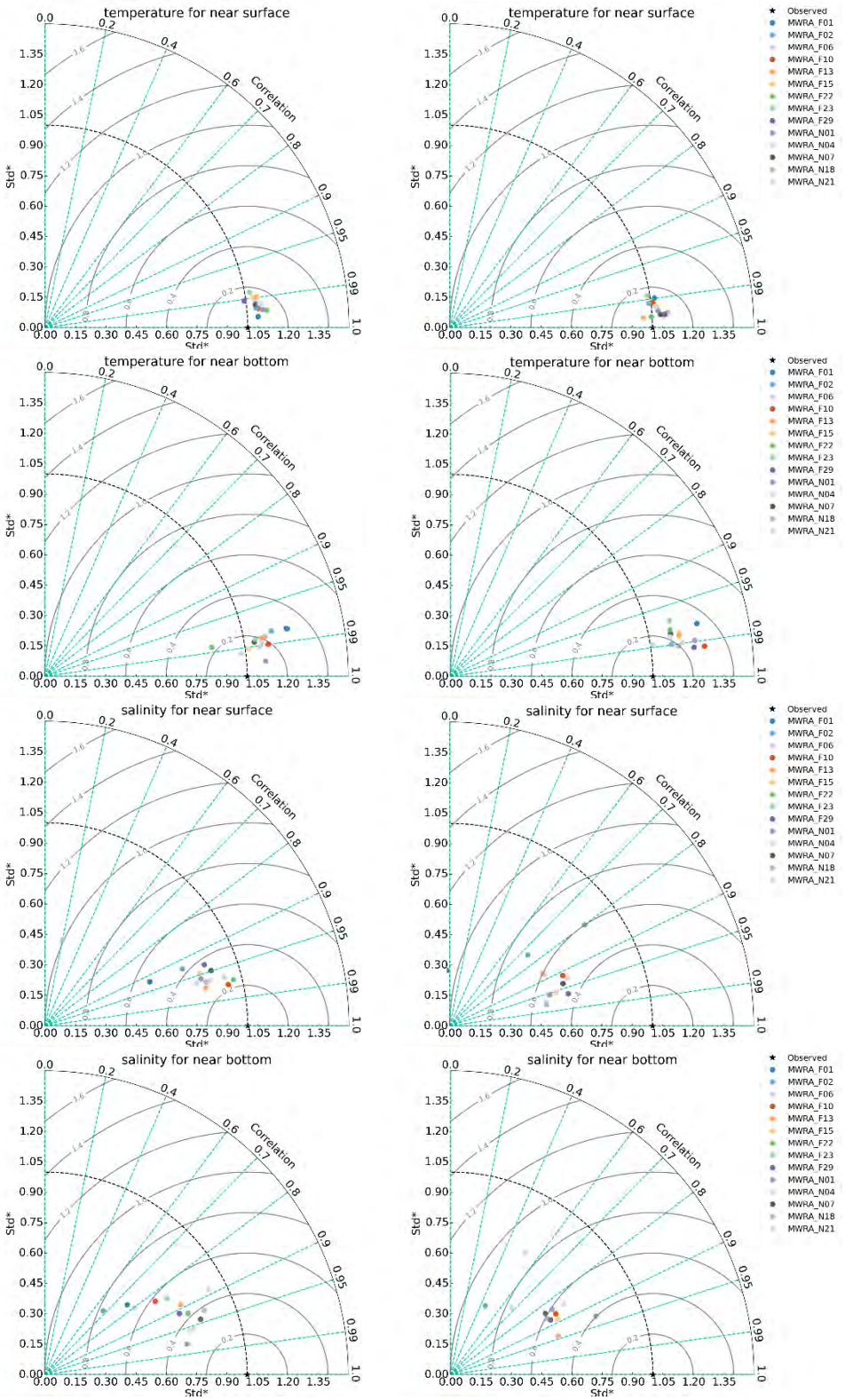

Fig. A-2 Taylor diagrams of hydrodynamic model for MWRA vessel-based survey observations. Temperature (upper frames), salinity (lower frames); 2014 (left column) and 2015 (right column).

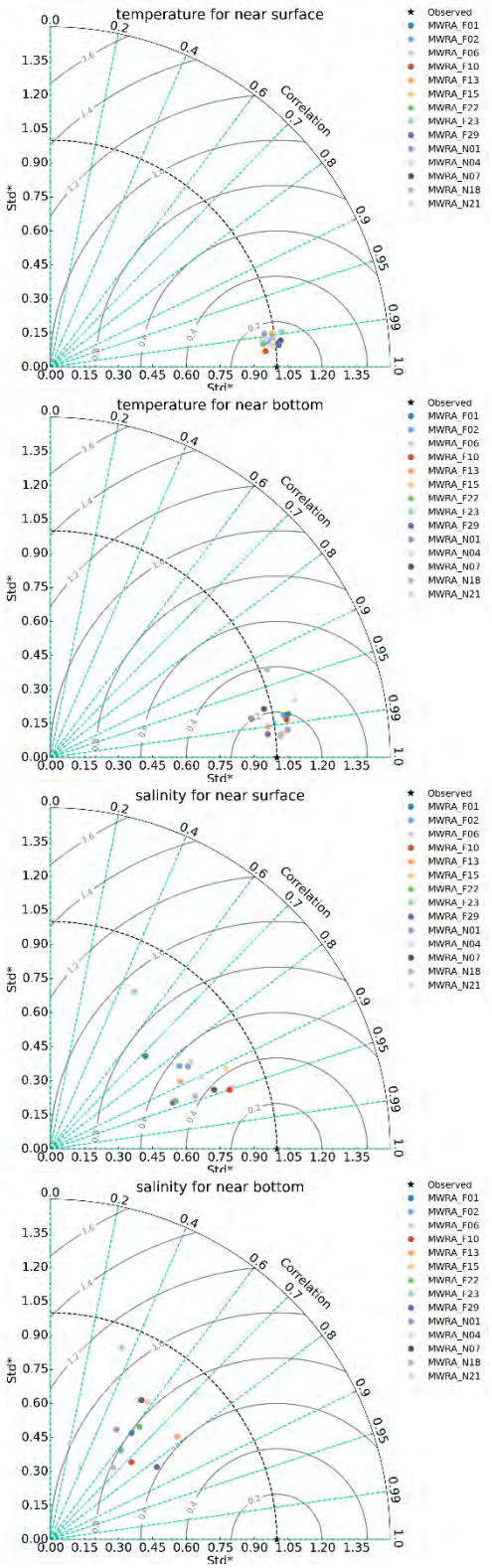

Fig. A-3 Taylor diagrams of hydrodynamic model for MWRA vessel-based survey observations. Temperature (upper frames), salinity (lower frames); 2016.

A.2 Water Quality

In the following figures, Taylor diagrams of the individual years of the validation simulation are presented. These can be consulted in addition to the combined Taylor plots for the years 2012-2016 in Figure 5-1 and Figure 5-2.

As described in Section 2.1, for the 2017 BEM run, the representation of effluent nutrient concentrations has been corrected compared to the runs for 2012-2016 (Deltares, 2021). An analysis of the effect of this correction upon the results in 2016 has shown that the effects of correcting the loads effects are minor and localized in the direct vicinity of the outfall (Section 2.1). The effect of the correction of the loads upon the Taylor diagrams and statistics for the period 2012-2016 used here is negligible.

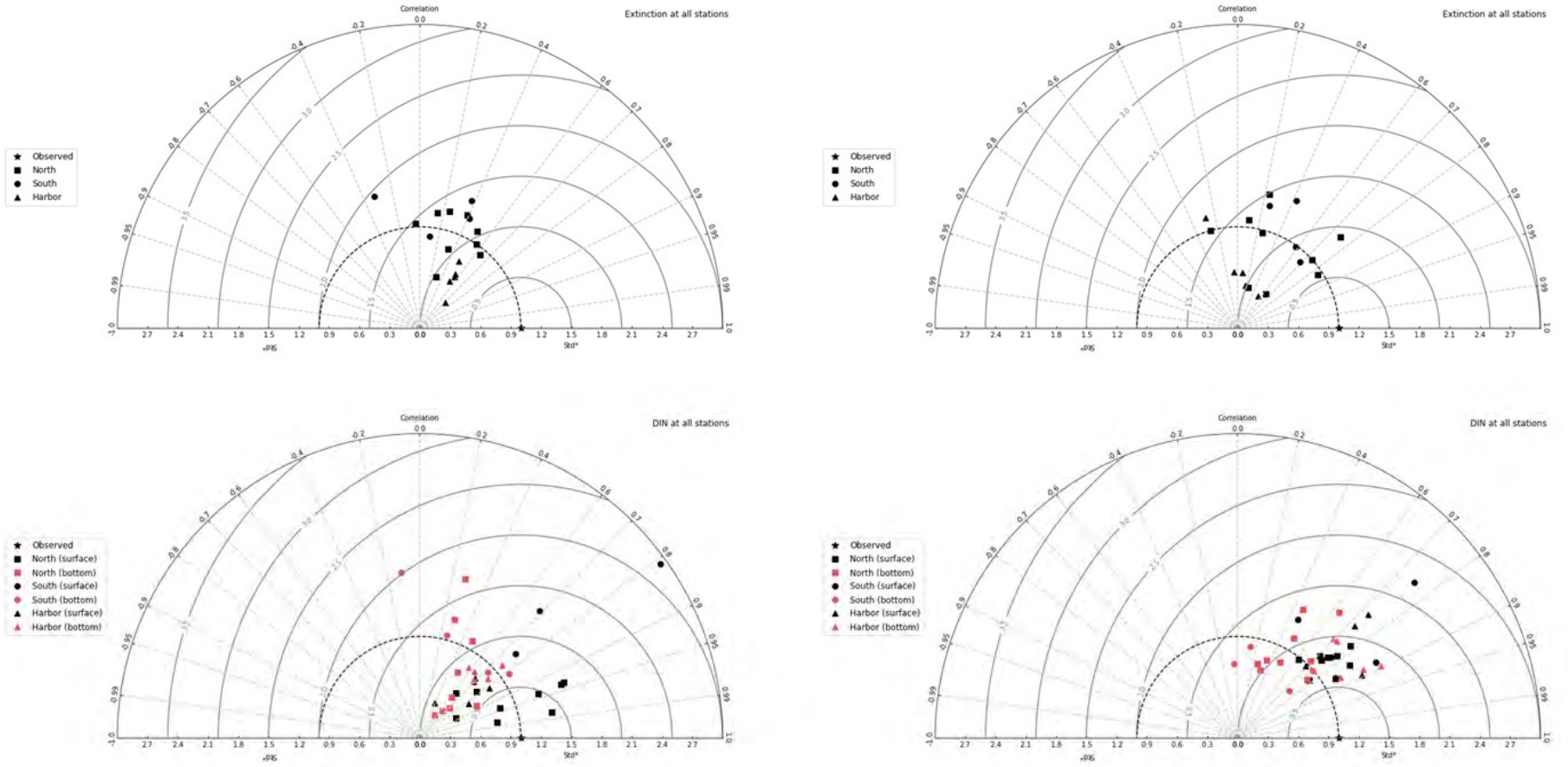

Fig. A-4 Taylor diagrams for MWRA vessel-based survey observations. Top panels show the parameter Extinction and bottom panels Dissolved Inorganic Nitrogen. Left panels show results for the year 2012 and right panels for the year 2013

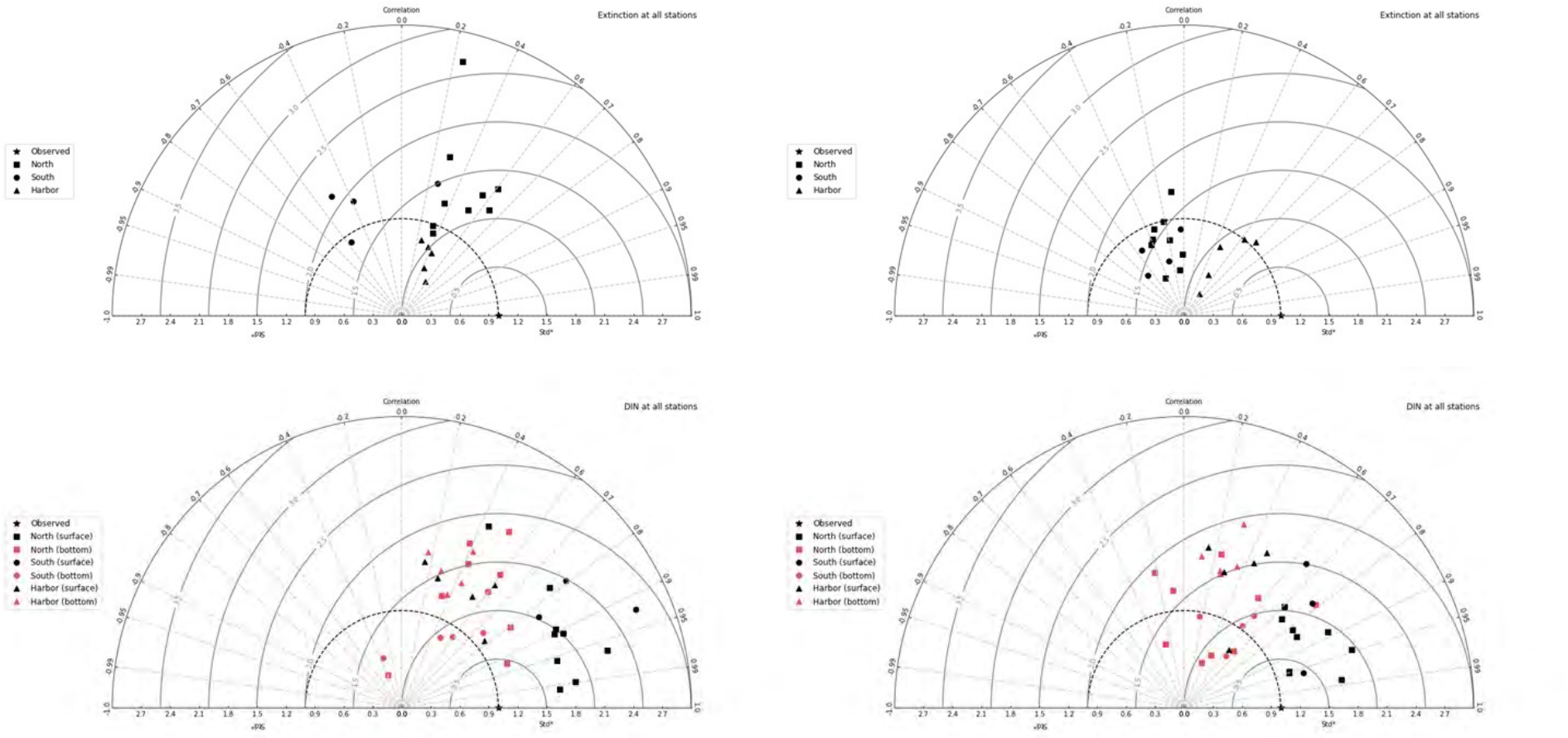

Fig. A-5 Taylor diagrams for MWRA vessel-based survey observations. Top panels show the parameter Extinction and bottom panels Dissolved Inorganic Nitrogen. Left panels show results for the year 2014 and right panels for the year 2015

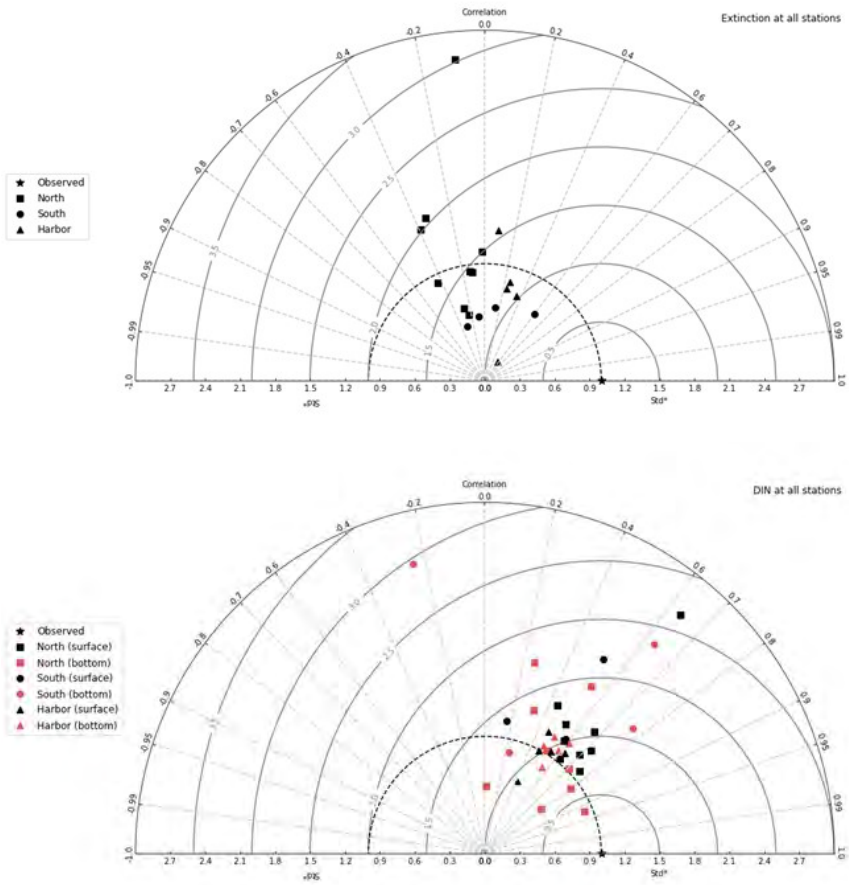

Fig. A-6 Taylor diagrams for MWRA vessel-based survey observations. Top panels show the parameter Extinction and bottom panels Dissolved Inorganic Nitrogen. Left panels show results for the year 2016.

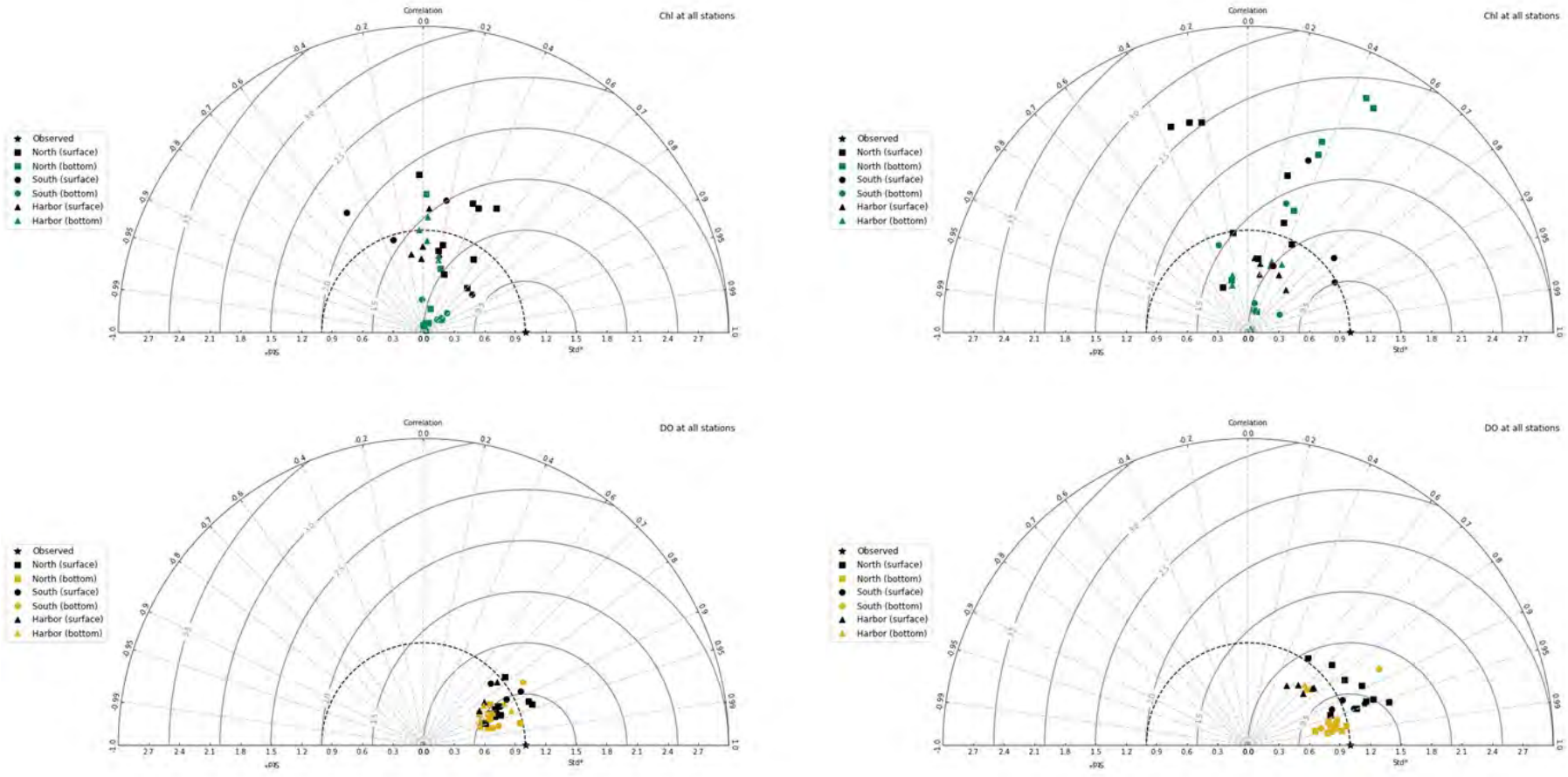

Fig. A-7 Taylor diagrams forfor MWRA vessel-based survey observations. Top panels show the parameter Chlorophyll-a and bottom panels Dissolved Oxygen. Left panels show results for the year 2012 and right panels for the year 2013.

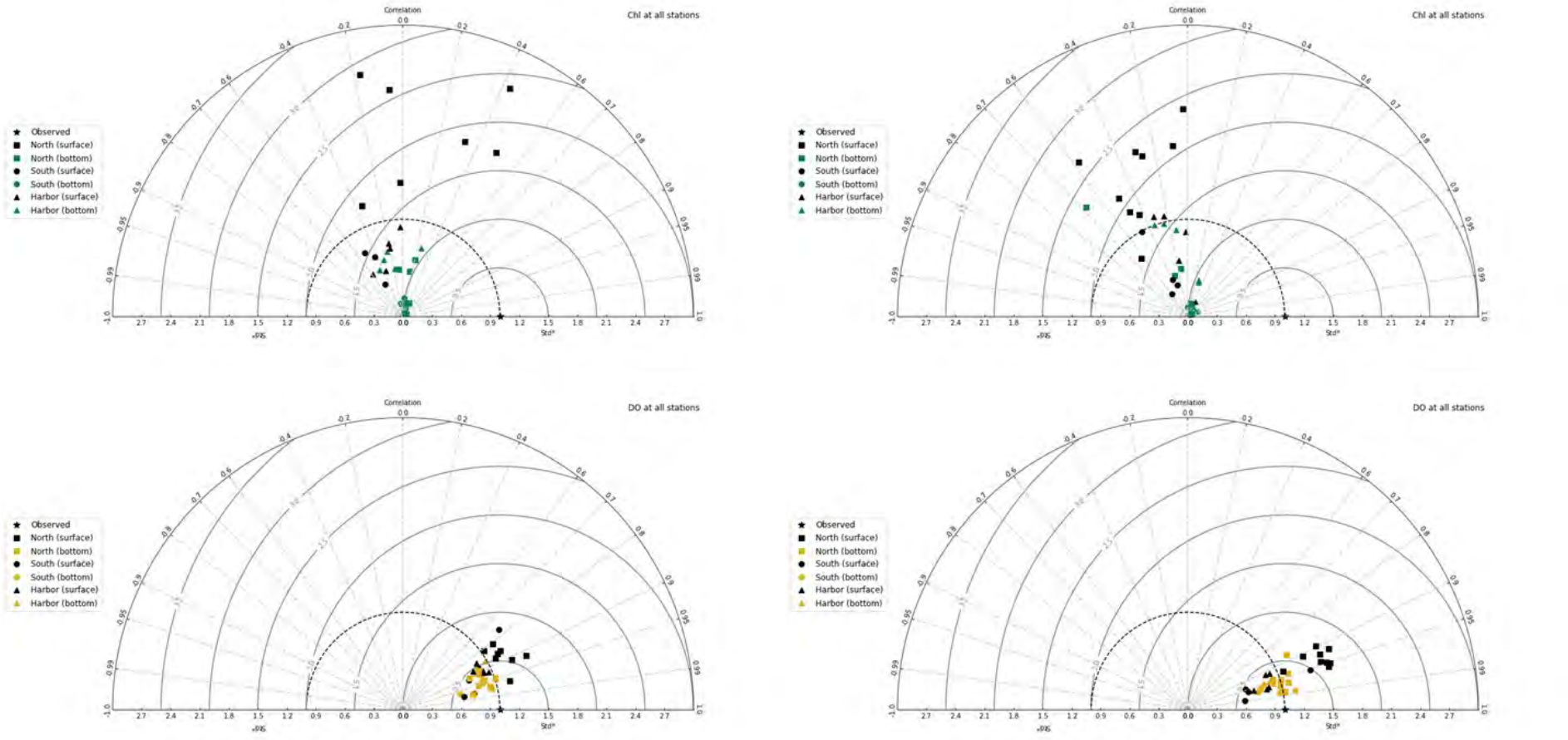

Fig. A-8 Taylor diagrams forfor MWRA vessel-based survey observations. Top panels show the parameter Chlorophyll-a and bottom panels Dissolved Oxygen. Left panels show results for the year 2014 and right panels for the year 2015

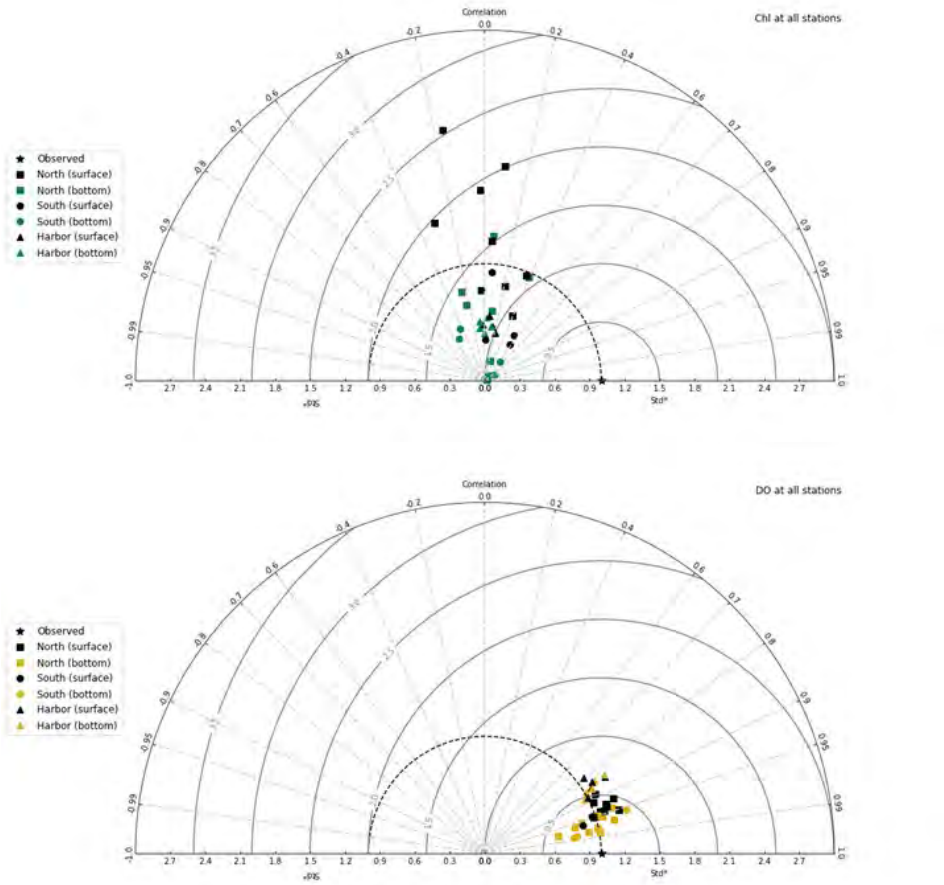

Fig. A-9 Taylor diagrams forfor MWRA vessel-based survey observations. Top panels show the parameter Chlorophyll-a and bottom panels Dissolved Oxygen. Left panels show results for the year 2016.

B Comparison plots for corrected outfall loads

Comparison plots between the former representation of the loads (Deltares, 2021) and the corrected representation are provided. These plots include:

- Model-observation time-series plots for DIN, chlorophyll a, and dissolved oxygen (DO) concentrations;
- Taylor diagrams for DIN, chlorophyll a and dissolved oxygen (DO) concentrations;
- Cross-sections plots through the DITP outfall for DIN, chlorophyll a and dissolved oxygen (DO) concentrations.

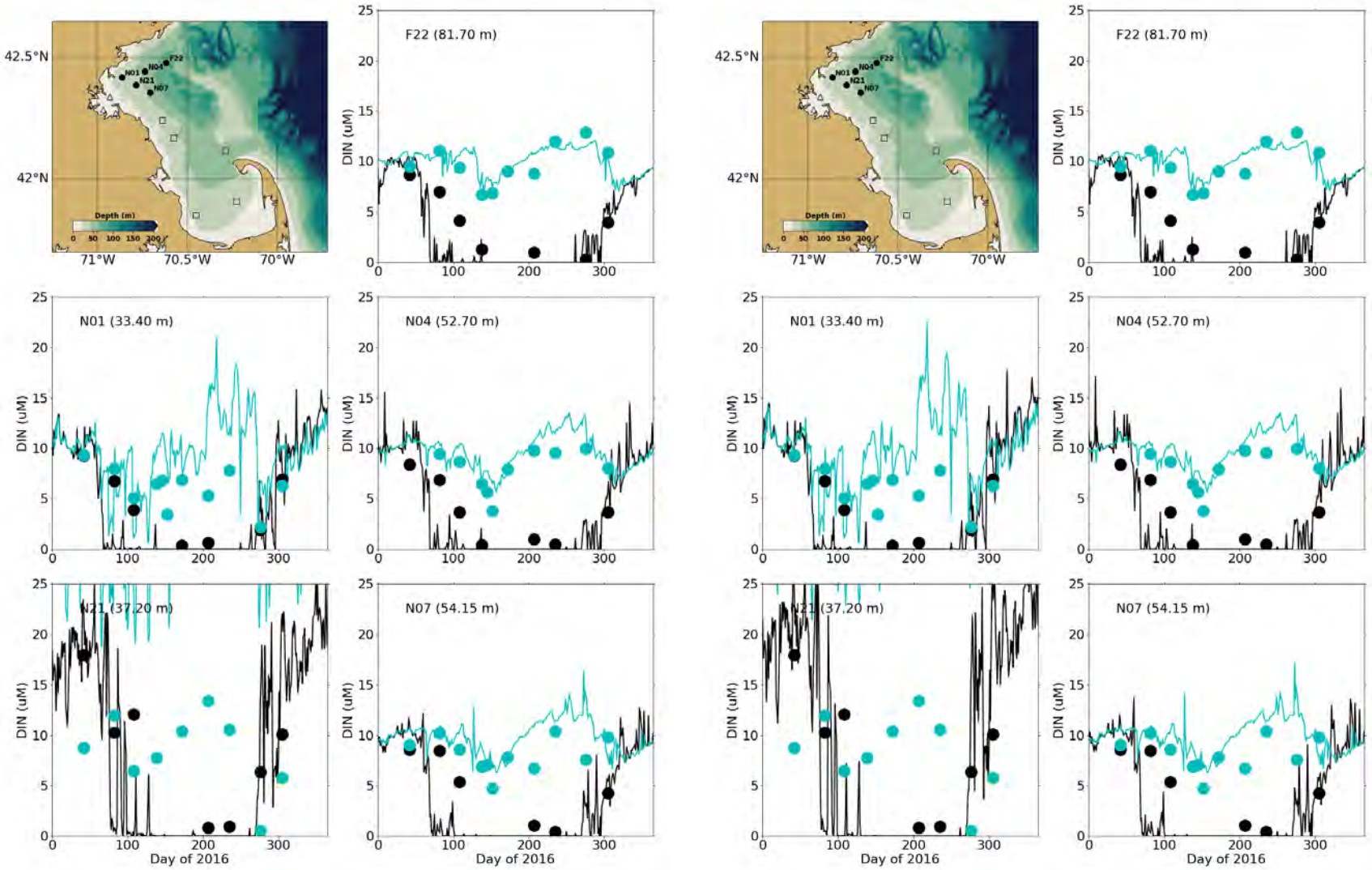

Fig. B-1 Comparison of simulated (lines) and observed (dots) DIN time-series for the year 2016 near the surface (black) and near the seabed (blue). Left panel: former representation of nutrients in DITP; right panel: corrected representation

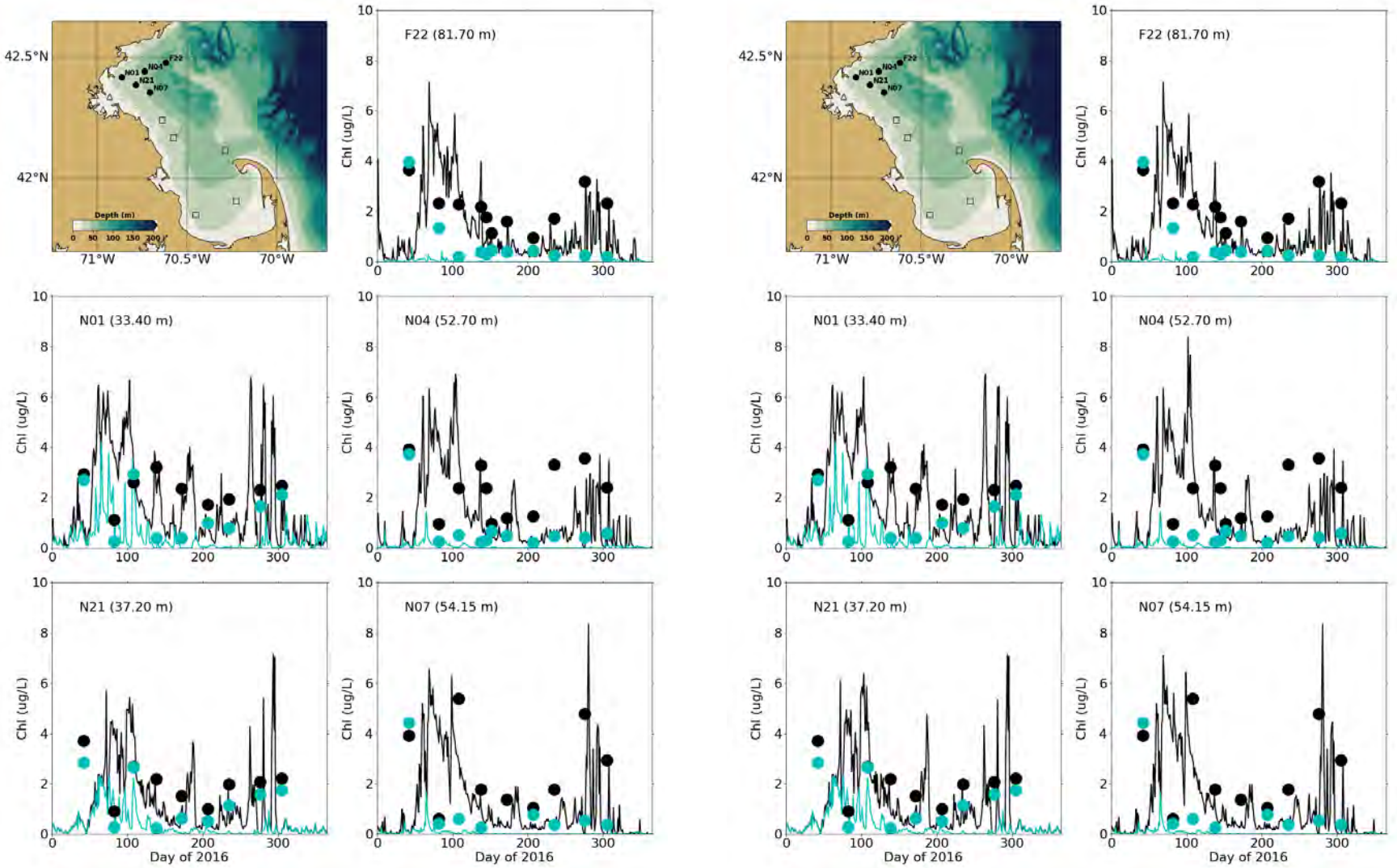

Fig. B-2 Comparison of simulated (lines) and observed (dots) chlorophyll a time-series for the year 2016 near the surface (black) and near the seabed (blue). Left panel: former representation of nutrients in DITP; right panel: corrected representation.

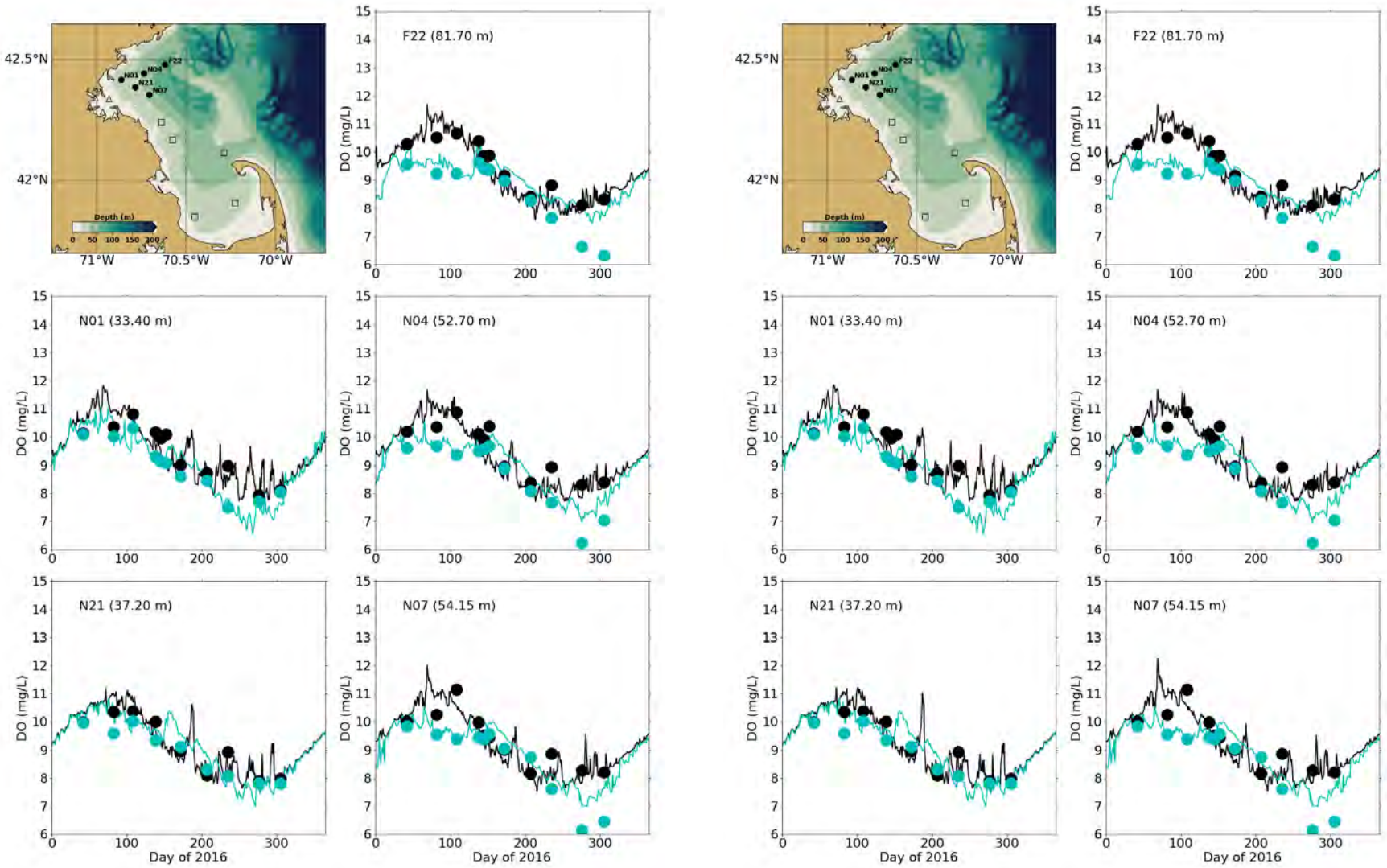

Fig. B-3 Comparison of simulated (lines) and observed (dots) DO time-series for the year 2016 near the surface (black) and near the seabed (blue). Left panel: former representation of nutrients in DITP; right panel: corrected representation

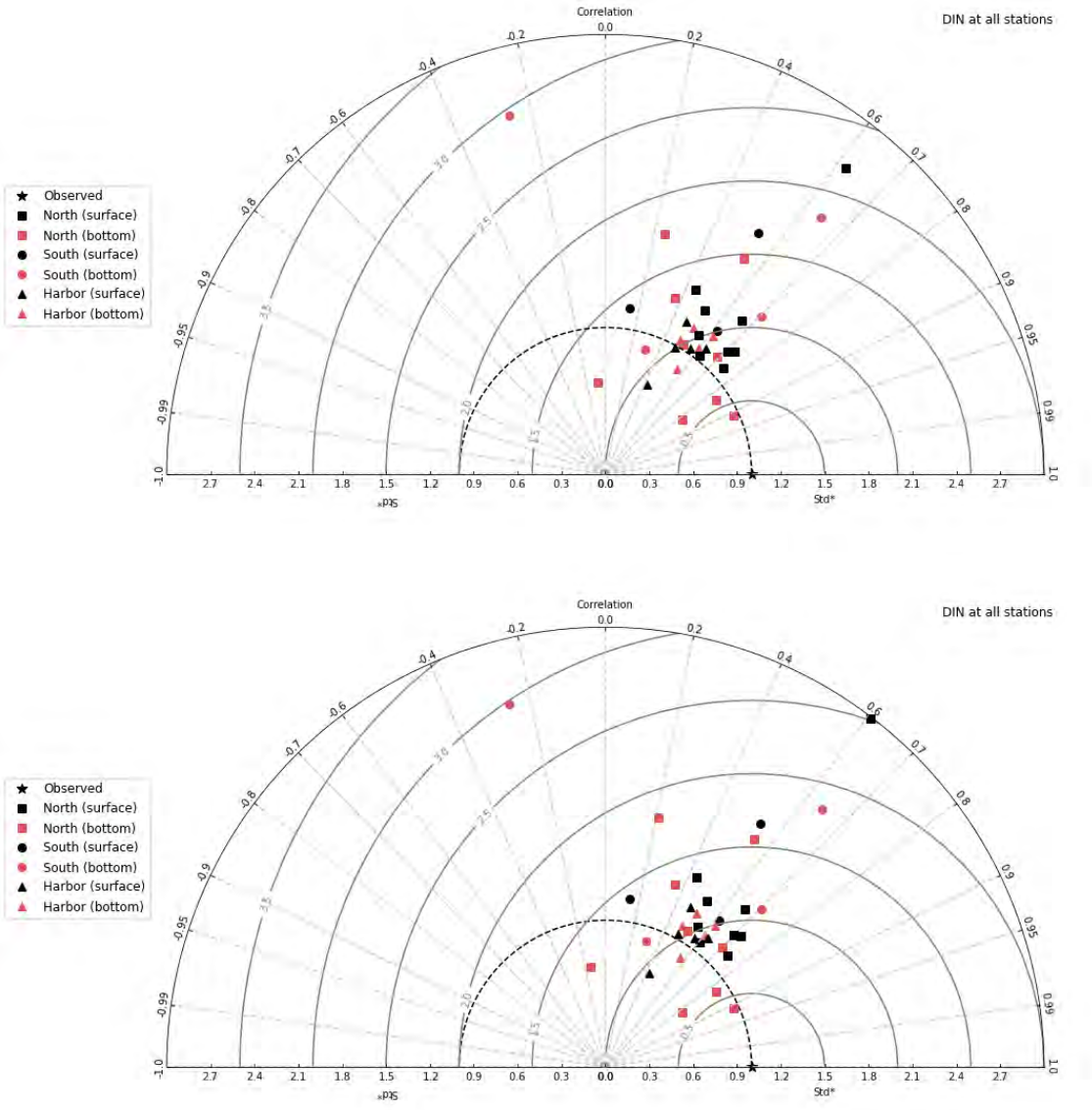

Fig. B-4 Comparison of Taylor diagrams for DIN concentrations for the year 2016. Top panel: former representation of nutrients in DITP; lower panel: corrected representation

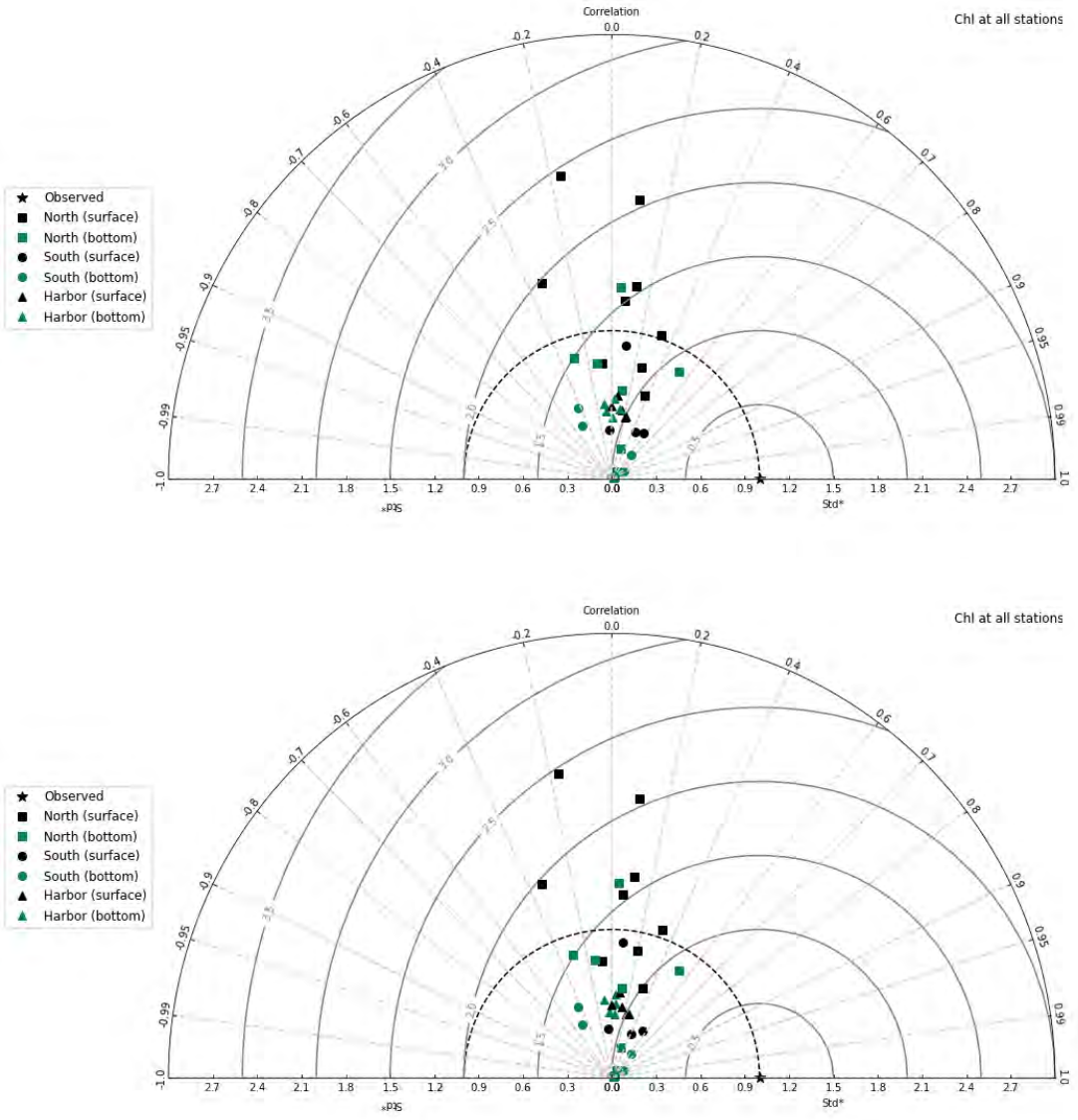

Fig. B-5 Comparison of Taylor diagrams for chlorophyll a concentrations for the year 2016. Top panel: former representation of nutrients in DITP; lower panel: corrected representation

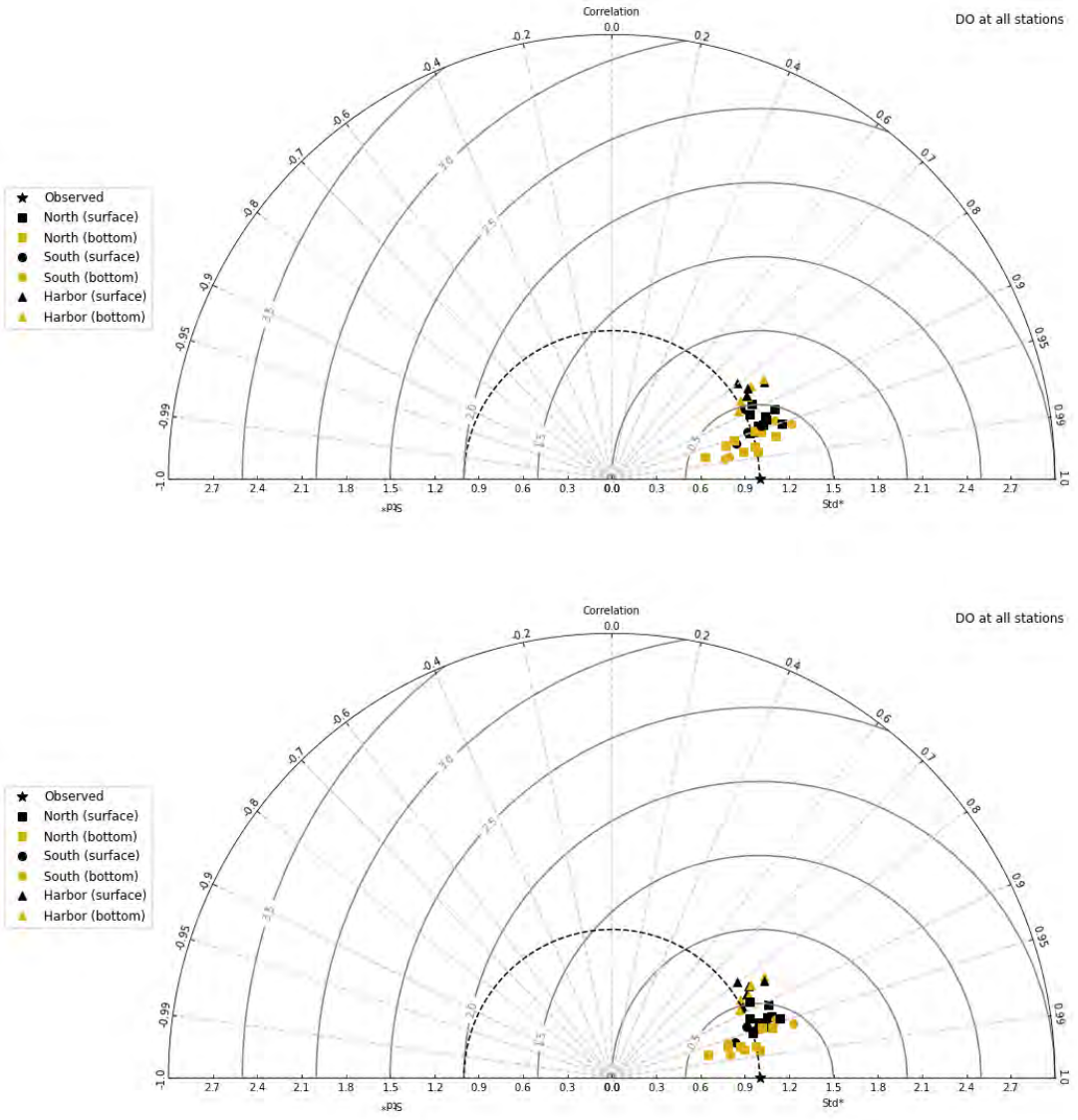

Fig. B-6 Comparison of Taylor diagrams for DO concentrations for the year 2016. Top panel: former representation of nutrients in DITP; lower panel: corrected representation.

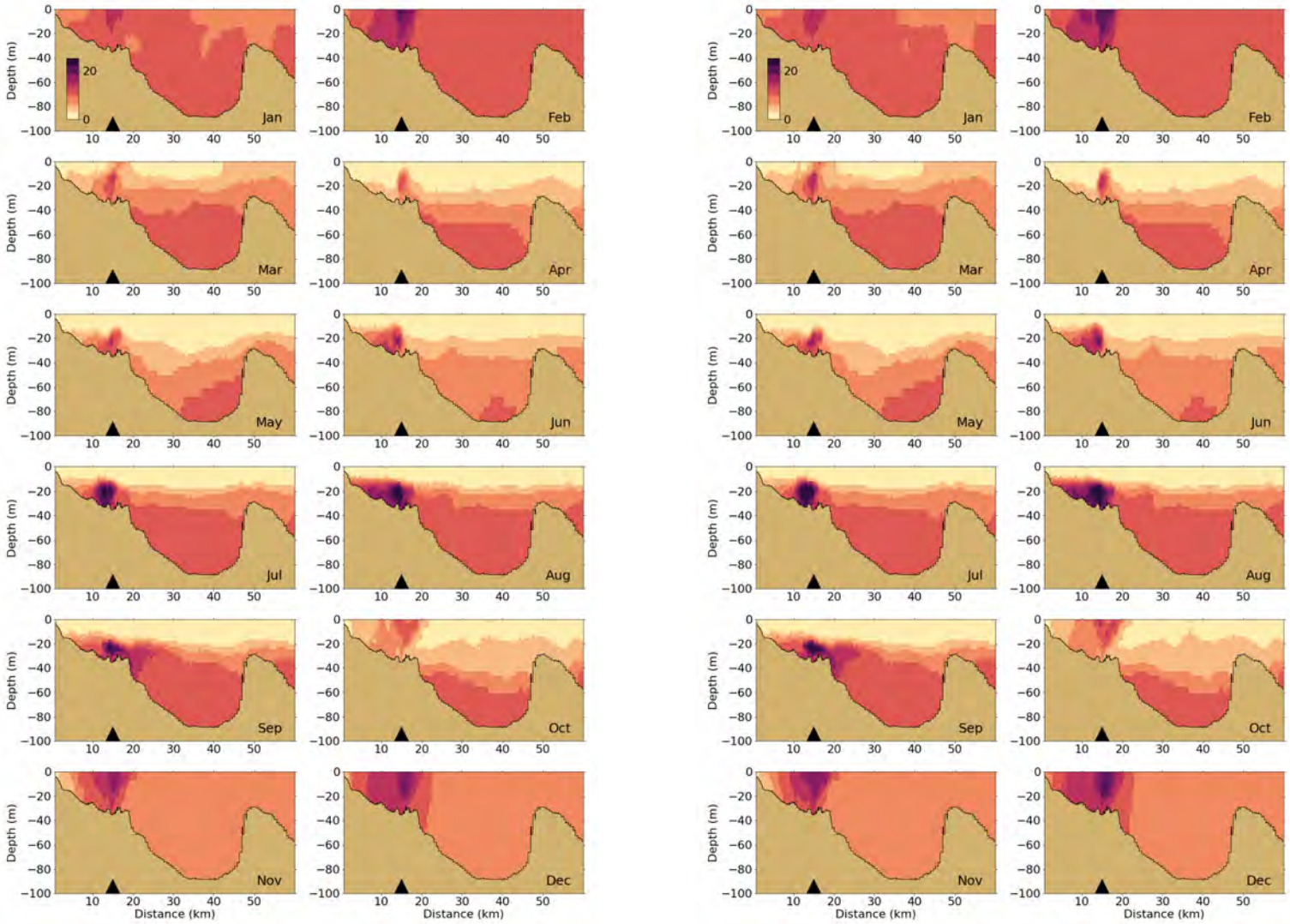

Fig. B-7 Comparison of cross-sections through the DITP outfall for DIN concentrations for the year 2016. Left panel: former representation of nutrients in DITP; right panel: corrected representation

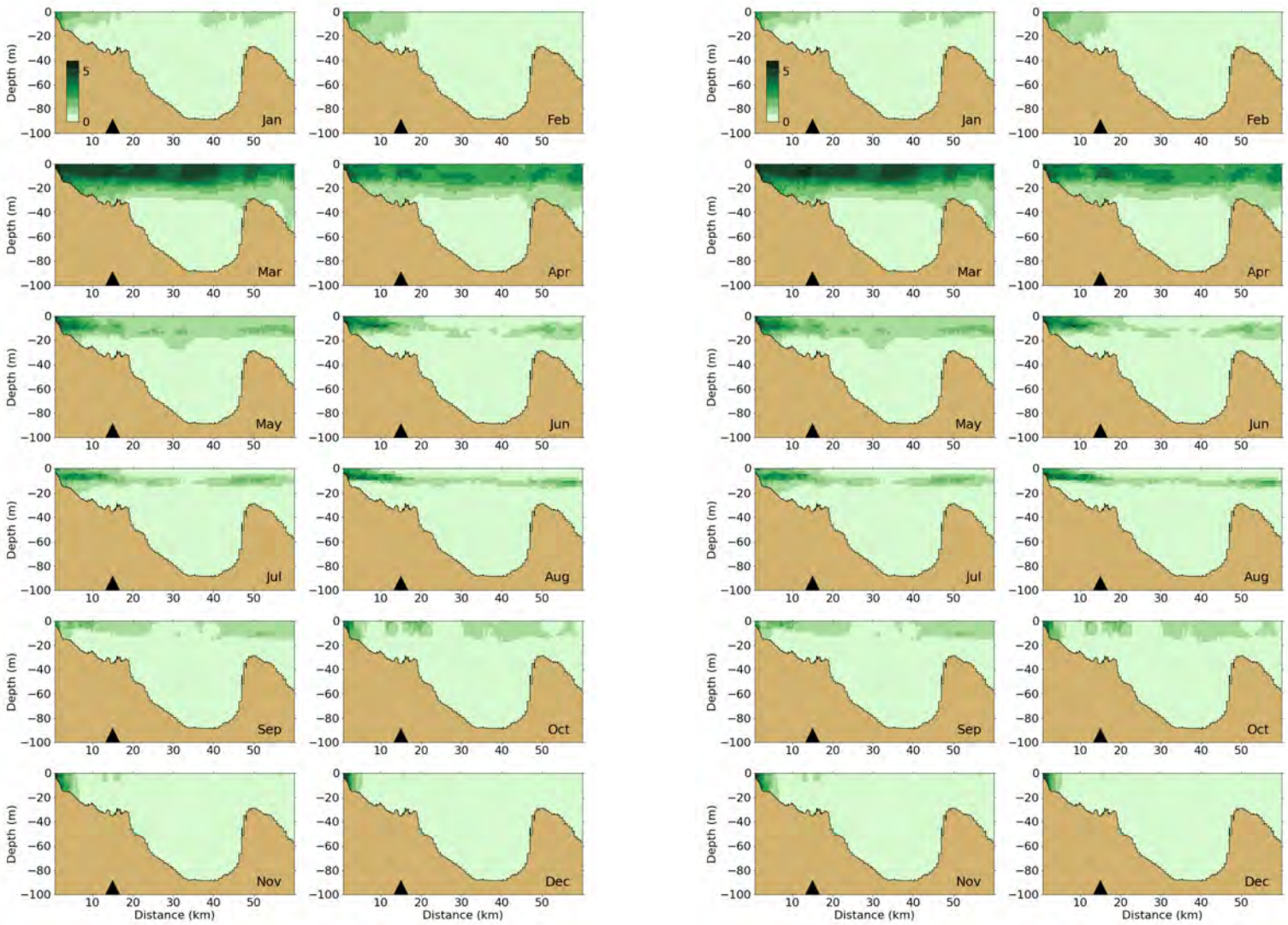

Fig. B-8 Comparison of cross-sections through the DITP outfall for chlorophyll a concentrations for the year 2016. Left panel: former representation of nutrients in DITP; right panel: corrected representation

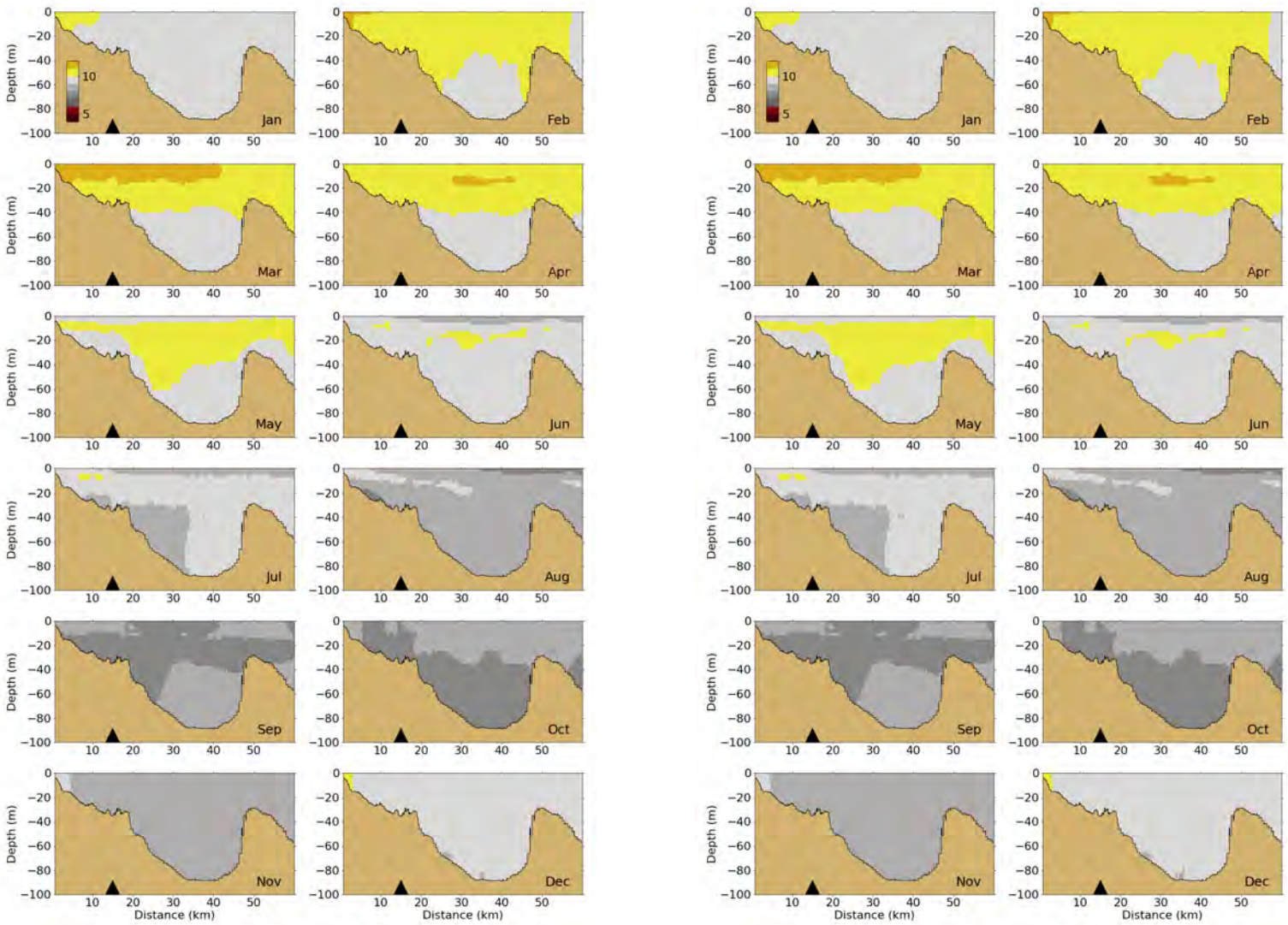

Fig. B-9 Comparison of cross-sections through the DITP outfall for DO concentrations for the year 2016. Left panel: former representation of nutrients in DITP; right panel: corrected representation.

Massachusetts Water Resources Authority
100 First Avenue • Boston, MA 02129
www.mwra.com
617-242-6000